TRIPLET EXCITON DIFFUSION IN ORGANIC CRYSTALS

by

STEPHEN ARNOLD

A dissertation submitted to the Graduate Faculty in Physics in partial fulfillment of the requirements for the degree of Doctor of Philosophy, The City University of New York.

1970

This manuscript has been read and accepted for the Graduate Faculty in Physics in satisfaction of the dissertation requirement for the degree of Doctor of Philosophy.

August 19, 1970
date

John C. Lamark
Chairman of Examining Committee

August 19, 1970
date

Robert M. Lea
Deputy Executive Officer

Professor Mark Miksic

Professor Bernard Kramer

Professor William Miller

Doctor William Whitten
Supervisory Committee

The City University of New York

Acknowledgments

The author wishes to express his sincere gratitude to his advisor, Professor Arthur C. Damask. The skills and values which he imparted were as significant as his explicit help in providing the facilities, equipment, and encouragement that made this work possible.

The author also wishes to express his appreciation to Doctor William B. Whitten for his discussions, frequent suggestions, and his valuable advise.

Appreciation is here expressed for the support of this research by The Army Research Office, Durham. The author has also benefited by the use of the facilities provided by the Brookhaven National Laboratory.

TABLE OF CONTENTS

LIST OF TABLES

LIST OF FIGURES

CHAPTER 1

Introduction

This work deals with two problems which fall into the general category of the diffusion of triplet excitons in organic crystals. The first problem was the investigation of triplet exciton trapping by dislocations in anthracene, and the second was the measurement of Davydov splitting in pyrene. In this chapter the pertinent characteristics of pyrene and anthracene are presented, previous work is discussed, and the thesis objectives are stated.

A. Pertinent Characteristics of Anthracene and Pyrene

The anthracene and pyrene molecules are illustrated in Figure 1.1. These molecules are held in a planar rigid structure by bonding between trigonal hybrids, as illustrated for pyrene in Figure 1.2. The σ bonds are symmetrical about the bond axis giving localized C-C and C-H bonds. The π bonds are to either side of the plane which contains the carbon atoms. The π electrons associated with any carbon atom are equally shared by its neighbors in the molecule, so that the π electrons are completely delocalized. This delocalization of the π electrons is a contributing factor to the binding energy of crystals composed of organic molecules. The π electrons are easily polarized, and the interaction between mutually induced dipoles, commonly known as the London Force, holds the crystal together. Crystals which are bound together by this weak interaction are known as molecular crystals.

Fig.1.1. Molecular structure of: (a) anthracene; and (b) pyrene.

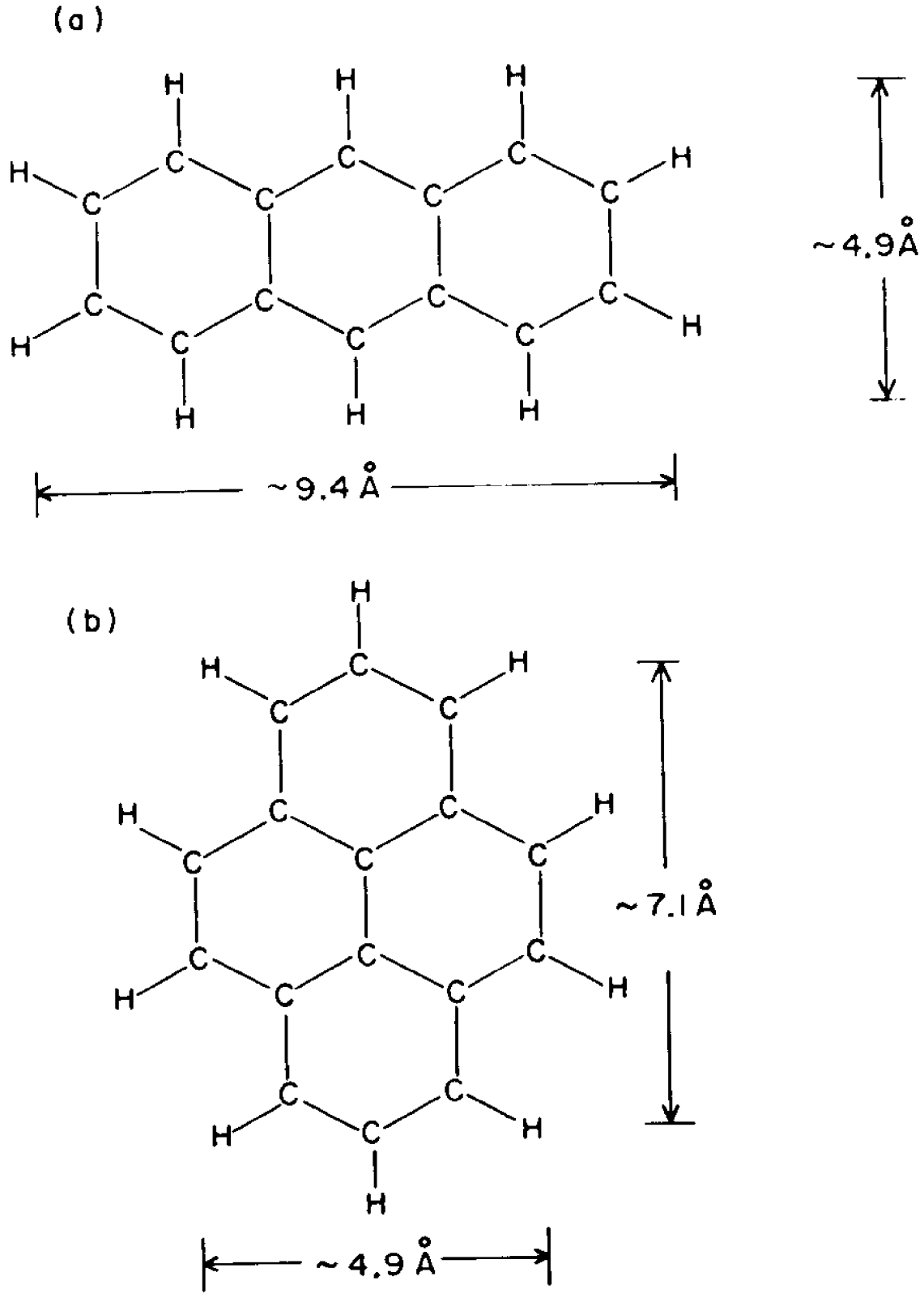

Fig. 1.2. (a) Combined trigonal hybrid orbital and p_z orbital; (b) Localized σ orbitals; and (c) Delocalized π orbitals.

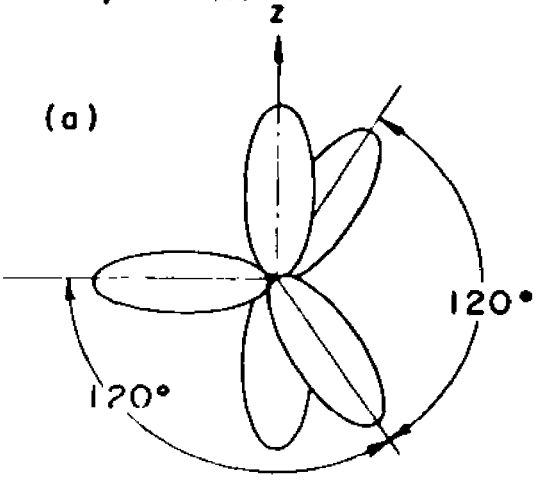

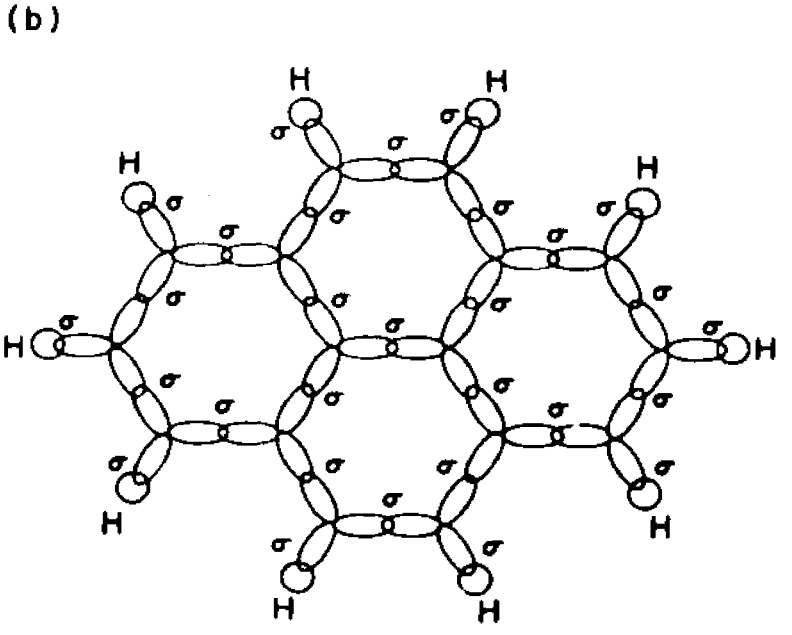

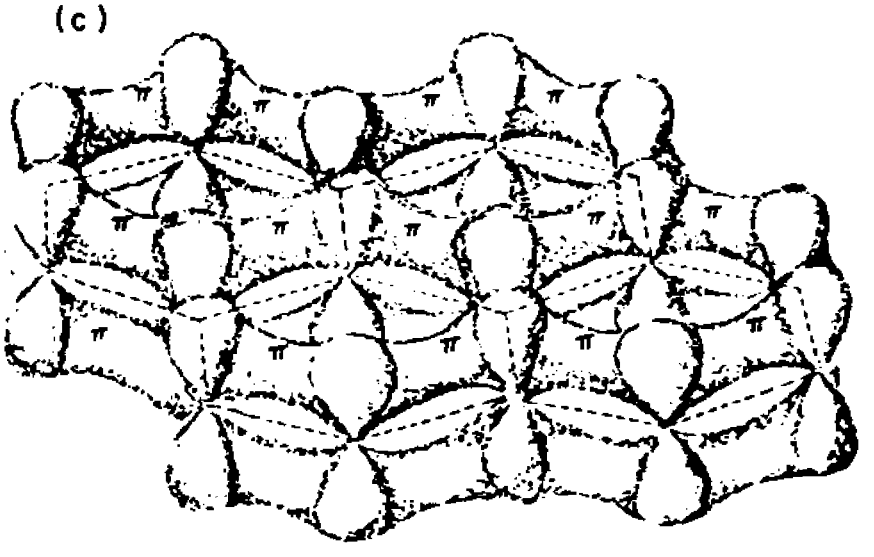

Due to the weak crystal forces, the low-lying molecular energy levels are relatively undisturbed in molecular crystals. Figure 1.3a shows the low-lying energy levels for a typical molecular crystal, including vibrational levels. The ground state is composed of an even number of electrons having opposite spins, and is therefore a singlet state. An excited state is generated by raising a π electron from the zero vibrational level of the ground state to a different electronic state. This can be done in two ways. If the spin is conserved in generating the excited state, it will be a singlet, otherwise, it will be a triplet. Figures 1.3b and 1.3c show the low-lying energy levels of anthracene[1] and pyrene[2,3] respectively. Vibrational levels are not shown in these figures.

Normally the triplet state is considered to be unaccessible because the selection rule, S=0, does not allow spin multiplicity to change with an electronic transition. In most cases, however, a small amount of spin orbit coupling degrades spin as a good quantum number, and the triplet state can be populated. In anthracene the highest value of the absorption coefficient for the triplet state is one-millionth that of the singlet state.[1,4]

An electron which is raised to one of the vibrational levels of an excited singlet or triplet state will rapidly (in about 10^{-12} seconds) lose its excess vibrational energy through coupling with lattice vibrations until it finds itself in the lowest vibrational level of the first excited singlet or triplet state. Since the S_1 to S_o transition is

Fig. 1.3. The first excited singlet and triplet states of: (a) A typical organic molecule; (b) anthracene; and (c) pyrene.

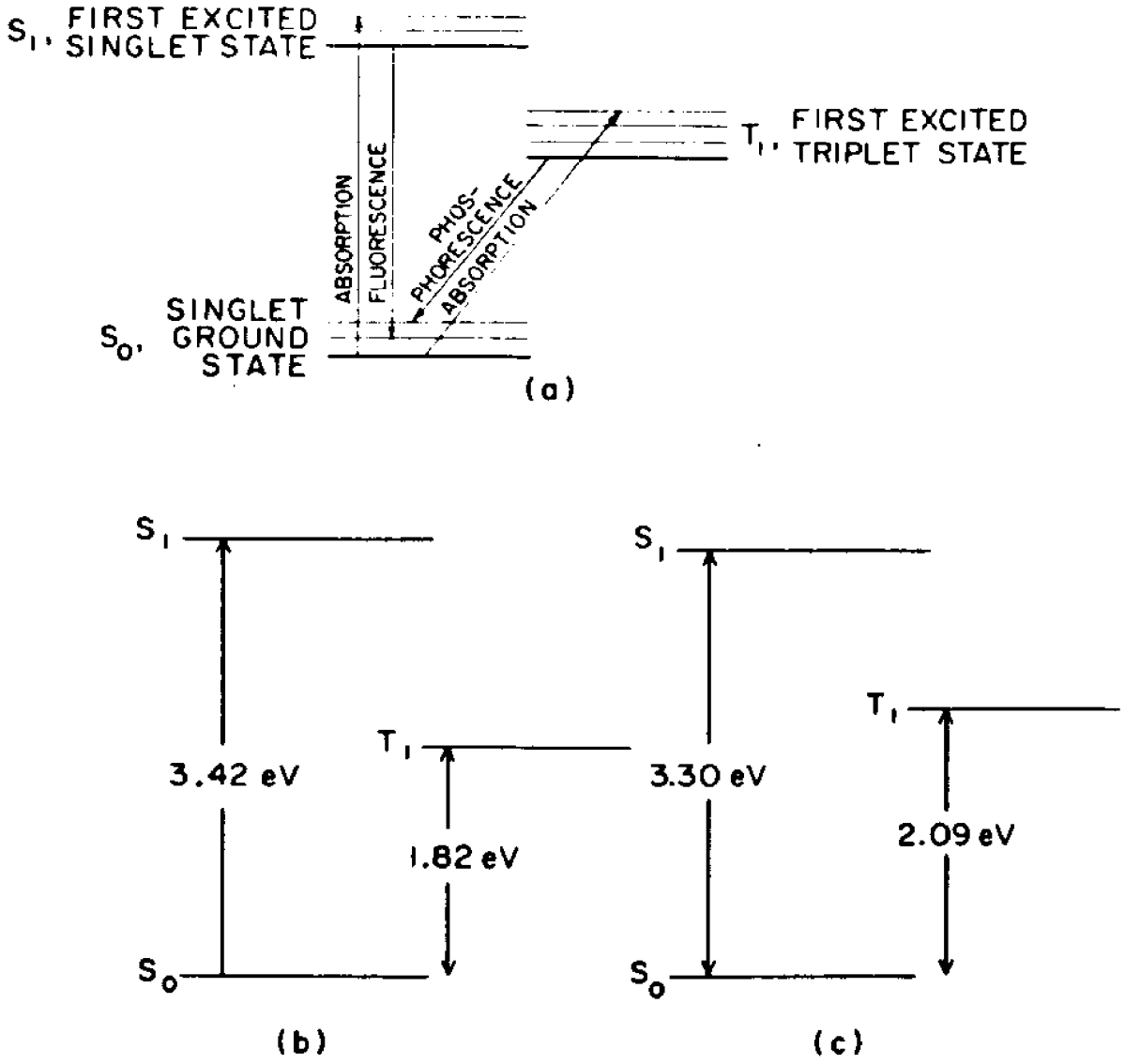

favorable, almost all the S_1 excitation is lost through radiative decay to the vibrational levels of the ground state. The lifetime of the S_1 state is typically about 10^{-9} seconds and the radiation is called fluorescence. In contrast the T_1 to S_o transition is not favorable, and most of the radiation is lost nonradiatively. In anthracene the radiative lifetime of this transition is approximately 60 seconds.[5] The radiation from this relatively long-lived state is commonly called phosphorescence.

Normally in solids the excitation of an electron is associated with a positively charged hole which is left behind. In the low-lying excited states the electron and hole form an electrically neutral bound pair. This bound pair is clearly not a stationary state of the entire crystal. If the history of the bound pair is followed subsequent to its formation, by using the rest of the crystal as a perturbation, the probability of finding the excitation on the original molecule decreases, and on neighboring molecules increases. It was in this way that Frenkel[6] first introduced the idea of an excitation wave for rare gases, and later pointed out that the process could be likened to the motion of a quasi particle, the exciton, through the crystal.

The triplet exciton, generated by exciting the triplet state, has a long diffusion length in comparison to the singlet exciton. In anthracene, for example, the diffusion lengths for singlet and triplet excitons are 0.05[7] and 10[8] microns respectively. Because the triplet exciton moves onto many molecules during its lifetime, a good chance exists for adjacent molecules

to be in the triplet state at the same time in spite of the fact that the triplet exciton density is small, due to the weak absorption of the triplet state. A slight coupling between these adjacent molecules allows their excitations to eventually combine on one molecule. If the spins of the two triplet excitons add to zero at the moment of combination and the combined energy is enough to cause an S_0 to S_1 transition, an excited singlet state will be formed. The combination of two triplets may also give rise to a triplet or quintet state, but the radiative decay from either of these states will be relatively small due to its spin forbidden nature. The creation of a singlet exciton from two triplet excitons is called triplet-triplet annihilation, and the light given off from the decay of the excited singlet state is called delayed fluorescence. The triplet absorption spectrum, which is exceedingly difficult to measure by direct means, can be determined indirectly by observation of this delayed fluorescence.

B. Past Work and Thesis Objectives

The long diffusion of the triplet exciton causes its lifetime to be strongly controlled by defect trapping. These defects may be either structural or impurity imperfections. Lupien and Williams[8] have found that the lower the impurity content of crystalline anthracene, the greater the triplet exciton lifetime. However no study has yet been made on the effects of structural defects on triplet exciton lifetime.

Recent work by Singh and Lipsett[10] indicates peaks in the delayed fluorescence intensity vs. temperature spectrum

in anthracene crystals. Siebrand[11] proposed a model to fit these data by assuming the peaks are due to an assortment of traps. This model can also be used to analyze the effects which structural defects have on triplet excitons, if such defects can be induced in a controlled manner. It is known that crystals plastically bent to a radius r will have a dislocation density given by[12]

$$N = 1/br \qquad 1.1$$

where b is the Burgers vector. N will be discussed further in chapter 4, section C.

The goal of the first problem was to find the effect which dislocations have on the triplet exciton motion. This was accomplished by the two fold process of: (1) measuring the steady state delayed fluorescence and triplet decay time vs. temperature for crystals before and after bending; and (2) analyzing the resulting data with Siebrand's triplet exciton trapping model.

Since crystal defects play an important role in the diffusion of triplet excitons, it is of interest to explore other techniques for the measurement of triplet exciton diffusion. Most measurements of the triplet diffusion constant in the past have involved experiments in which a small area of crystal is steadily illuminated and the diffusion of the exciton is followed by measuring the intensity of the delayed fluorescence.[8, 13-17] It now appears possible in certain cases to arrive at the exciton diffusion constant for a perfect crystal by doing experiments in an imperfect one. Davydov[18] has shown that the first triplet level in crystals which contain

two or more molecules per unit cell will be split. The split levels are oppositely polarized. The splitting can be measured by looking at the delayed fluorescence intensity vs. wavelength for each of the two polarizations. This technique is suitable because the delayed fluorescence spectrum is equivalent to the absorption spectrum. The splitting enables a qualitative dispersion relation to be set up and from this dispersion relation the exciton r.m.s. velocity can be calculated. The half width of the excitation spectrum gives a measure of the scattering time of the diffusing excitons. From the r.m.s. velocity and the scattering time the diffusion constant can be calculated. Recent work by Avakian et al[19] on anthracene has shown that this type of measurement is feasable.

In view of this, the goal of the second problem was to arrive at a diffusion constant of triplet excitons in pyrene by measuring the half width of the triplet absorption spectrum and the Davydov splitting.

References - Chapter 1

1. P. Avakian, E. Abramson, R.G. Kepler, and J.C. Caris, J. Chem. Phys. 39, 1127 (1963).
2. J. Ferguson, J. Chem. Phys. 28, 765 (1958).
3. P. Avakian and E. Abramson, J. Chem.Phys. 43, 821 (1965).
4. I. Nakada, J. Phys. Soc. Japan 20, 346 (1965).
5. G.C. Smith, Phys. Rev. 166, 839 (1968).
6. J. Frenkel, Phys. Rev. 37, 17 (1931).
7. O. Simpson, Proc. Roy. Soc. (london) A 238, 402 (1956).
8. P. Avakian and R.E. Merrifield, Phys. Rev. Letters 13, 541 (1964).
9. Y. Lupien and D.F. Williams, Mol. Crystals 5, 1 (1968).
10. S. Singh and F.R. Lipsett, J. Chem. Phys. 41, 1163 (1964).
11. W. Siebrand, J. Chem. Phys. 42, 3951 (1965).
12. A.H. Cottrel, Dislocations and Plastic Flow in Crystals, Oxford Press (London), 1953, p.29.
13. R.G. Kepler and A.C. Switendick, Phys. Rev. Letters 15, 56 (1965).
14. V. Ern, P. Avakian and R.E. Merrifield, Phys. Rev. 148, 862 (1966).
15. D.F. Williams and J. Adolph, J. Chem. Phys. 46, 4252 (1967).
16. D. F. Williams, J. Adolf, and G.W. Schneider, J. Chem. Phys. 45, 575 (1966).
17. M.Levine, J. Jortner and A. Szoke, J. Chem. Phys. 45, 1591 (1966).
18. A.S. Davydov, Zh. Eksperim, i Teo Fiz 18, 210 (1948).
19. P. Avakian, V. Ern, R.E. Merrifield and A. Suna, Phys. Rev. 165, 974 (1968).

CHAPTER 2

Siebrand's Model of Triplet Exciton Trapping

In this chapter Siebrand's model[1] of the triplet exciton trapping process is reviewed. The model is then extended to include a description of the decay of the delayed fluorescence.

A. Differential Equations

In the model of triplet exciton trapping constructed by Siebrand[1], the triplets are generated by direct excitation of the triplet state. In this model there are N_1 traps of depth ϵ_i with triplet density y_1. The free singlet and triplet exciton densities, x and y, are obtained from the following equations

$$\frac{dy}{dt} = \alpha I + \sum_i q_i y_i - \left(\beta_0 + \sum_i p_i + \gamma \sum_i c_i y_i + \gamma y\right) y \qquad 2.1$$

$$\frac{dy_i}{dt} = \alpha_i I + p_i y - \left(q_i + \beta_i + \gamma c_i y\right) y_i \qquad 2.2$$

$$\frac{dx}{dt} = -\alpha x + \tfrac{1}{2}\gamma y \left(y + \sum_i c_i y_i\right) \qquad 2.3$$

I is the incident intensity, αI is the rate of generation of free triplet excitons and $\alpha_i I$ is the rate of generation of triplet excitons at the trapping sites. a and β_0 are the rate constants for the decay of free triplet and singlet excitons, respectively, and the β_i's are the rate constants for the de-

cay of trapped triplets. γ and $c_1\gamma$ are the rate constants for triplet-triplet and triplet-trapped triplet annihilation, respectively, and p_i and q_i are the rate constants for trapping and release, respectively, at the i^{th} level. The latter two rate constants are given by

$$p_i = Z_i N_i \qquad 2.4$$

and

$$q_i = q_o e^{-\epsilon_i/kT} \qquad 2.5$$

where N_i and ϵ_i are the density and the trap depth, respectively, for the i^{th} trap. Z_i is the triplet exciton velocity times the trap cross-section, and q_o is the pre-exponential factor in the release rate. q_i is assumed to be the only temperature dependent rate constant.

Equations 2.1, 2.2, and 2.3 can be simplified by making some reasonable assumptions. For lack of further knowledge it is assumed that the c_i's are unity, i.e., we neglect the difference between the rate constants for triplet-triplet and triplet-trapped triplet annihilation. Also $\alpha_1 I$, the direct absorption of light at the trapping sites, is neglected for impurities because their concentration is small (see chapter 3, section A), and for mechanical defects because measurements of the triplet absorption spectrum in anthracene crystals[2] are in agreement with the measurements made in solution,[3] i.e., there are no mechanical defects in solution. In addition for small triplet exciton densities the bimolecular terms can be discarded except in the equation for dx/dt[4] (in the equation for dx/dt the bimolecular terms are the only source of singlet excitons).

With these assumptions equations 2.1, 2.2 and 2.3 become

$$\frac{dy}{dt} = \alpha I + \sum_i q_i y_i - (\beta_0 + \sum_i p_i) y \qquad 2.6$$

$$\frac{dy_i}{dt} = p_i y - (q_i + \beta_i) y_i \qquad 2.7$$

$$\frac{dx}{dt} = -\alpha x + \tfrac{1}{2} \gamma y \left(y + \sum_i y_i\right) \qquad 2.8$$

B. Steady State Delayed Fluorescence Intensity

The delayed fluorescence results from the annihilation of triplet-triplet and triplet-trapped triplet pairs. These annihilations produce singlet excitons which subsequently decay and give off the fluorescence which is seen. Therefore from equation 2.8 the delayed fluorescence I_f is given by

$$I_f = ax \qquad 2.9$$

When the incident intensity is constant the triplet and singlet populations will be in steady state. The delayed fluorescence from equation 2.8, with dx/dt = 0, is

$$I_f = \tfrac{1}{2} \gamma y (y + \sum_i y_i) \qquad 2.10$$

Also from equation 2.7, with $dy_1/dt = 0$, the trapped triplet densities are

$$y_1 = A_1 y \qquad 2.11$$

where $A_1 = p_1/(q_1 + \beta_1)$

Substituting equation 2.11 into equation 2.6 with dy/dt=0, the free triplet density is

$$y = \frac{\alpha I}{\beta_0}\left[\frac{1}{1+\sum_i A_i \rho_i}\right] \qquad 2.12$$

where

$$\rho_i = \beta_i/\beta_0$$

Putting equations 2.11 and 2.12 into equation 2.10, the steady state delayed fluorescence intensity is

$$I_F = \frac{1}{2}\gamma\left(\frac{\alpha I}{\beta_0}\right)^2\left[\frac{1+\sum_i A_i}{\left(1+\sum_i \rho_i A_i\right)^2}\right] \qquad 2.13$$

It should be noted that the fluorescence intensity is proportional to the square of the incident intensity. This is only true if the bimolecular annihilation terms in equations 2.1 and 2.2 can be neglected.[4] Since an analysis of the experimental data using all of the bimolecular terms in equations 2.1 and 2.2 is unwieldy, the incident intensity was lowered to a point at which the square law was true before any data were taken (see chapter 3, section E). Such a precaution also eliminates the need for introducing saturation effects into the exciton trapping rate. Saturation effects would introduce an additional bimolecular term in equations 2.1 and 2.2. However, Goode and Lipsett[4] have shown that this term will be negligible if the square law is valid.+

+For the incident intensity used in this experiment (see chapter 3, section E) it is calculated that since the ratio of trapped triplet excitons to free triplet excitons for the traps introduced by plastic deformation is 10^{-5}, saturation effects can be neglected.

Maxima and minima occur in the steady state delayed fluorescence when $dI_f/dT = 0$, or

$$\sum_i \frac{dA_i}{dT}\left[1 + \sum_j \rho_j A_j - 2\rho_i\left(1 + \sum_j A_j\right)\right] = 0 \qquad 2.14$$

Since the A_i's decrease monotonically with increasing temperature, equation 2.14 will be zero if

$$1 + \sum_j \rho_j A_j - 2\rho_i\left(1 + \sum_j A_j\right) = 0 \qquad 2.15$$

The physical significance of equation 2.15 is clarified by considering the situation that there is only one trap level, labeled 4, which is operative. Then equation 2.15 reduces to

$$\rho_4 = \left(2 + A_4\right)^{-1} \qquad 2.16$$

Under this condition the second derivative of equation 2.13 (with one trap, labeled 4) is found to be negative, indicating that the extremum is a maximum. Since $A_4 > 0$ it follows from equation 2.16 that $\beta_4 < \frac{1}{2}\beta_0$. Therefore, in the case of a single trapping level, the steady-state delayed fluorescence exhibits a maximum if, and only if, the lifetime of the trapped triplet exciton is more than twice as long as the lifetime of the free exciton.

C. Decay of the Delayed Fluorescence Intensity

In the triplet exciton trapping experiment both steady state and transient delayed fluorescence measurements were car-

ried out. The data from the steady state measurements can be analyzed with equation 2.13. In order to analyze the decays of the delayed fluorescence which result from cutting off the incident excitation, Siebrand's work was extended to include the transient case. To analyze the decays, equations 2.6, 2.7 and 2.8 must be solved with I=0. Such a solution can be obtained with the aid of an additional assumption if only one type of trap is effective. Since the singlet excitons decay so rapidly compared to the triplets,[5] we may say dx/dt = 0 shortly after the excitation is removed. Therefore, with one type of trap, say i=4, equations 2.6, 2.7 and 2.8 become

$$\frac{dy}{dt} = q_4 y_4 - (\beta_o + p_4) y \qquad 2.17$$

$$\frac{dy_4}{dt} = p_4 y - (q_4 + \beta_4) y_4 \qquad 2.18$$

$$0 = -ax + \frac{1}{2}\gamma y (y + y_4) \qquad 2.19$$

From equations 2.9 and 2.19 the delayed fluorescence is

$$I_F = \frac{1}{2}\gamma y (y + y_4) \qquad 2.20$$

In order to evaluate equation 2.20 for the delayed fluorescence, y and y_4 must be determined by solving equations 2.17 and 2.18. This is done by the following procedure: First, equation 2.17

is differentiated and becomes

$$\frac{d^2y}{dt^2} = q_4 \frac{dy_4}{dt} - (\beta_o + p_4)\frac{dy}{dt} \qquad 2.21$$

Second, equation 2.18 is substituted for dy_4/dt into equation 2.21, and one obtains

$$\frac{d^2y}{dt^2} = q_4 p_4 y - q_4 (q_4 + \beta_4) y_4 - (\beta_o + p_4)\frac{dy}{dt} \qquad 2.22$$

Third, equation 2.17 is solved for y_4 and substituted into equation 2.22, and the result is

$$\frac{d^2y}{dt^2} = (q_4 + \beta_4 + p_4 + \beta_o)\frac{dy}{dt} - \left[(q_4 + \beta_4)(\beta_o + p_4) - q_4 p_4\right] y \qquad 2.23$$

Equation 2.23 has the general solution

$$y = D_1 e^{-\beta_+ t} + D_2 e^{-\beta_- t} \qquad 2.24$$

where

$$\beta_\pm = \frac{1}{2}(p_4 + \beta_o + q_4 + \beta_4) \pm \frac{1}{2}\sqrt{(q_4 + \beta_4 - p_4 - \beta_o)^2 + 4 q_4 p_4} \qquad 2.25$$

By following a similar procedure, y_4 is found to obey the same differential equation as y.

$$y_4 = D_3 e^{-\beta_+ t} + D_4 e^{-\beta_- t} \qquad 2.26$$

In order to complete the solution to the decay of the delayed fluorescence, it is necessary to use the initial conditions to evaluate D_1, D_2, D_3 and D_4. Just before the incident intensity is cut off the free and trapped triplet densities are in steady state and can be obtained from equations 2.12 and 2.11 respectively. When this is done one has

$$y(0) = \alpha I \left[\frac{1}{\beta_0 + \dfrac{P_4 \beta_4}{q_4 + \beta_4}} \right] \qquad 2.27$$

and

$$y_4(0) = \frac{P_4 y(0)}{q_4 + \beta_4} \qquad 2.28$$

By evaluating equation 2.24 at t=0, one obtains the relation

$$D_2 = y(0) - D_1 \qquad 2.29$$

D_3 and D_4 can be related to D_1 by substituting equations 2.24, 2.26 and 2.29 into equation 2.17 and equating like exponential terms. When this is done the result is

$$D_3 = \frac{(\beta_o + P_4 - \beta_+)}{q_4} D_1 \qquad 2.30$$

and

$$D_4 = \frac{(\beta_o + P_4 - \beta_-)}{q_4} (y_o - D_1) \qquad 2.31$$

D_1 is obtained by substituting equations 2.30 and 2.31 into equation 2.26, and evaluating it at t=0, so that

$$D_1 = \frac{y(o)}{\beta_- - \beta_+} \left(\beta_- - \beta_o - P_4 + \frac{P_4 q_4}{\beta_4 + q_4} \right) \qquad 2.32$$

To summarize, for the case of one trap, say i=4, the delayed fluorescence is given by

$$I_F = \frac{\gamma}{2} (y^2 + y y_4) \qquad 2.20$$

and the time dependence of the free and trapped triplet densities after the incident intensity is cut off is

$$y = D_1 e^{-\beta_+ t} + D_2 e^{-\beta_- t} \qquad 2.24$$

$$y_4 = D_3 e^{-\beta_+ t} + D_4 e^{-\beta_- t} \qquad 2.26$$

where

$$D_1 = \frac{y(0)}{\beta_- - \beta_+}\left(\beta_- - \beta_0 - P_4 + \frac{P_4 q_4}{\beta_4 + q_4}\right) \qquad 2.32$$

$$D_2 = y(0) - D_1 \qquad 2.29$$

$$D_3 = \frac{(\beta_0 + P_4 - \beta_+)}{q_4} D_1 \qquad 2.30$$

$$D_4 = \frac{(\beta_0 + P_4 - \beta_-)}{q_4}(y_0 - D_1) \qquad 2.31$$

and

$$y(0) = \frac{\alpha I}{\beta_0 + \frac{P_4 \beta_4}{\beta_4 + q_4}} \qquad 2.27$$

$$\beta_\pm = \tfrac{1}{2}(P_4 + \beta_0 + q_4 + \beta_4) \pm \tfrac{1}{2}\sqrt{(q_4 + \beta_4 - P_4 - \beta_0)^2 + 4 q_4 P_4} \qquad 2.25$$

In the special case in which there are no traps equation 2.17 becomes

$$\frac{dy}{dt} = -\beta_0 y \qquad 2.33$$

The solution to equation 2.33 is

$$y = y(0)\, e^{-\beta_0 t} \qquad 2.34$$

where, from equation 2.27 with $p_4=0$, $y(0)=\alpha I/\beta_o$.
By substituting equation 2.34 into equation 2.20 with $y_4=0$, one obtains

$$I_f = \frac{\gamma}{2}\left(\frac{\alpha I}{\beta_o}\right)^2 e^{-2\beta_o t} \qquad 2.35$$

It should be observed that the single decay process illustrated by equation 2.35 indicates that the multiple decay exhibited by equation 2.24 is a direct consequence of trapping.

In cases in which the delayed fluorescence appears to have only one decay constant, it is convenient to fit the data to

$$I_f = I_{f_o} e^{-2\beta t} \qquad 2.36$$

where I_{f_o} is the fluorescence at the start of the measurement, and β is called the triplet decay rate (or triplet decay constant). Single exponential decay will occur when one of the D_i's in equation 2.24 and 2.26 is much larger than the other three. This can happen, as demonstrated in the appendix to chapter 4, when β_4 is much greater than both β_o and p_4. The definition of β is convenient because a comparison of equation 2.36 with equation 2.35 shows that in the case in which trapping is ineffective, β will be identical to the free triplet decay rate β_o.

References - Chapter 2

1. W. Siebrand, J. Chem. Phys. 42, 3951 (1965).

2. P. Avakian, H. Abramson, R.G. Kepler, and J.C. Caris, J. Chem. Phys. 39, 1127 (1963).

3. M.R. Padhye, S.P. McGlynn, and M. Kasha, J. Chem. Phys. 24, 588 (1956).

4. D.H. Goode and F.R. Lipsett, J. Chem. Phys. 51, 1222 (1969).

5. J.B. Birks, T.A. King, and I.H. Munro, Proc. Phys. Soc. (London) 80, 355 (1962).

CHAPTER 3

Experimental Apparatus and Procedure for Trapping Experiment

A. Availability and Quality of Anthracene Crystals

The anthracene crystals were prepared at, and made available by the Solid State Physics Group of the Brookhaven National Laboratory.

The crystals were prepared by starting with synthetic anthracene (Eastman H 480) and further purifying it by chromatography, vacuum sublimation, and zone refining.[1] The residual impurity concentration was too small to be detected by gas chromatography (less than 1 ppm). Single crystals were grown by the Bridgman method.

The dislocation content of the undeformed anthracene samples was estimated by counting etch pits on the ab cleavage plane (see section B for the preparation of a sample from the crystal boule). Etching was accomplished by immersing the crystals in fuming sulfuric acid diluted 1:10 with concentrated sulfuric acid, and then rapidly washing the samples in water.[2] A microscope focused on the ab plane revealed well defined rhombic etch pits. The undeformed samples were found to have typically 1×10^5 to 5×10^5 pits/cm^2.

B. Preparation of a Sample from a Crystal Boule

The crystal boule was cleaved with a razor along the ab cleavage plane, which was located with the aid of cleavage cracks. A section about 2 mm in thickness was cut parallel to the cleaved surface with a xylene-soaked string saw. The string saw was used

because it was found that a razor tended to bend thin sections in the cleavage process. The crystal was then cemented to a glass slide with "Duco" cement, and both sides were planed flat with a razor blade, used as a microtome. An optical finish was obtained by brushing the crystal with a "Kleenex" tissue saturated with xylene. In order to align the crystal for the bending which followed, a straight edge was cut in the ab plane, parallel to the a direction. The a direction can be easily located in anthracene because it is the direction of maximum birefringence[3] (see Fig. 3.1). The typical sample was 1 cm^2 in the ab plane and approximately 1 mm thick along the c' direction (the direction perpendicular to the ab plane).

The triplet lifetime (measurement described in Section E(7)) in these prepared crystals was found to increase with annealing time and temperature. It was found that saturation of the lifetime could be obtained by annealing for 1 hour at 443°K. Accordingly, all crystals were annealed in this manner prior to bending.

C. Bending of a Sample

According to Robinson and Scott,[4] slip can occur in anthracene on both the (001)[010] and (001)[110] systems. The (001)[010] system was chosen as the crystal bending direction because of the ease in orienting a sample along the b direction (see Fig. 3.1).

The crystal bending was accomplished by placing the anthracene sample in a half cylindrical shell so that the a direction of the crystal, the direction of its straight edge, was a-

Fig.3.1. Orientation of an anthracene crystal by double refraction. (a) An unaligned crystal placed over intersecting vertical and horizontal lines. (b) A crystal aligned relative to intersecting vertical and horizontal lines with its a axis parallel to the horizontal line.

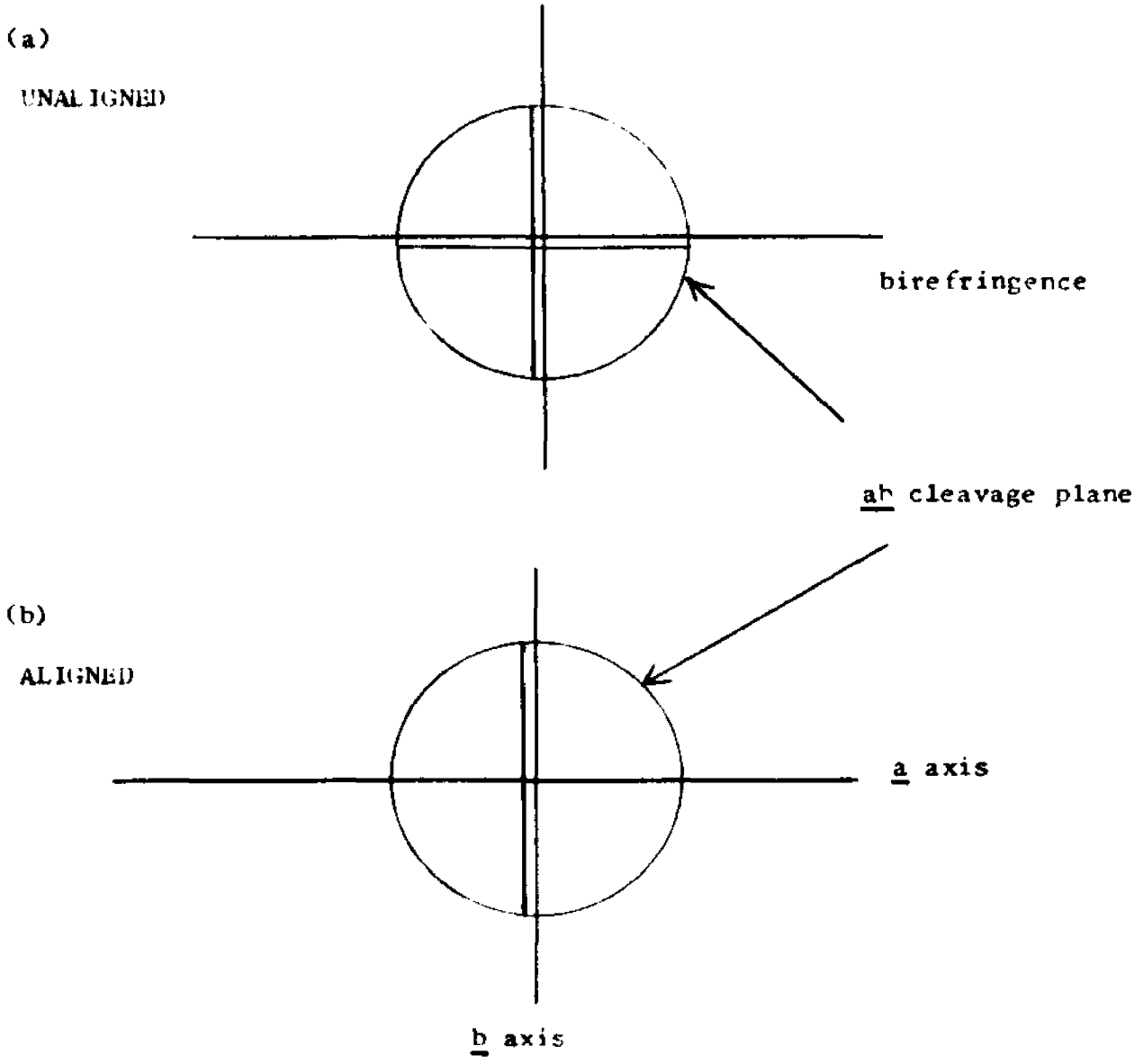

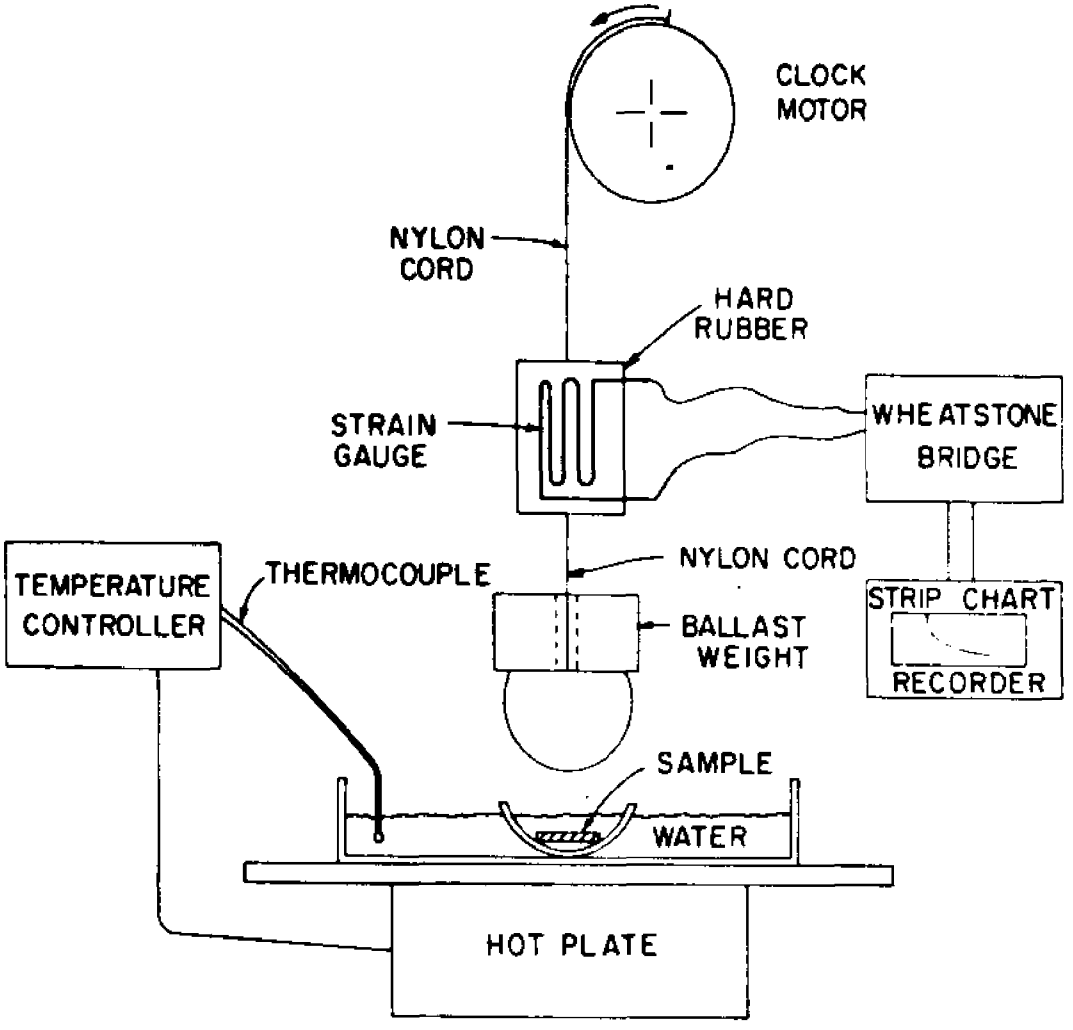

Fig. 3.2. PLASTIC DEFORMATION APPARATUS

long the axis of the shell. By lowering a solid cylinder onto the crystal in a shell of desired curvature, the crystal could be bent to the curvature of the shell along the b direction. To facilitate the bending, the crystal was bathed in water which was maintained at 50°C.[4] (Preliminary experiments had shown that annealing at even 60°C for one hour following the bending had no measurable effect on the triplet lifetimes, and it is therefore assumed that no dislocations anneal during the bending.) Ballast was applied to the weight of the solid cylinders in order to supply the critical shear stress necessary for slip. A strain gauge was used to monitor the instantaneous downward force on the crystal. The bending apparatus is shown in Figure 3.2. The bending process was terminated when the strain gauge indicated that the crystal was supporting the full weight of the solid cylinder plus ballast.

D. Condition of the Bent Crystals

The bent crystals were visually clear except for an occasional surface crack which was noticed after bending to 0.71 cm^{-1}, the largest curvature used in the experiment.

Evidence for dislocations was obtained from x-ray diffraction. When an unbent crystal was x-rayed in transmission, the radiograph showed distinct diffraction maxima (see Fig. 3.3a). After the crystal was bent, the diffraction maxima were found to smear (see Fig. 3.3b). Upon annealing the crystal at 443°K for 1 hour the smears divided into a number of distinct images (see Fig. 3.3c). Diffraction characteristics of this type indicate the formation of polygonization boundaries.[5] These boundaries

Fig. 3.3. X-ray transmission radiographs of; (a) an unbent crystal; (b) a crystal after bending; and (c) a bent crystal after annealing for 1 hour at $443^{o}K$.

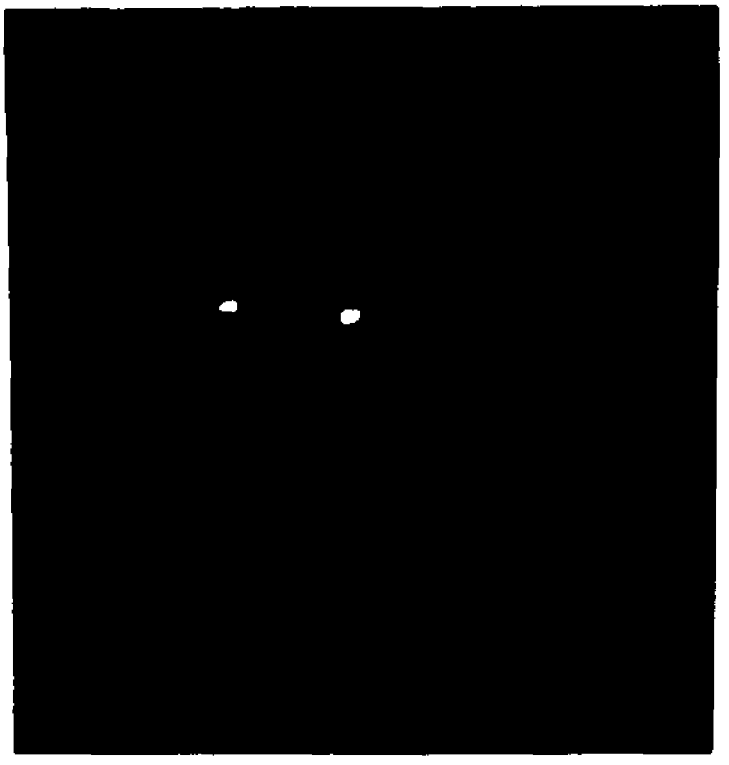

(a)

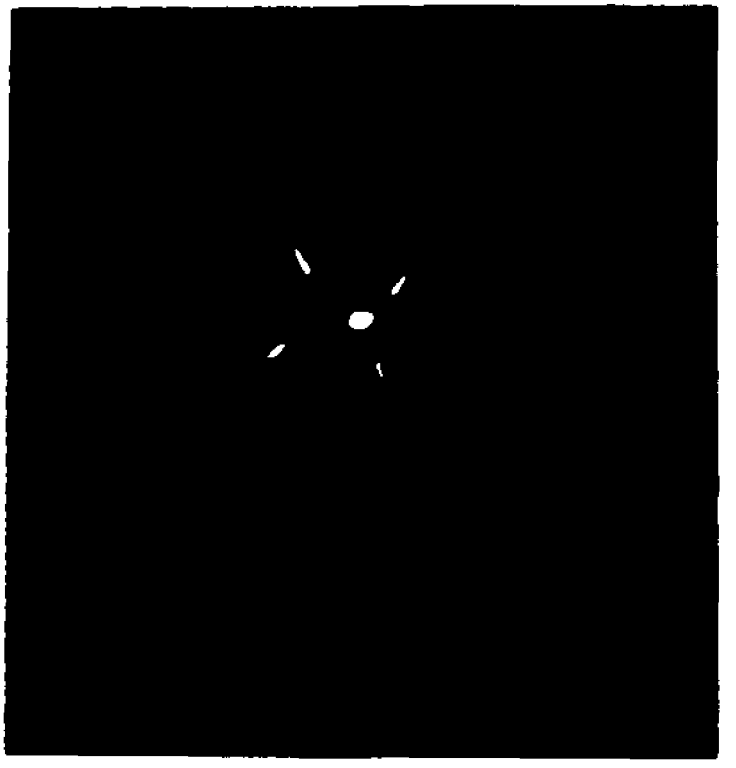

(b)

(c)

are known to be formed when thermally activated dislocations move together and decrease the crystal strain energy by forming small-angle grain boundaries.

E. Apparatus for Trapping Experiment

The trapping experiment involved the measurement of the steady state and transient delayed fluorescence intensity as a function of temperature in the range from 6° to 390° K. These measurements were made before and after the crystal was bent.

The apparatus used in performing the trapping experiment consisted of the following: (1) a liquid helium cryostat; (2) a vacuum and helium gas system; (3) a low temperature crystal holder and temperature controller; (4) a high temperature crystal holder and temperature controller; (5) an optical system; (6) an electrical system for measuring the steady state delayed fluorescence; (7) an electrical system for recording the delayed fluorescence decay (see Fig. 3.4).

(1) Liquid Helium Cryostat

The liquid helium cryostat was manufactured by the Janis Research Company, Inc. The cryostat was designed to operate in the range from 4° to 300° K. It consisted of an outer Dewar which contained liquid nitrogen, a Dewar which contained liquid helium, and a chamber in which the sample was cooled. The sample chamber was accessible to light through quartz windows. A diagram of the cryostat is shown in Figure 3.5.

The cooling process was accomplished in three steps. In the first step both the liquid nitrogen and liquid helium Dewars were filled with liquid nitrogen and the sample cooled down to

1. Liquid helium cryostat

2. Helium gas system

3. Low temperature controller

4. High temperature controller

5. Optical system

6. Electrical system for measuring the steady state delayed fluorescence

7. Electrical system for recording the delayed fluorescence decay

Fig. 3.4. Apparatus for trapping experiment

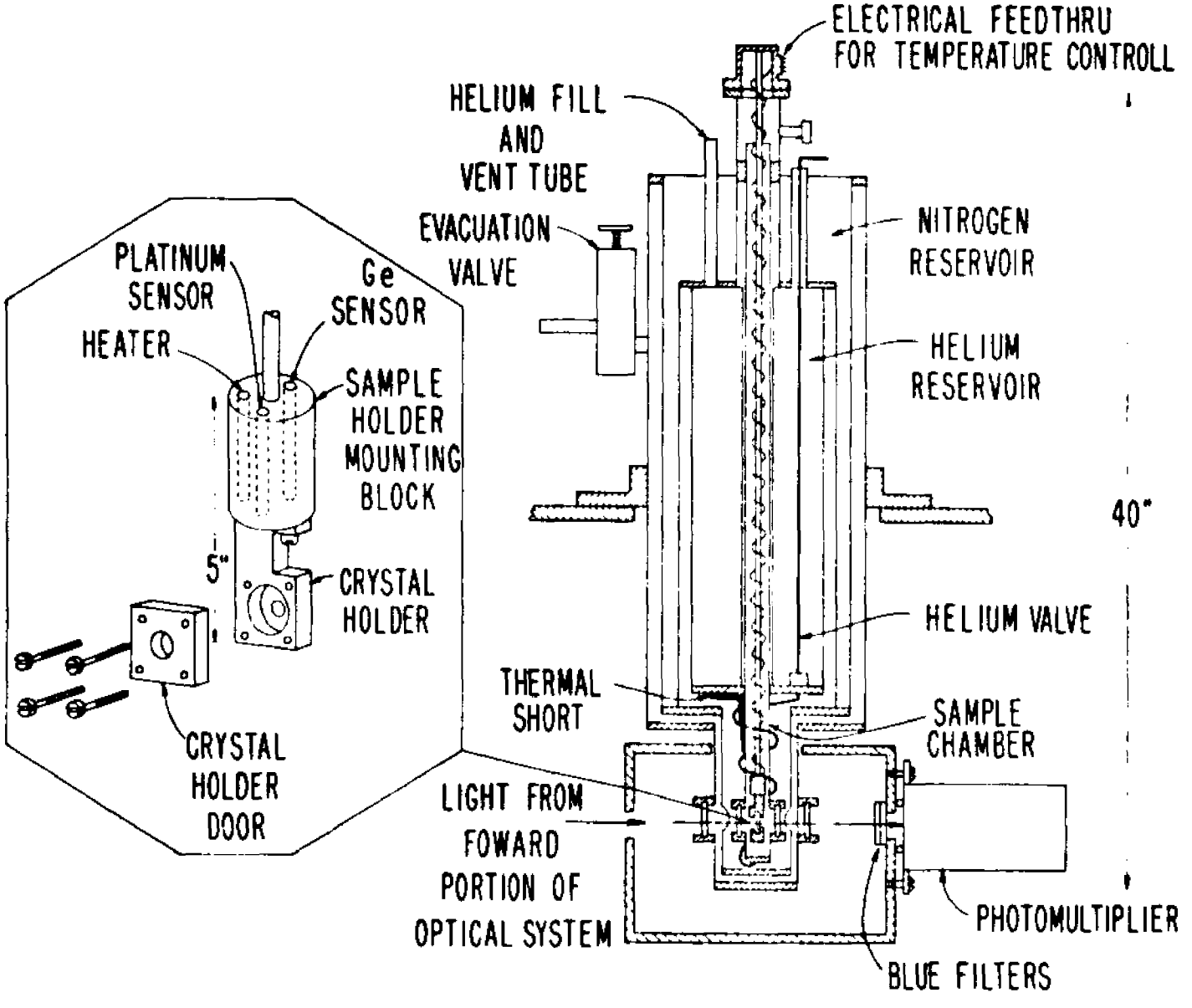

Fig.3.5. Cryostat and low temperature sample holder

90°K in 10 hours. To aid in this precooling, a thermal short was constructed between the bottom of the helium Dewar and the sample chamber (see Fig. 3.5). In the second step liquid helium was substituted for the liquid nitrogen in the helium Dewar and the sample was further cooled to 15°K in about 2 hours. At this point the sample chamber was partially evacuated and liquid helium was allowed to flow in by opening a capillary tube between the helium Dewar and the sample chamber. When the sample was immersed in the liquid helium, the vacuum line was closed and measurements were made as the sample began to warm up.

(2) Vacuum and Helium Gas System

In order to preserve the liquid nitrogen and liquid helium in the cryostat a vacuum system was used which consisted of a cold trap followed by a diffusion pump and a forepump (see Fig. 3.6a). With this system the cryostat was pumped down to a pressure of 1 micron before adding the liquid helium.

To assure frost-free operation of the sample chamber it was pressurized with helium at 1 atmosphere before the cryostat was cooled. This was accomplished by pumping the sample chamber down to 50 microns, closing the vacuum line and then pressurizing the sample chamber with helium (see Fig. 3.6b).

(3) Low Temperature Crystal Holder and Temperature Controller

The low temperature crystal holder consisted of a copper bar with a cavity drilled in it, and a copper door (see Fig. 3.5) The cavity and door had holes drilled through them so that the ab plane of the crystal could be illuminated from one side, while the delayed fluorescence was viewed by a photomultiplier from the

Fig.3.6. Block diagram of: (a) the cryostat vacuum system; and (b) the helium gas system.

(a)

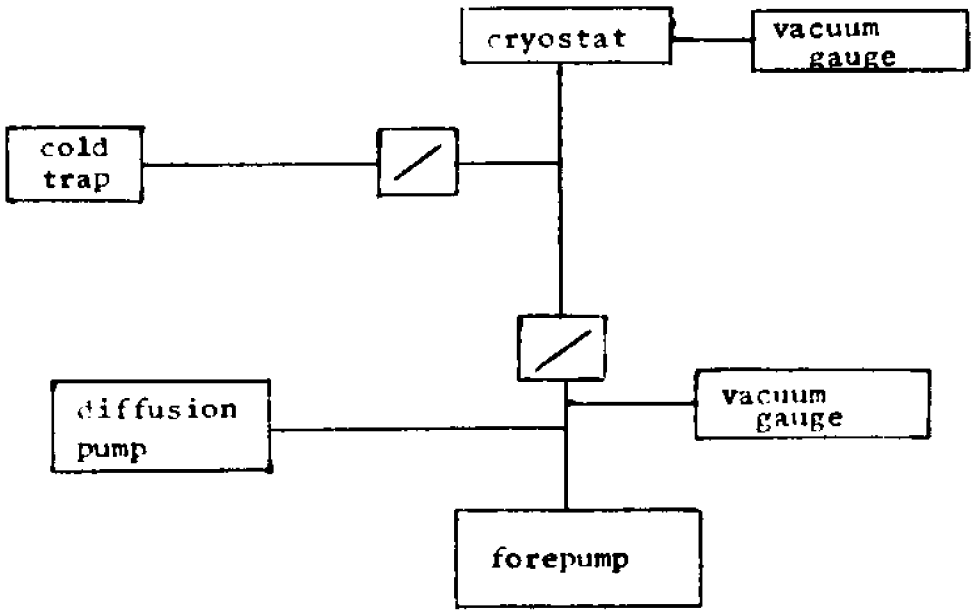

(b)

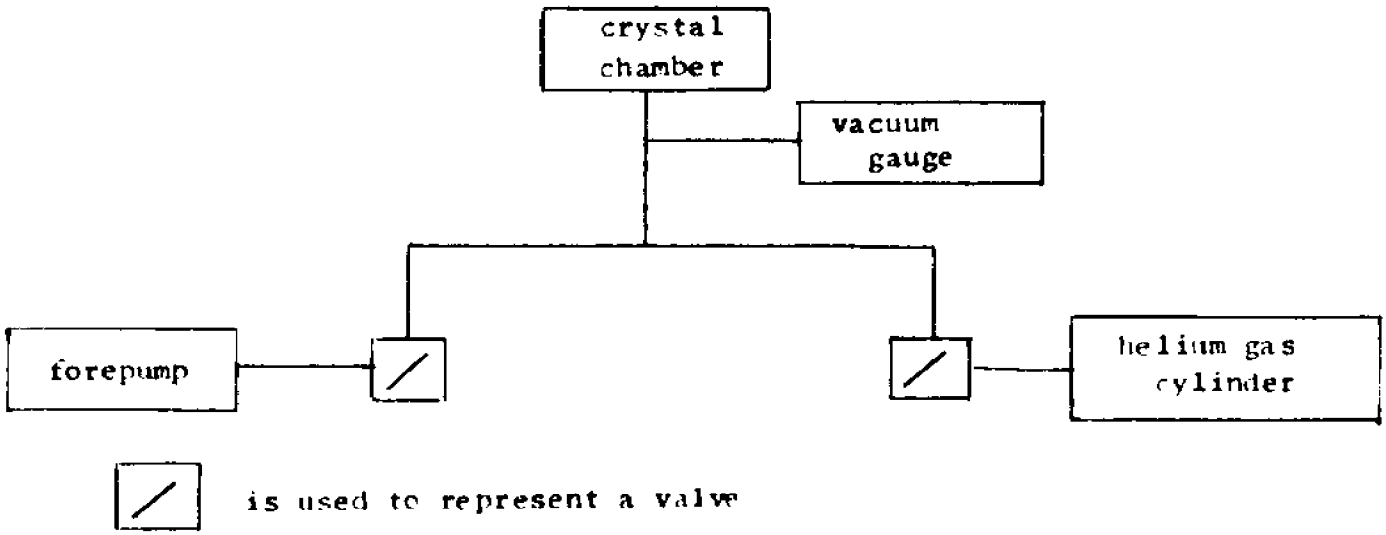

is used to represent a valve

other. The crystal was held in place with General Electric RTV Silicone Rubber.

The crystal holder was bolted to a mounting block which was provided with the cryostat. The mounting block consisted of a solid copper cylinder implanted with a germanium temperature sensor, a platinum temperature sensor and a 15 Ω heater (see Fig. 3.5). The mounting block was suspended from a three foot long stainless steel tube which was anchored to a cap at the top of the cryostat (see Fig. 3.5). An electrical "feed-thru" mounted on the cap provided access to the sensors and heater in the mounting block.

The temperature of the mounting block was controlled with a Cryogenics Research Model TC-103 temperature controller. The controller operated in the following manner. When a desired temperature sensor resistance was dialed into the controller the difference between the real and desired sensor resistance established an off balance current in an AC bridge. This off balance current was amplified and used to drive a heater power supply in the proper direction to bring the sensor resistance to a desired value. The germanium sensor was used from 6° to 15°K, and the platinum sensor was used from 15° to 300°K.

(4) <u>High Temperature Sample Holder and Temperature Controller</u>

The high temperature sample holder consisted of a brass cylinder, two quartz windows, two brass flanges, two copper-constantan thermocouples, a nichrome heater winding, and a helium gas inlet pipe (see Fig. 3.7). This sample holder was used to make delayed fluorescence measurements between 300°K and 390°K.

Since anthracene easily oxidizes on the surface at these temperatures, the sample was kept in a 1 atmosphere helium environment. This was accomplished by attaching the helium gas pipe (see Fig. 3.7) to the helium gas system (see Fig. 3.6).

The temperature of a sample was controlled by connecting thermocouple A and the heater (see Fig. 3.7) to an automatic temperature controller (West Instrument Corp., Model JP). The sample temperature was measured from thermocouple B with a calibrated Hewlett Packard strip chart recorder.

(5) Optical System

The optical system is shown schematically in Figure 3.8. The purpose of this system was to directly generate only triplet excitons, and to observe the delayed fluorescence which results. A 1000 W xenon lamp was used as the source. Since the triplet levels absorb light at wavelengths less than 7000 Å,[6] while the singlet levels absorb below 4000 Å,[7] the low wavelength portion of the xenon spectrum was eliminated. This was accomplished by using the CS 3-67 and CS 3-68 filter combination which acts as a long wavelength pass filter with a cut-off at 5240 Å. The delayed fluorescence emitted by the crystal is composed of wavelengths greater than 4000 Å. In order to keep from detecting the incident light, a 3400 Å to 5000 Å band-pass filter combination (CS 4-72 and CS 5-58) was used before the photomultiplier. This band-pass combination also passes light above 14,000 Å where the xenon source is active. To eliminate this infrared a $CuSO_4$ filter was placed before the xenon source. It was found that 2 cm of a 0.31 molal solution was enough to eliminate

Fig. 3.7. High temperature sample holder

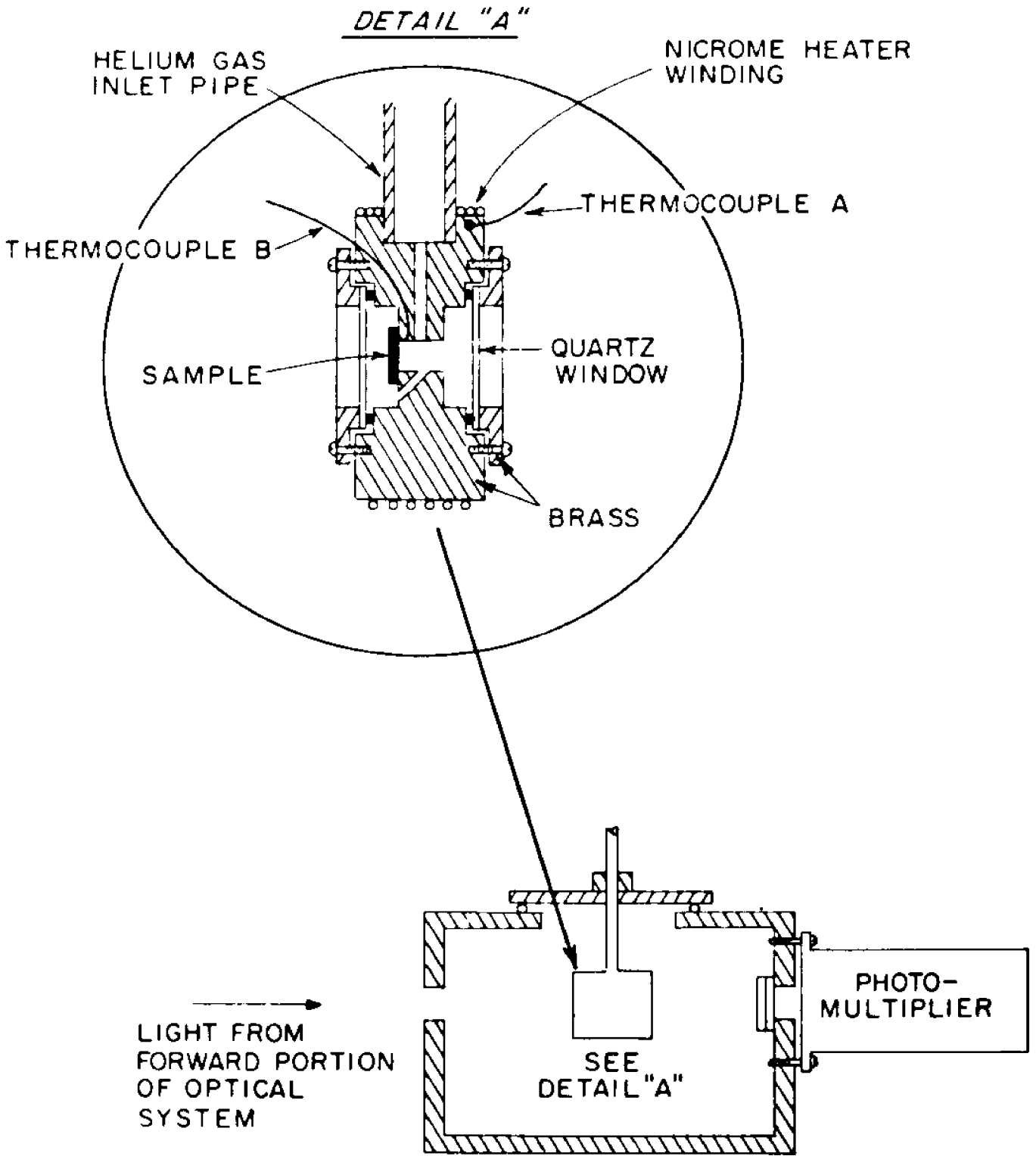

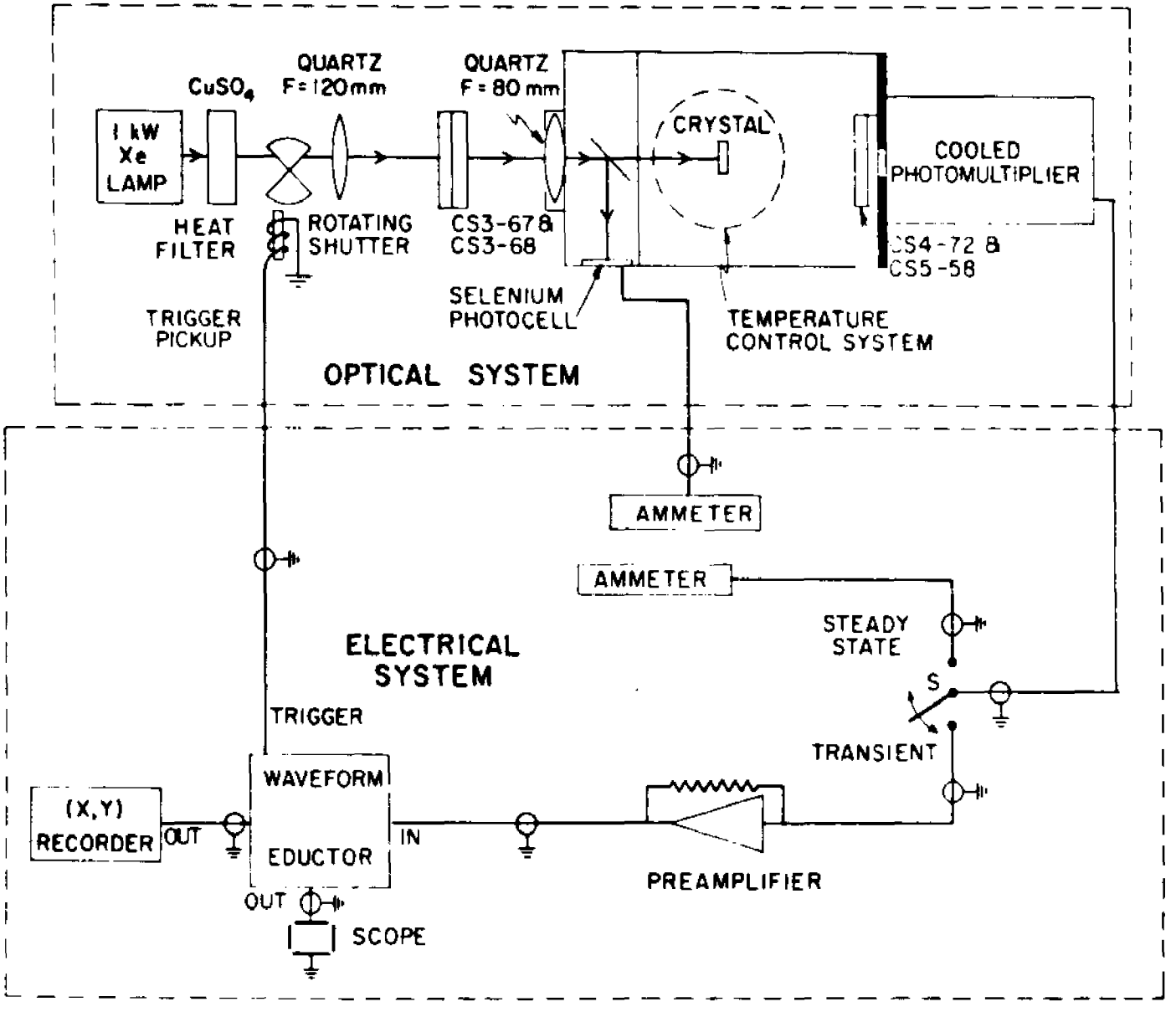

Fig. 3.8. Electrical and optical systems for the trapping experiment

all the detectable infrared.

To guarantee that only triplet excitons were being generated directly, and that the triplet density was small (see chapter 2, section B) the steady-state fluorescence was tested for its quadratic nature. This was done by cutting down the incident intensity by a factor of two with a neutral density filter and observing that the fluorescence decreased by a factor of four.

(6) Electrical System for Measuring the Steady-State Delayed Fluorescence

The electrical system used in the trapping experiment is shown in Figure 3.8. In order to measure the steady-state fluorescence intensity the rotating shutter was held open and switch S was turned to its steady state position (see Fig. 3.8). In this position the current from the EMI 9558 photomultiplier was measured with an ammeter. The shutter was then closed and the photomultiplier dark current recorded. To improve the signal to noise ratio and to maintain constant photocathode sensitivity, the photomultiplier was cooled to 0°C, within ± 0.25°C, by a temperature stabilized tube chamber (Products for Research Inc. Model TE-102 TS).

The incident intensity was monitored and held at 4.5 milliwatts/cm^2 within ±2%. The monitoring was accomplished by using a quartz beam splitter to reflect a portion of the incident intensity onto a selenium photocell (see Fig. 3.8). The current from the photocell was measured by an ammeter which was calibrated in intensity units with a thermopile.

(7) Electrical System for Recording the Delayed Fluorescence Decay

When the incident intensity is cut off, the delayed fluorescence of the crystal decays. If this decay is viewed directly from the photomultiplier, it is found to be very noisy. To get an accurate number for the decay rate many pictures would have to be analyzed. To eliminate this task a PAR Waveform Eductor was used to average out the random noise. The PAR Waveform Eductor is a storage bank containing one hundred RC circuits. When a trigger signal is fed to the Eductor it begins to sweep across the one hundred RC circuits in a desired time and places whatever information is found at its input in the individual capacitors. The process is repeated as many times as there are trigger signals. Signals which occur with the same frequency as the trigger signal will be integrated to their value, while signals which occur in a random relation to the trigger signal will be integrated to zero.

In order to provide repetitive decays for the Eductor, the rotating shutter shown in Figure 3.9 was constructed. The shutter consisted of a 200 rpm syncronous motor, an iron shutter blade, and an induction coil trigger pickup. The position of the shutter is shown in Figure 3.8. Each time the shutter closed a positive pulse from the induction coil triggered the Eductor to sweep across its memory for 30 milliseconds. By turning switch S to the transient position (see Fig. 3.8) the repetitive decays were syncronously stored. The memory of the Eductor was continuously monitored by an oscilloscope. When the memory became sta-

Fig.3.9. Rotating shutter

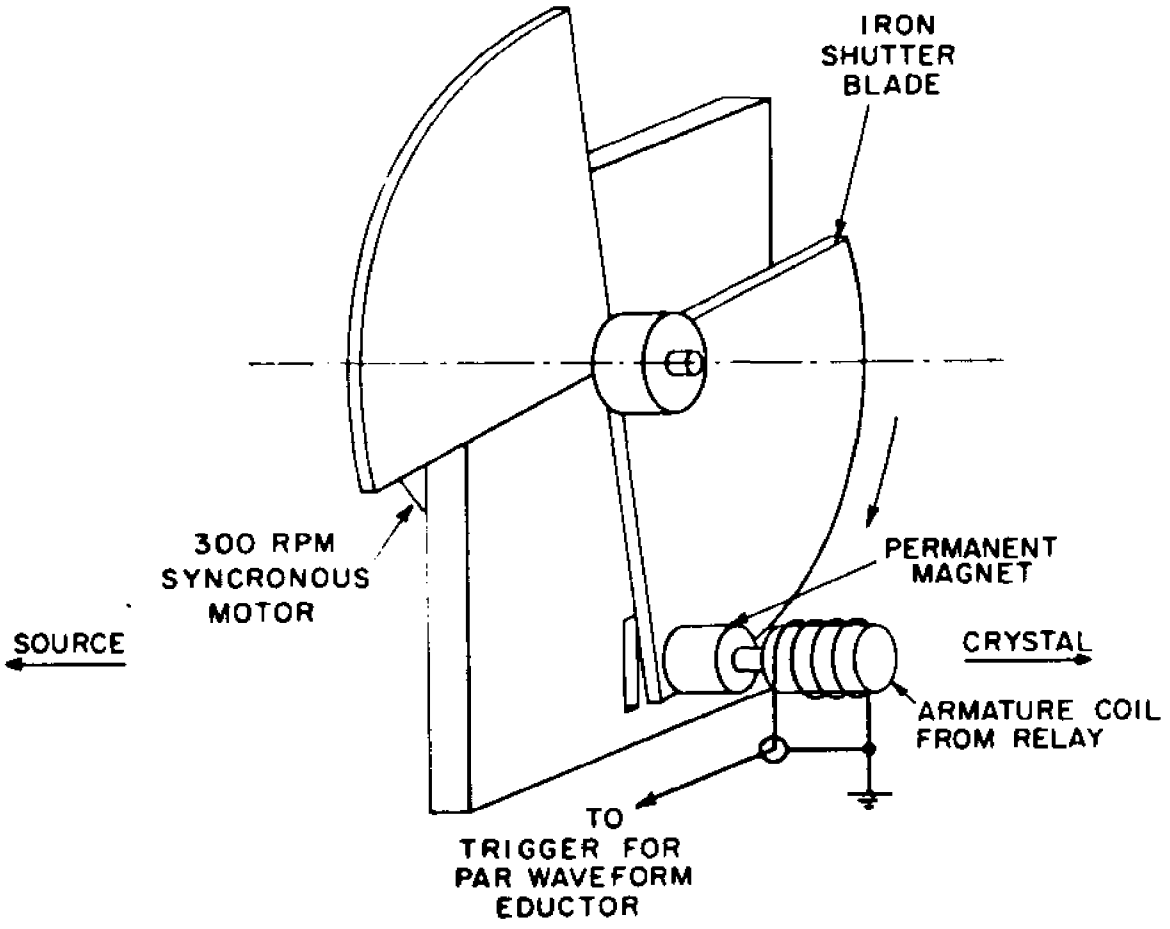

tionary, it was read out on an X-Y recorder. The shutter was then fixed in the closed position and the dark current of the photomultiplier was recorded by triggering the Eductor internally.

References - Chapter 3

1. A.I. Korn, Thesis, City University of New York, 1969.

2. N.T. Corke, A.A. Kawada, and J.N. Sherwood, Nature 213, 62 (1967).

3. I. Nakada, J. Phys. Soc. of Japan 17, 113 (1962).

4. P.M. Robinson and H.G. Scott, Acta Metall. 15, 1581 (1967).

5. A.H. Cottrell, Dislocations and Plastic Flow in Crystals, Oxford Press (London), 1953.

6. P. Avakian, E. Abramson, R.G. Kepler, and J.C. Caris, J. Chem. Phys. 39, 1127 (1963).

7. A.V. Bree and L.E. Lyons, J. Chem. Soc., 5206 (1960).

CHAPTER 4

Results and Discussion of Trapping Experiment

A. Calculation of the Triplet Decay Rate from the Delayed Fluorescence Decay Data

An example of the fluorescence decay data after the subtraction of the dark current is shown in Figure 4.1a. Each channel of the Eductor is represented by a single step in this data. Because the shutter took about 1.5 milliseconds to close, data from the first 2 milliseconds of the decay was not used in the calculation of β, the triplet decay rate. The natural logarithm of the delayed fluorescence following the complete closure of the shutter is shown in Figure 4.1b. The points in this figure correspond to the channels of the Eductor. From the definition of β given in equation 2.36, $I_f = I_{f_o} e^{-2\beta t}$, the slope of the straight line through the points in Figure 4.1b is -2β. To improve the accuracy of the calculated triplet decay rate, the straight line was fitted by the method of least squares.

B. Results

The measured delayed fluorescence vs. temperature spectrum in the region from 6° to 273°K for an anthracene crystal before and after bending to a radius of curvature of 1.4 cm is shown in Figure 4.2. The data for the unbent crystal indicate maxima in the fluorescence intensity at 10°, 45° and 175°K. In the bent crystal these maxima are still present, although displaced downward, and, in addition, the shape is quite different

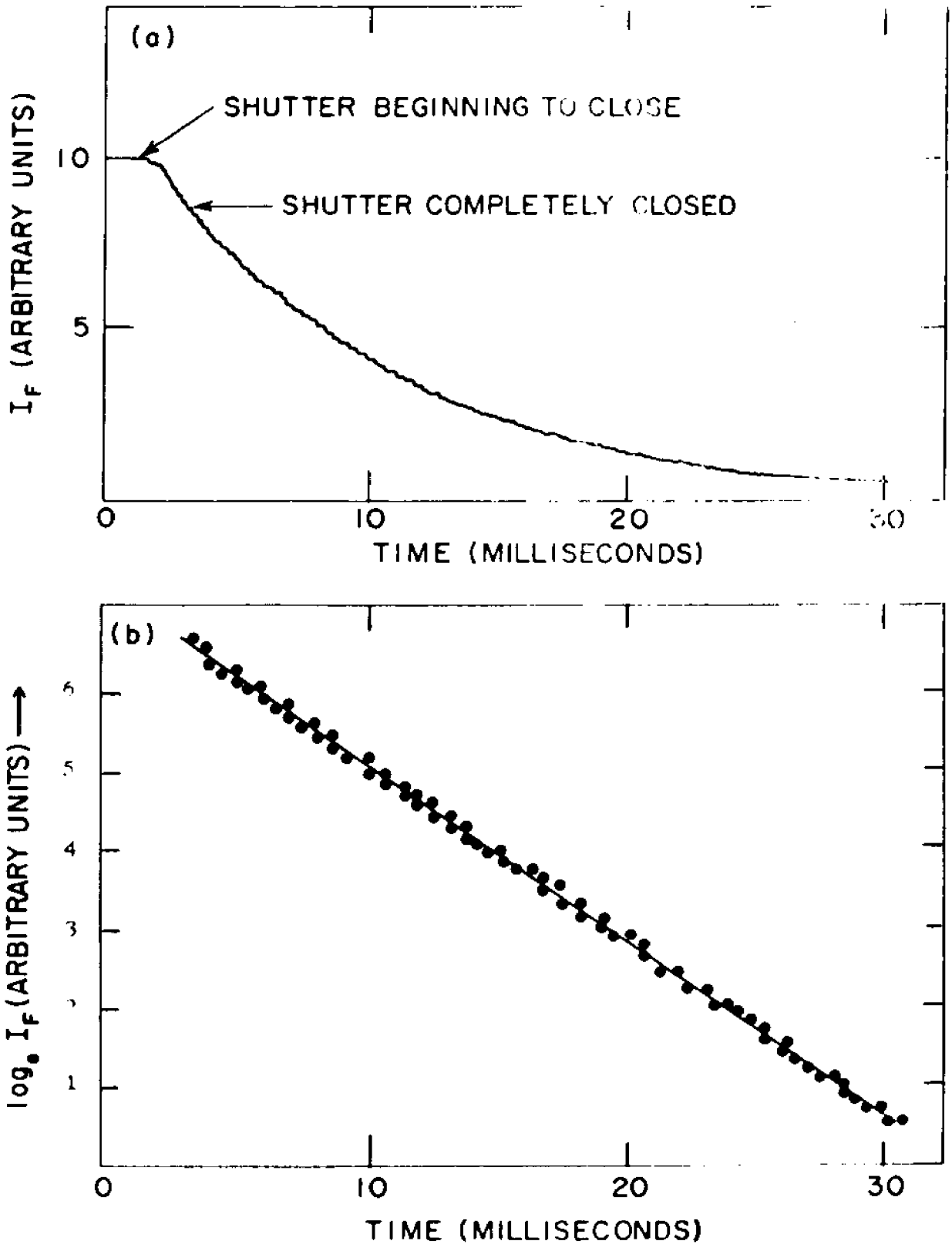

Fig. 4.1. (a) Typical exponential delayed fluorescence decay data; and (b) Evaluation of the triplet lecay constant from fluorescence decay data.

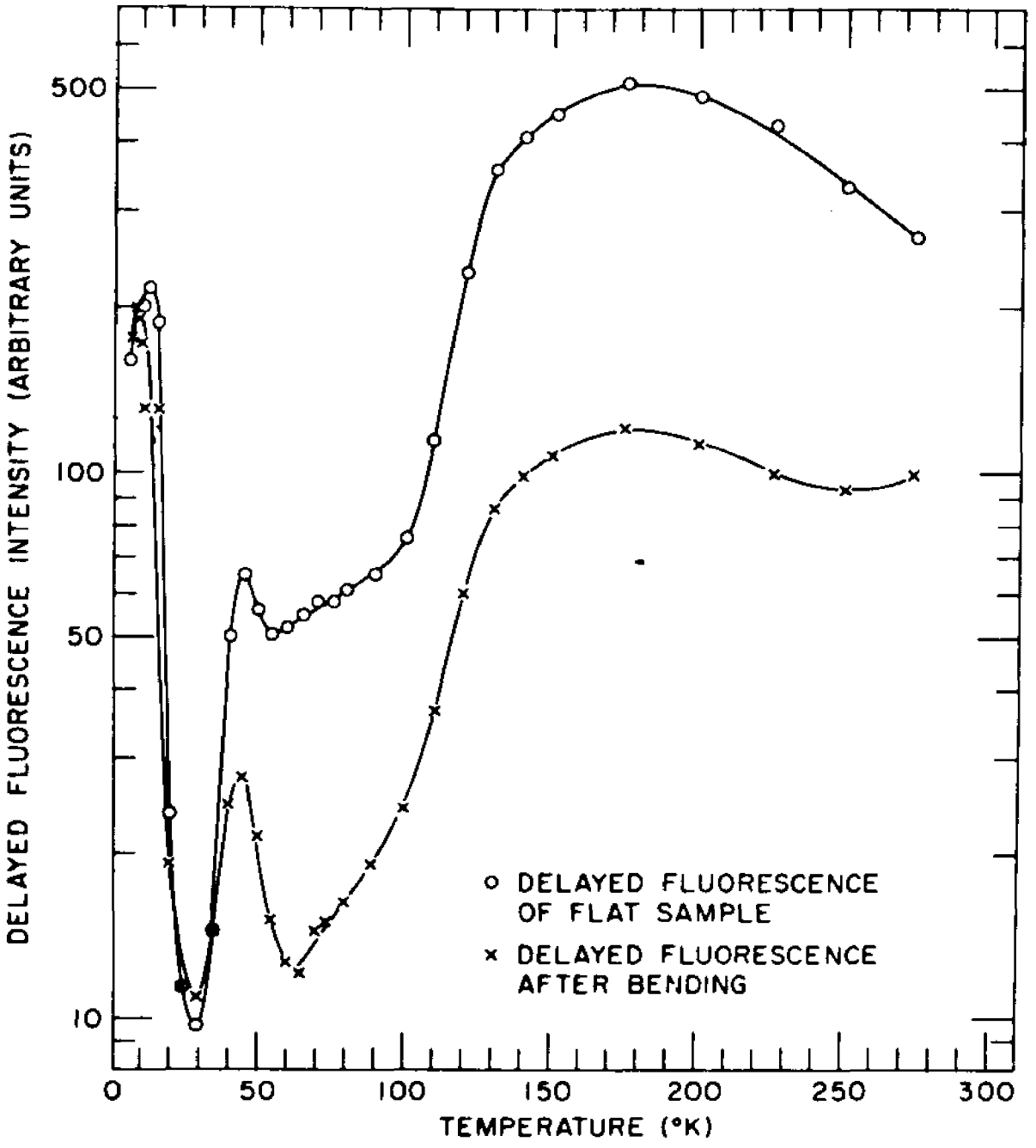

Fig. 4.2. Delayed fluorescence intensity versus temperature in the region from 6° to 273°K for a crystal before and after bending to a 1.4 cm radius of curvature.

between 230° and 290°K. The results of similar measurements in the region from 90° to 390°K are shown in Figure 4.3, as well as the triplet decay constant data. The coincidence of the data for both the flat and the bent condition of the crystal at 390°K is not a result of an annealing process; repeated measurements made on the same sample gave the same temperature characteristics of fluorescence and triplet decay constant. A recovery of the original values of the fluorescence and triplet decay constant can be obtained by annealing a bent crystal for one hour at 443°K.

The maximum in the delayed fluorescence of the undeformed crystal at 175°K has been shown by Siebrand[1] to be due to temperature dependent reabsorption, which is in no way related to triplet exciton trapping. If this reabsorption were not present and if we assume that there are no traps effective in the undeformed sample above 200°K, as we will discuss later, the delayed fluorescence should be independent of temperature above this point. Since the delayed fluorescence of the bent crystal recovers asymptotically to its unbent value above 250°K, the maximum in the delayed fluorescence of the bent crystal at 315°K, as shown in Figure 4.3, is clearly not due to traps introduced by the bending; this maximum is probably caused by temperature dependent reabsorption.

The delayed fluorescence shows evidence of at least two simultaneous decay processes occuring in the range of 6°-50°K. An example of this at 15°K is shown in Figure 4.4. From 50°K to 390°K there was little evidence of more than one decay proc-

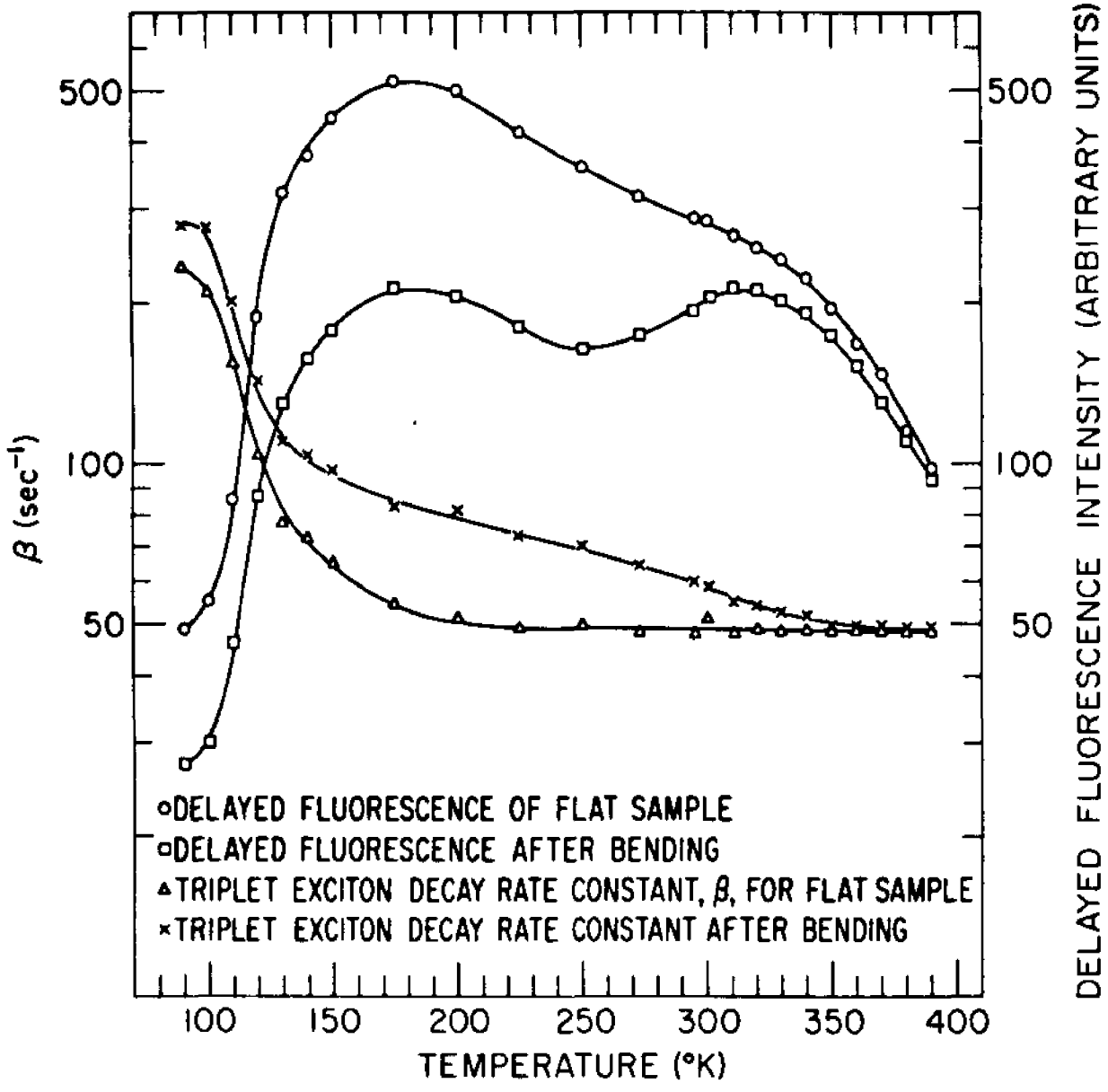

Fig. 4.3. Delayed fluorescence intensity and triplet decay rate in the region from 90° to 390°K for a crystal before and after bending to a 1.4 cm radius of curvature.

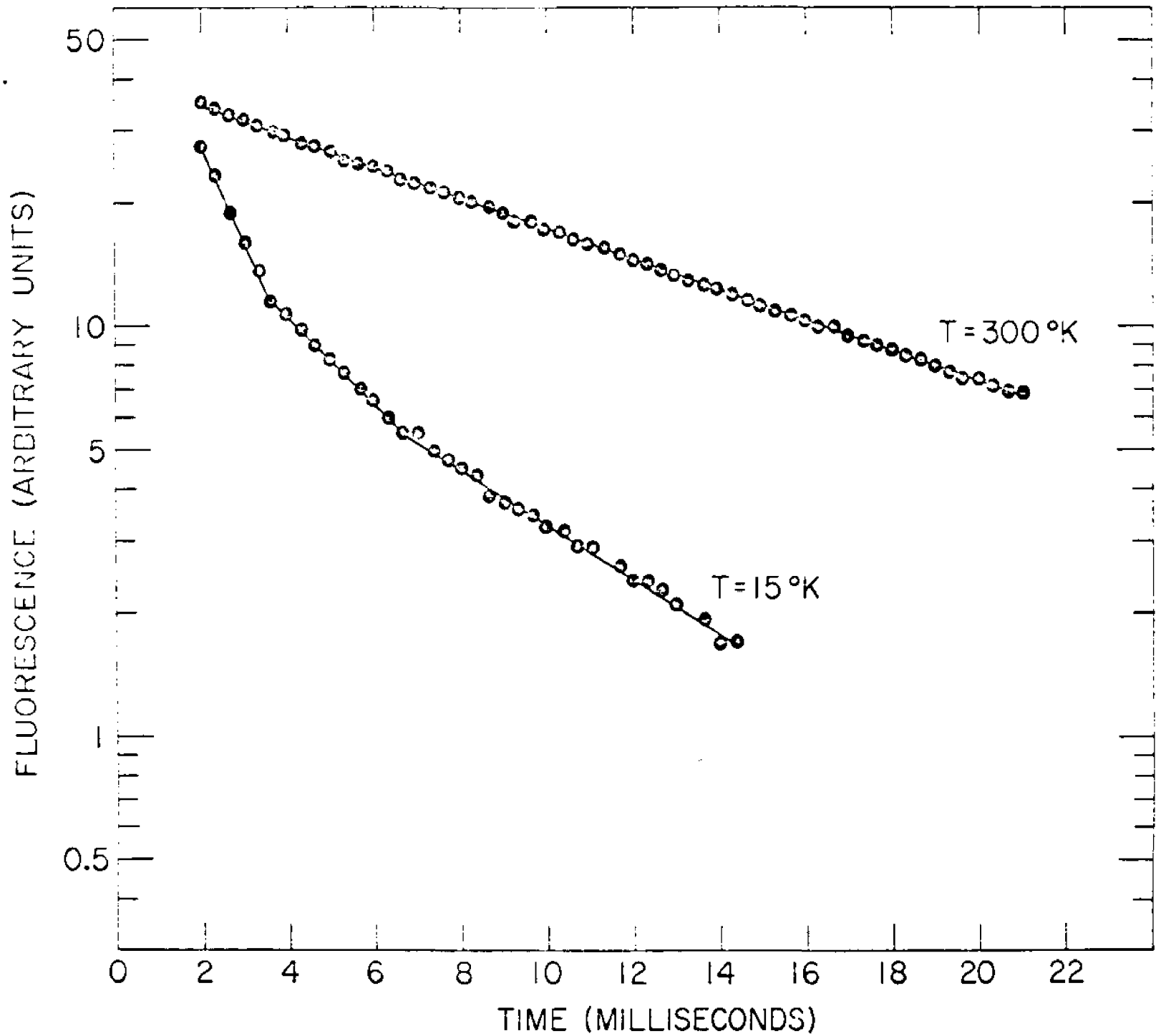

Fig. 4.4. Delayed fluorescence decay data at 15°K and 300°K.

ess, as illustrated by the 300°K curve of Figure 4.4. A qualitative explanation of the decay process is given in the appendix to this chapter.

If dislocations are the trapping centers which cause the increase in the triplet decay constant of the bent crystal with respect to the unbent one at room temperature, it is expected that this increase should be proportional to dislocation density. Since the dislocation density is proportional to crystal curvature, the increase in triplet decay constant should be proportional to this curvature. Triplet decay constants obtained at room temperature from a crystal bent to different curvatures are shown in Figure 4.5. These data were found to be reproducible in different crystals and verify the proportionality of triplet decay constant to curvature for small curvatures. The deviation of the data point at 0.7 cm^{-1} from linearity can be explained as follows. At large curvatures some dislocations will have formed small-angle grain boundaries so that they no longer individually act as traps, i.e., the grain boundary does not act with the same trapping efficiency as would the dislocations within it were they dispersed through the crystal. These small angle grain boundaries are visible to the unaided eye in crystals bent to curvatures of 0.7 cm^{-1} or above (see chapter 3, section D).

The formation of polygonization boundaries in a bent crystal by annealing it at 443°K for one hour (see chapter 3, section D), and the recovery of the triplet lifetime for this time and temperature gives added evidence that dislocations are the defects responsible for the trapping of the triplet excitons.

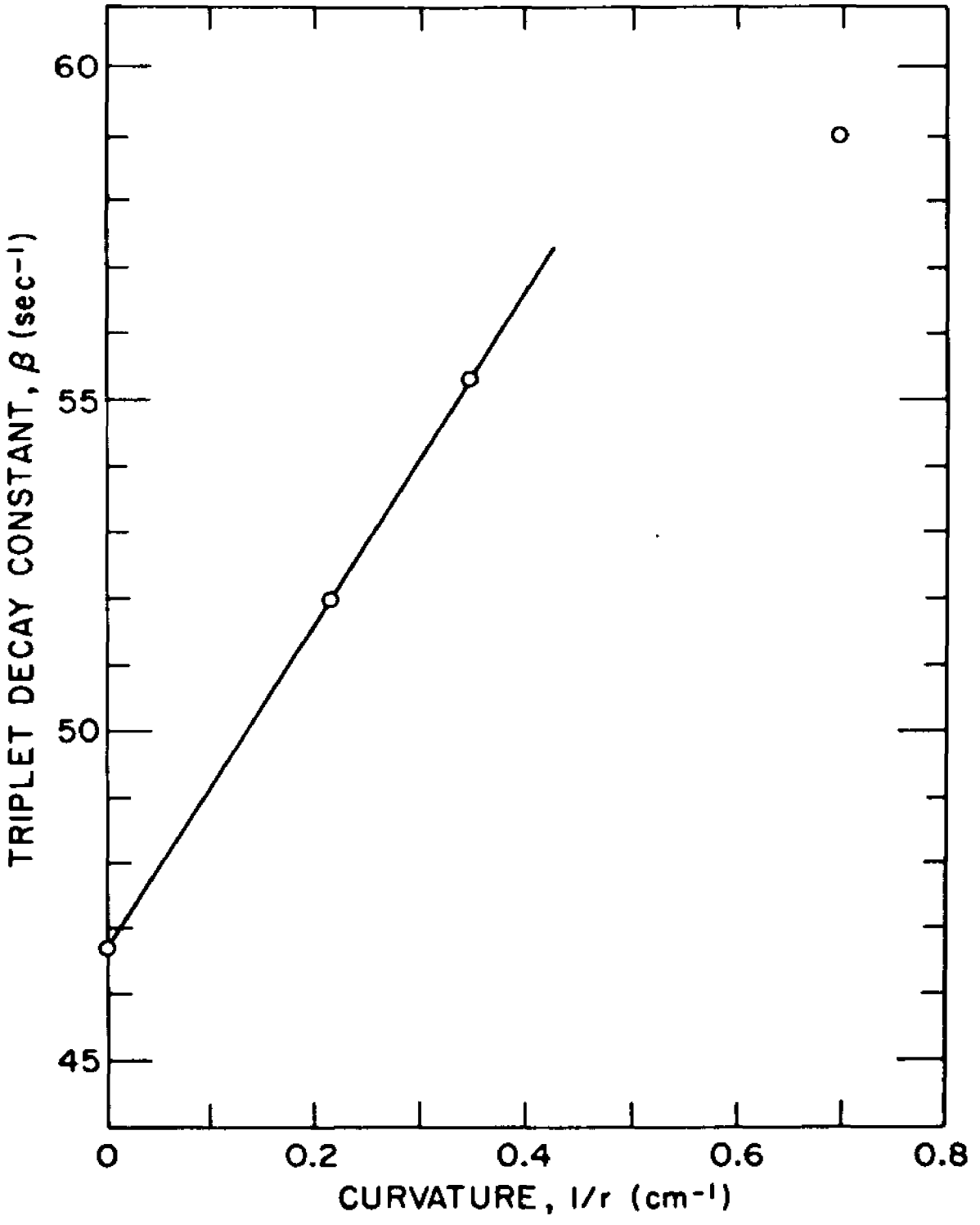

FIGURE 4.5

Triplet decay constant, β, versus curvature

The density of dislocations produced by plastic deformation can be obtained by calculation from equation 1.1, N=1/rb, with the Burgers vector taken to be the b lattice parameter, 6.04 Å,[2] or directly by etch pit counting. Unfortunately, it was not possible to obtain an etch pit count for the bc plane of a deformed specimen. However, clearly resolved etch pits could be observed in the ab cleavage plane (see chapter 3, section A). Good correspondence was shown between the change in triplet lifetime and estimates of dislocation densities by the following experiment. An unbent anthracene crystal suspected of having a large number of dislocations was etched in the ab plane, and the etch pit count was found to be 2×10^6 cm^{-2}. If the dislocations are randomly distributed this count indicates a dislocation density of 4×10^6.[3] This crystal showed a decrease in decay constant from 300°K to 380°K of 7 sec^{-1}. For the bent crystal of Figure 4.3 this number is 11 sec^{-1}. The calculated dislocation density for an anthracene crystal bent to a radius of 1.4 cm is 11.6×10^6 cm^{-2}. One may now show a correspondence in these two samples of the change in decay constant per unit dislocation density in going from 300° to 380°K. This ratio for the etched crystal is 0.57×10^6 cm^{-2}-sec and for the bent crystal is 1.1×10^6 cm^{-2}-sec, which shows agreement within a factor of two.

A measurement was made to see if there is a strain rate dependence of trapping center production. A crystal was bent at eight times the normal rate, but no change in the decay constant within the reproducibility of the experiment was observed. This indicates that point defects, which may be produced by a velocity

dependent mechanism from moving dislocations, either are not produced in significant quantities or play a negligible role in triplet trapping.

C. Discussion

The temperature dependence of the fluorescence of the unbent crystals (Figures 4.2 and 4.3) is similar to the results of other investigations.[4,5] As mentioned in chapter 1, Siebrand[1] has been able to fit the data of Singh and Lipsett[5] by using a triplet exciton trapping model (see chapter 2) with three trap levels, which will be numbered 1 to 3 in order of increasing depth. (Note that this is the reverse of Siebrand's numbering system.) In the following discussion it will be shown that the presence of one additional trap can be used to explain the essential differences between the data taken before and after the bending process. These differences are: (1) the reduction of the steady-state fluorescence intensity below 390°K (Figures 4.2 and 4.3); (2) the increase in the decay constant of the transient fluorescence intensity with decreasing temperature below 390°K (Figure 4.3); and (3) the change in shape of the steady-state fluorescence intensity with temperature above 200 K°(Figure 4.3).

The triplet exciton trapping model presented in chapter 2 can now be applied to our results for the temperature dependence of the delayed fluorescence and triplet lifetime in undeformed anthracene. Since no investigator has reported a triplet lifetime above ~23 msec, and since the delayed fluorescence of the unbent crystal in Figure 4.3 shows little evidence of detrapping

above 200°K, it is assumed that no traps are effective in this region for the unbent crystal. Therefore, the change in fluorescence intensity and triplet lifetime above this temperature must be due to traps introduced by the bending. Since the dislocations form the only trapping sites which are effective above 200°K, the trapping in this region will be approximated by a single trap, labeled 4. To obtain the parameters for this trap an assumption must be made about the size of the decay constant of the trapped triplet exciton, β_4. The lack of a maximum in the delayed fluorescence above 200°K, after excluding reabsorption effects, indicates that β_4 must be larger than half the free triplet decay constant, β_o (see chapter 2, section B). To simplify the analysis it will be assumed that β_4 is large enough so that the density of trapped triplets is in steady state during the delayed fluorescence decay. Using this assumption in equation 2.18, one obtains

$$y_4 = \frac{p_4 y}{q_4 + \beta_4} \qquad 4.1$$

Substituting equation 4.1 into equation 2.17, the rate of change of the free triplet density, dy/dt, becomes

$$\frac{dy}{dt} = -\left(\beta_o + \frac{p_4 \beta_4}{q_4 + \beta_4}\right) y \qquad 4.2$$

Since the trapped triplet density, y_4, is proportional to the free triplet density, y, the delayed fluorescence, given by equation 2.20, will decay in the following manner

$$I_f = I_{f_o} e^{-2\left(\beta_o + \frac{p_4 \beta_4}{q_4 + \beta_4}\right)t} \qquad 4.3$$

A comparison of equation 4.3 to equation 2.36, the defining equation for β, shows that

$$\beta = \beta_o + \frac{p_4 \beta_4}{q_4 + \beta_4} \qquad 4.4$$

Equation 4.4 indicates that the triplet density will decay with decay rate β_o at high temperatures, as expected, and that the decay rate should be $\beta_o + p_4$ at low temperatures where q_4 is no longer effective. β_o, as shown in Figure 4.3, is 48 sec^{-1}. A comparison of the delayed fluorescence vs. temperature for a crystal before and after bending indicates that q_4 begins to be effective in depopulating the triplets from trap 4 at about 220°K. At this temperature β is 74 sec^{-1}. Using this number and the value for β_o, p_4 is approximately 26 sec^{-1}. With equation 4.4 in the form

$$\ln\left(\frac{p_4}{\beta - \beta_o} - 1\right) = -\frac{\epsilon_4}{kT} + \ln\left(\frac{q_o}{\beta_4}\right) \qquad 4.5$$

other parameters can be readily determined. Figure 4.6 shows a plot of the left hand side of equation 4.5 vs. 1/kT, above 220°K, for the decay constant data given in Figure 4.3. ϵ_4, the slope of the line in Figure 4.3, is 0.3 ev. $\frac{q_o}{\beta_4}$, the vertical intercept, is 2×10^5. Under conditions of thermal equi-

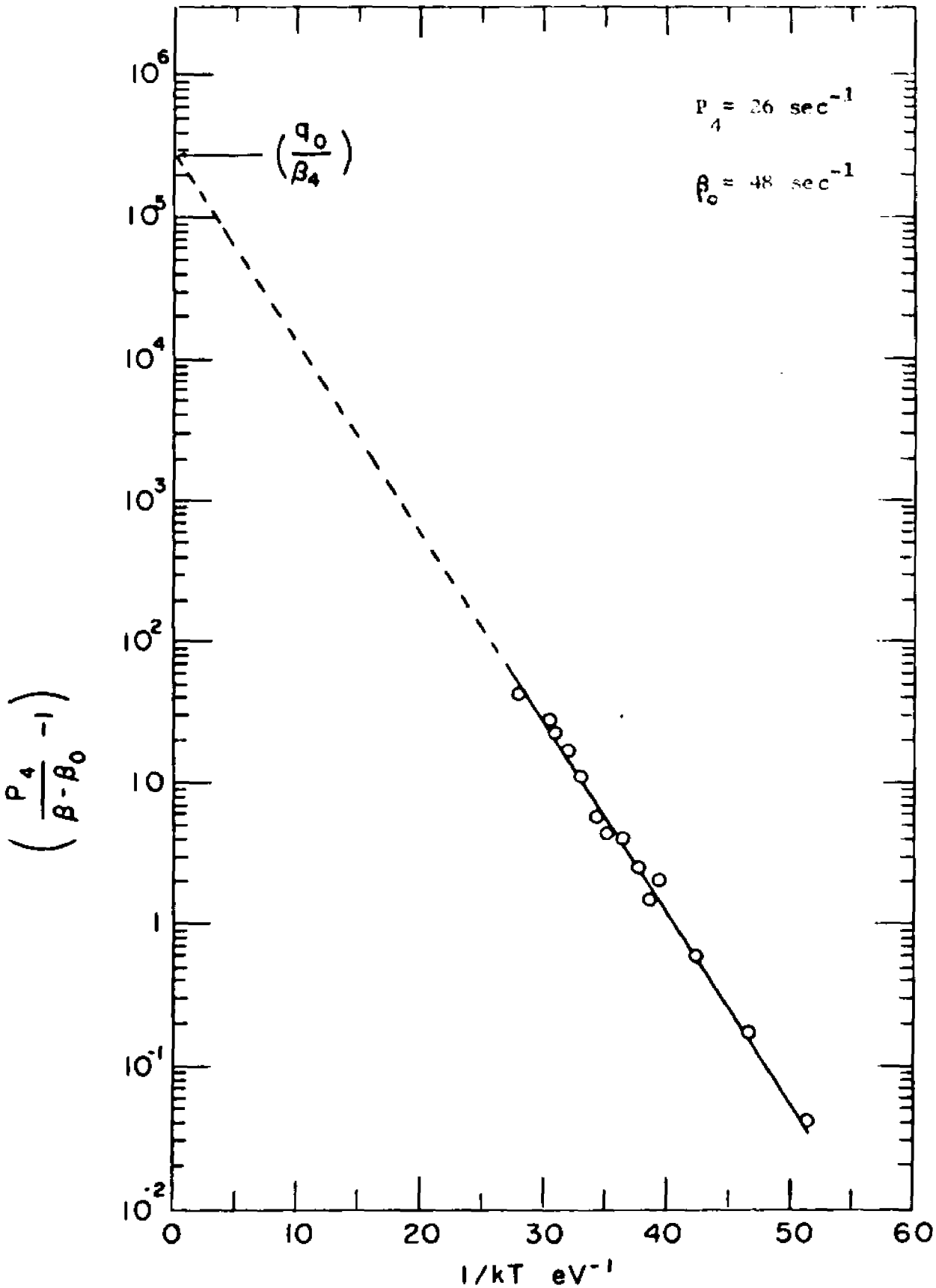

Fig. 4.6. Left hand side of Eqn. 4.5 vs. 1/kT

librium the escape-attempt frequency, q_o, is given by[6]

$$q_o = Z N_c \qquad 4.6$$

where Z is essentially the triplet exciton velocity times the average cross-section of a molecule, and N_c is the density of exciton states available to the escaping exciton. The average triplet exciton velocity in anthracene is 5×10^4 cm/sec,[7] and the average cross-section of an anthracene molecule is 31×10^{-16} cm^2. Using these numbers Z is 2×10^{-10} cm^3/sec. N_c, the density of exciton states is just the density of molecules, which in anthracene is 4×10^{21} cm^{-3}. The escape-attempt frequency from equation 4.6 is 8×10^{11} sec^{-1} and β_4 is 4×10^6 sec^{-1}.

Attempts were made to fit the triplet decay constant data above 200°K by using the general one trap formalism presented in chapter 2. It was found that small values of β_4, $(\beta_4 \simeq \beta_o)$, caused the calculated fluorescence decay to be nonexponential, and intermediate values of β_4, $(\beta_o < \beta_4 < 10^4)$, gave no reasonable agreement with the experimental data. This is added evidence that the assumption of a large β_4 is correct.

Added evidence of the correctness of the parameters obtained for trap 4 from the triplet decay constant data is gained by showing that the steady-state fluorescence data can be fitted by these same parameters. Figure 4.7 shows a plot of the delayed fluorescence data from Figure 4.3 in the region above 200°K. The intensity ratio of the fluorescence of the bent crystal to the fluorescence before bending is plotted because it is independent of crystal reabsorption and other processes not related to

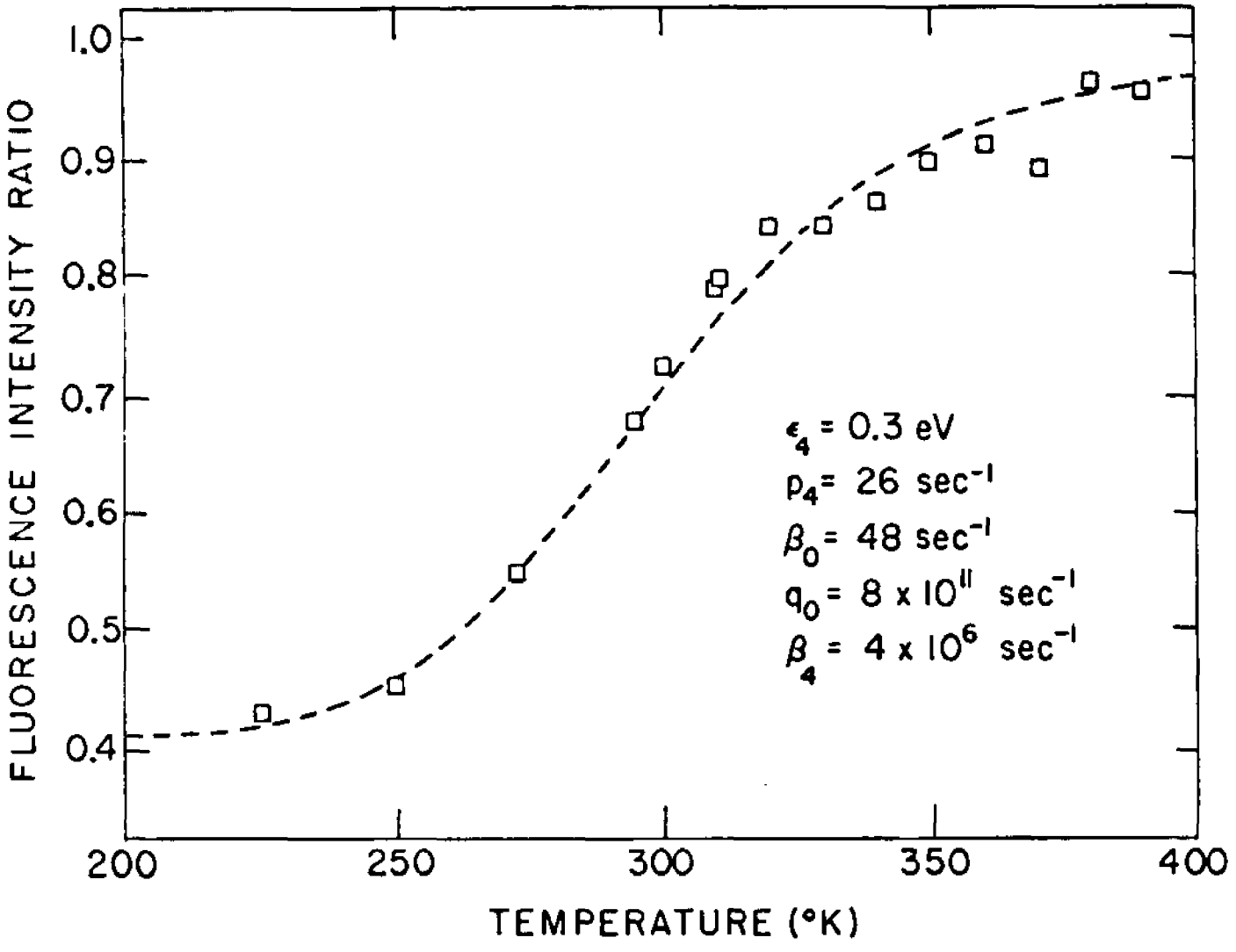

Fig. 4.7. Fluorescence intensity ratio (ratio of the fluorescence intensity of a bent crystal to the fluorescence intensity before bending) versus temperature and theoretical curve (dashed line).

triplet exciton trapping. The dashed line in Figure 4.7 is the theoretical intensity ratio obtained from equation 2.13 using one trap, labeled 4, for the deformed sample and zero traps for the undeformed sample. The parameters used for trap 4 in this figure are identical to those obtained from the triplet decay constant data of the bent sample.

A computer calculation of equation 2.13 for the temperature range 6° to 273°K was obtained by varying the parameters of three different traps to match the experimental curve of an unbent crystal such as that shown in Figure 4.2. The best result, in arbitrary intensity units, is shown by the dashed line in Figure 4.8 and the parameters are given in Table 4.1. These traps have essentially the same depths as those used by Siebrand[1] in matching comparable data of Singh and Lipsett.[5] Comparison of the dashed line of Figure 4.8 with the data for the unbent crystal (Figure 4.2) shows reasonable agreement in the low temperature region up to 110°K. The differences above this temperature are believed to arise from reabsorption of the crystal, whose temperature dependence is unknown, and nonlinear effects which were not included in equation 2.13. A similar calculated curve is shown in Figure 4.8 for the bent crystal in which one additional trap, i=4, was used. If the ratio of the data of the bent to the unbent crystal is used, as mentioned earlier, factors independent of trapping, such as reabsorption, are eliminated. The ratios of both the data and the calculated curves are shown in Figure 4.8. In this latter comparison of theory to experiment good agreement is seen above 100°K. The disagreement

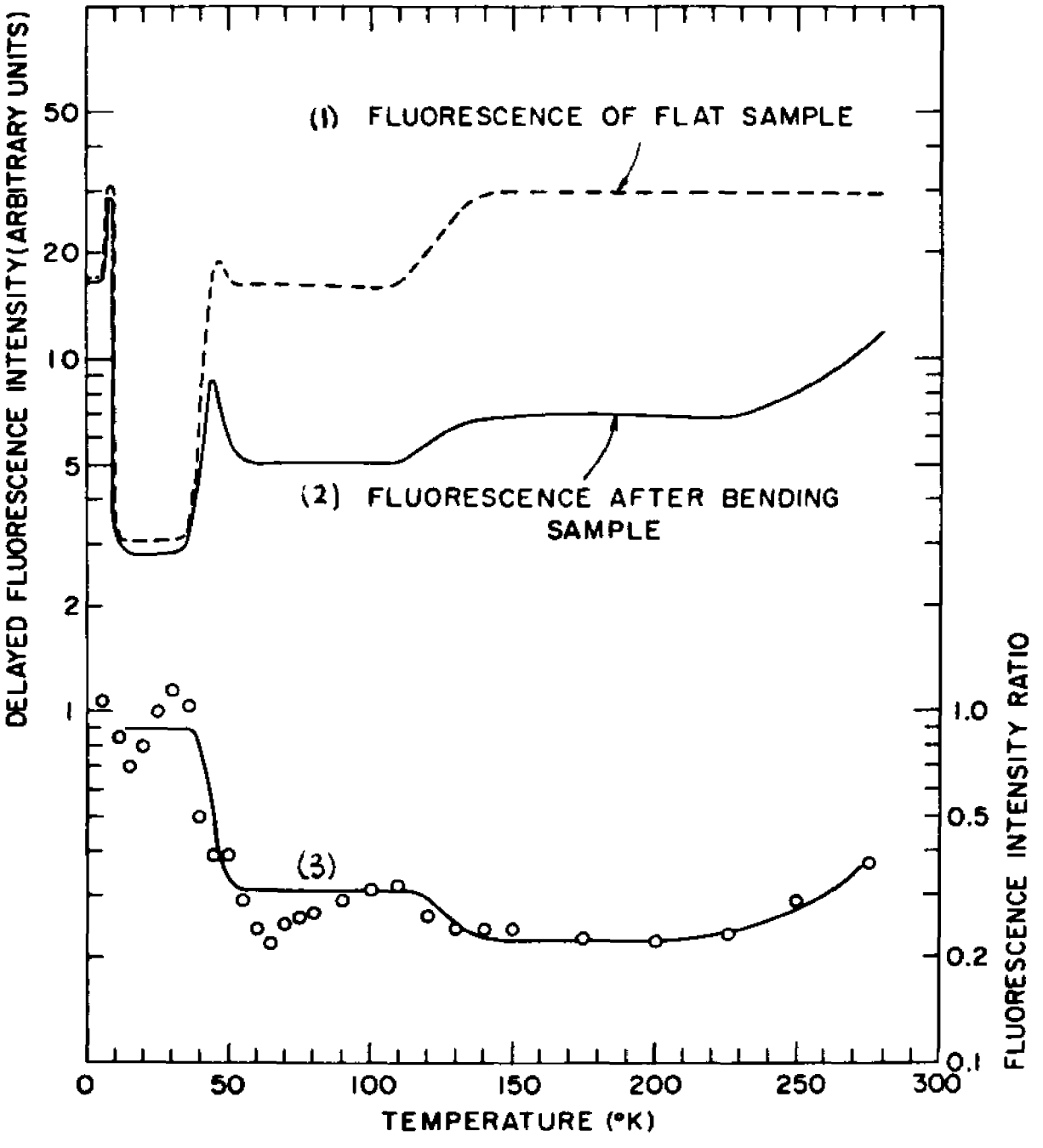

Fig. 4.8. (1) Theoretical curve of the delayed fluorescence vs. temperature for an unbent sample.
(2) Theoretical curve of the delayed fluorescence vs. temperature for a sample after bending.
(3) Ratio of curve (2) to curve (1) with experimental data

in the temperature range of 50° to 90° K arises from the inaccuracy of the experimental data due to small signal to noise ratio at low intensity. The scatter of the data from 15° to 30° K about the theoretical ratio arises from the limited precision of temperature control in this region in which there is such a large change of fluorescence with temperature. The parameters in Table 4.1 are those which gave the best fit to the ratio of the experimental data of Figure 4.2.

Although the data of Figures 4.7 and 4.8 were taken in different crystals, the best fit of the theoretical curves for both requires the same trap depth of 0.3 ev while the trap concentration, which is reflected in p_4, is seen to differ by a factor of two. All the decay constant data taken on crystals above 200° K can be fitted with $p_4=26$ sec^{-1}, while the intensity data in the same temperature region sometimes require a larger p_4 for a best fit. It is believed that this disparity arises because the steady-state intensity and the triplet decay constant are affected differently by inhomogeneities in the dislocation distribution. The effect can be explained by the following argument. The steady-state delayed fluorescence intensity in the region above 200° K, from equation 2.13, is

$$I_f = \frac{1}{2}\gamma\left(\frac{\alpha I}{\beta_0}\right)^2 \frac{\left[1+\frac{p_4}{q_4+\beta_4}\right]}{\left[1+\frac{\beta_4 p_4}{\beta_0(q_4+\beta_4)}\right]^2} \qquad 4.7$$

because trap 4 is the only trap which affects I_f in this region. Since β_4 is much larger than p_4, equation 4.7 can be approximated by

TRAP	4	3	2	1
ϵ_i(ev)	0.3	0.23	.083	.02
$P_i(sec^{-1})$	52	20	100	600
$\beta\ (sec^{-1})$	$4x10^{6}$	240	20	0.5
$N_i = p/Z(cm^{-3})$	$3x10^{11}$	$1x10^{11}$	$5x10^{11}$	$3x10^{12}$

CONSTANT PARAMETERS

*$Z = 2x10^{-10}\ cm^{3}\text{-}sec^{-1}$

$\beta_c = 48\ sec^{-1}$

$\sigma_0 = 8x10^{11}\ sec^{-1}$

TABLE 4.1

Parameters used in curves (1) and (2) of Fig.4.8.

* Z is obtained by multiplying the average physical cross-section of an anthracene molecule by the triplet exciton velocity.

$$I_f = \frac{1}{2} \frac{\gamma (\alpha I)^2}{\beta_0 + \frac{\beta_4 p_4}{q_4 + \beta_4}} \qquad 4.8$$

A comparison of equations 4.8 and 4.4 reveals that the steady state delayed fluorescence should be inversely proportional to the triplet decay constant. Because of this the triplet decay constant seen above 200°K is representative of the area of lowest dislocation content, while the fluorescence, which is inversely proportional to the local triplet decay constant, is suppressed in regions of high dislocation density. Therefore in the case of an inhomogeneous distribution of dislocations, the values of p_4 arrived at from the decay constant and fluorescence data will not be in agreement.

The above analysis has shown that the fluorescence vs. temperature characteristics of a plastically deformed sample can be explained by a single additional trap. The effectiveness of this trap must now be considered. Under the assumption of a diffusion limited trapping process, the rate constant p_4 is $p_4 = v\sigma N_4$, where v is the average triplet exciton velocity and σ is the geometrical cross-section of the trap.+ The calculated dislocation density for an anthracene crystal bent to a radius of 1.4 cm is 1.2×10^7 dislocation per cm^2. If each mole-

+Although dislocations are properly treated as line defects with an effective trapping radius, in the present analysis they are considered to be a chain of point defects for convenience. The two treatments should be equivalent except for a geometrical factor of order unity.

cule along a dislocation line acts as an individual trap, the trap density N_4 will be 1.4×10^{14} traps/cm^3. Using 5×10^4 cm/sec for the average triplet exciton velocity[7] and the average physical cross-section of an anthracene molecule of 31×10^{-16} cm^2, p_4 is 3×10^4 sec^{-1}. The present experimental values of p_4 are three orders of magnitude smaller than the value estimated on the assumption of diffusion-limited trapping.

Since the good agreement in dislocation content between etch pit counts and plastic deformation computations shows that the estimates of dislocation density are reasonable, it appears that the trapping cross-section must be about 3.3×10^{-18} cm^2, a value several orders of magnitude smaller than the geometrical cross-section. Such a small cross-section can mean that there is a small probability of capture of the exciton by the trap upon its encounter. A similar idea of capture probability has been used by Tomura and Takahashi to explain their observation of small singlet exciton trapping cross-sections by impurities in anthracene.[8] Because of the necessity of introducing an effective trap cross-section, calculations of trapping kinetics may be in error without this specific information. The present experiments yield the product of the effective cross-section and the concentration of traps. The concentrations N_i of the traps 1,2, and 3 given in Table 1 were obtained by the assumption of a cross-section of the molecule and are therefore only as valid as this assumption.

APPENDIX

The character of the fluorescence decay at various temperatures, as illustrated in Figure 4.4, can be explained qualitatively with the parameters used to fit the fluorescence intensity, Table 4.1. The triplet decay constant for the deepest trap, β_4, is very large compared to either p_4, its rate constant for trapping, or β_o, the free triplet decay constant (see Figure 4.7 and Table 4.1). Using this information, equation 2.25 reduces to

$$\beta_- \simeq \beta_o + p_4 - \frac{q_4 p_4}{q_4 + \beta_4 - p_4 - \beta_o} \qquad \text{(A1)}$$

and

$$\beta_+ \simeq q_4 + \beta_4 + \frac{q_4 p_4}{q_4 + \beta_4 - p_4 - \beta_o} \qquad \text{(A2)}$$

It is clear from these expressions that at any temperature β_+ is much larger than β_-. As a consequence, the coefficient which predominates above 200°K in equations 2.24 and 2.26 is D_2, and, from equation 2.17, the fluorescence exhibits a single decay given by

$$I_f = \frac{\gamma}{2} D_2^2 e^{-2\beta_- t} \qquad \text{(A3)}$$

Calculations based on equations (A1) and (A3) fit the decay data of Figure 4.3 equally well as does the general expression

(equations 2.20, 2.24, and 2.26) with the same parameters.

The shallower traps cannot be analyzed with a one-trap model; however, a qualitative discussion can be given. The long lifetimes in traps 1 and 2 are responsible for the multiple decay of the fluorescence observed in the region from 6°K to 50°K. To illustrate this, suppose that the crystal is at 8°K. At this temperature, the q_1's for traps 2, 3, and 4 are insignificant compared to their own decay rates and to q_1. As a consequence, traps 2-4 will be totally effective while trap 1 will be partially effective ($q_1 \simeq 0.4\beta_1$). In view of this, equations 2.1 and 2.2 may be approximated by

$$\frac{dy}{dt} = \alpha I + q_1 y_1 - (\beta_0 + p_1 + p_2 + p_3 + p_4) y \qquad \text{(A4)}$$

$$\frac{dy_1}{dt} = p_1 y - (q_1 + \beta_1) y_1 \qquad \text{(A5)}$$

When the shutter closes, all the traps combine their capture rates to quickly deplete the free triplet population. Because of its large capture rate and slow decay rate, trap 1 initially contains over one thousand times the free triplet population. As a consequence, a point is soon reached in the decay process at which the rate of release from trap 1 is equal to the rate of triplet depletion $\left[\text{i.e., } q_1 y_1 = (p_1 + p_2 + p_3 + p_4 + \beta_0) y\right]$. Beyond this point the free triplet population can be considered to be approximately in steady state because the triplets are captured

or decay as fast as they are released by trap 4. With this simplification the solutions to equations (A4) and (A5) indicate that both the free and trapped triplet populations will decay slowly with a rate constant of approximately β_1 . So long as the other trap populations are small in comparison to y_1, the steady-state approximation to equation 2.3, i.e., dx/dt=0, yields

$$I_f \simeq \frac{1}{2} \gamma y \left(y + y_1 \right)$$

Because of the initial fast decay of y followed by the slow decays of y and y_1, the fluorescence will no longer exhibit simple exponential decay. When the temperature of the crystal is above 50°K traps 1 and 2 will not be significantly populated, and, as a consequence, multiple decays will not be observed.

References - Chapter 4

1. W. Siebrand, J. Chem. Phys. 42, 3951 (1965).

2. A. McL. Mathieson, J.M. Robertson, and V.C. Sinclair, Acta Cryst. 3, 245 (1950).

3. G. Schoeck, J. Appl. Phys. 33, 1745 (1962).

4. D.H. Goode and F.R. Lipsett, J. Chem. Phys. 51, 1222 (1969).

5. S. Singh and F.R. Lipsett, J. Chem. Phys. 41, 1163 (1964).

6. R.H.Bube, Photoconductivity of Solids (J. Wiley and Sons Inc. New York, 1960), p.51.

7. P. Avakian, V. Ern, R.E. Merrifield, and A. Suna, Phys. Rev. 165, 974 (1968).

8. M. Tomura and Y. Takahashi, J. Phys. Soc. Japan 26, 1325 (1969).

CHAPTER 5

Theory of Davydov Splitting

In a molecular crystal the binding energy of any one electron to its "own" molecule is much larger than its binding energy to all the other molecules in the crystal. For this reason the crystal may be treated as an aggregate of noninteracting oriented molecules with the intermolecular interaction used as a perturbation. Using this approach it will be shown in this chapter that the presence of several molecules per unit cell causes a characteristic splitting of the absorption bands.

A. Derivation of the Secular Determinant for the Energy of an Excited State

The total Hamiltonian for the lattice is

$$H = \sum_{m\alpha} H_{m\alpha} + \sum_{m\alpha,n\beta}{}' V_{m\alpha,n\beta} \qquad 5.1$$

where $H_{m\alpha}$ is the self energy operator for the molecule in the α place of the m^{th} unit cell and $V_{m\alpha,n\beta}$ is the interaction operator between the $m\alpha$ and the $n\beta$ molecule. The prime on the second summation indicates that each pair of interactions is to be counted once, and all self interactions ($V_{m\alpha,m\alpha}$) are to be excluded.

If the interaction between the molecules is small it may be neglected in the zeroth approximation. In this case the wave function of the normal state of the crystal may be presented in the form of antisymmetrized products of the ground state wave

functions $\phi^{\circ}_{m\alpha}$ of the individual molecules

$$\Phi^{\circ} = a \prod_{m\alpha} \phi^{\circ}_{m\alpha} \qquad 5.2$$

where "a" is the appropriate antisymmetric operator. If one molecule $n\beta$ is excited the state of the crystal is

$$\Phi^{f}_{n\beta} = a \phi^{f}_{n\beta} \prod_{m\alpha \neq n\beta} \phi^{\circ}_{m\alpha} \qquad 5.3$$

where

$$\int \Phi^{f}_{n\beta} \Phi^{f}_{m\alpha} = \delta_{n\beta, m\alpha}$$

Since the molecules are under the influence of the crystal periodicity, a Bloch function should be formed from the $\Phi^{f}_{n\beta}$ wave functions. This function takes the form

$$\psi^{f} = k' \sum_{m\alpha} B_{\alpha} e^{i\underline{k}\cdot\underline{r}_{m}} \Phi^{f}_{m\alpha} \qquad 5.4$$

where k' is a normalization factor.

The secular equations for the energy of an excited state are obtained in the following manner. By operating on the excited state wave function (equation 5.4) with the Hamiltonian (equation 5.1), one obtains

$$\sum_{m\alpha} H_{m\alpha} \psi^{f} + \sum'_{m\alpha, n\beta} V_{m\alpha, n\beta} \psi^{f} = \epsilon^{f} \psi^{f} \qquad 5.5$$

where ϵ^{f} is the energy of the excited state of the crystal. By

multiplying equation 5.5 by $\Phi^{F*}_{p\delta}$ (the excited state of the crystal with only the $p\delta$ molecule excited), rearranging the terms and integrating over all the molecules in the crystal, one may write

$$\sum_{m\alpha} \int \Phi^{F*}_{p\delta} H_{m\alpha} \psi^F dV + \sum'_{m\alpha, n\beta} \int \Phi^{F*}_{p\delta} V_{m\alpha, n\beta} \psi^F dV - \epsilon^F \int \Phi^{F*}_{p\delta} \psi^F dV = 0 \quad 5.6$$

Substituting equation 5.4 for ψ^F and recognizing that $\Phi^{F*}_{p\delta}$ is independent of the summation over $m\alpha$, the first term in equation 5.6 becomes

$$\text{FIRST TERM IN EQN. 5.6} = k' \int \left[\sum_{c\gamma} B_\gamma e^{i\underline{k}\cdot\underline{r}_c} \Phi^{F*}_{p\delta} \sum_{m\alpha} H_{m\alpha} \Phi^F_{c\gamma} \right] dV \quad 5.7$$

Since $\Phi^F_{c\gamma}$ is the sum of permutation products of the molecular wave functions for all the molecules, equation 5.7 becomes

$$\text{FIRST TERM IN EQN. 5.6} = k' \sum_{c\delta} B_\delta e^{i\underline{k}\cdot\underline{r}_c} \left(E^F_{c\delta} + \sum_{m\alpha \neq c\delta} E^\circ_{m\alpha} \right) \int \Phi^{F*}_{p\delta} \Phi^F_{c\delta} dV \quad 5.8$$

where $E^F_{c\delta}$ and $E^\circ_{c\gamma}$ are the energies of a free molecule in its excited state and ground state respectively. Using the orthonormality relationship in equation 5.3, equation 5.8 becomes

$$\text{FIRST TERM IN EQN. 5.6} = k' B_\delta e^{i\underline{k}\cdot\underline{r}_p} \xi^F_\delta \quad 5.9$$

where $$\xi^F_\delta = \left(E^F_{p\delta} + \sum_{m\alpha \neq p\delta} E^\circ_{m\alpha} \right)$$

The second term in equation 5.6 can be written as

$$\text{SECOND TERM IN EQN. 5.6} = k' \sum_{q\rho} B_\rho \, e^{i\underline{k}\cdot\underline{r}_q} \, M_{p\delta,q\rho} \qquad 5.10$$

where

$$M_{p\delta,q\rho} = \int \Phi^{F*}_{p\delta} \sum_{m\alpha,n\beta}{}' V_{m\alpha,n\beta} \, \Phi^{F}_{q\rho} \, dV$$

Using the orthonormality relationship in equation 5.3, the third term in equation 5.6 can be written as

$$\text{THIRD TERM IN EQN. 5.6} = -k' B_\delta \, e^{i\underline{k}\cdot\underline{r}_p} \, \epsilon^F \qquad 5.11$$

Reconstructing equation 5.6 from equations 5.9, 5.10 and 5.11 we have

$$\xi^F B_\delta e^{i\underline{k}\cdot\underline{r}_p} + \sum_{q\rho} B_\rho e^{i\underline{k}\cdot\underline{r}_q} M_{p\delta,q\rho} - \epsilon^F B_\rho e^{i\underline{k}\cdot\underline{r}_p} = 0 \qquad 5.12$$

With a bit of algebra equation 5.12 becomes

$$\sum_\rho \left[\sum_q e^{i\underline{k}\cdot(\underline{r}_q - \underline{r}_p)} M_{p\delta,q\rho} + (\xi^F - \epsilon^F)\,\delta_{\delta\rho} \right] B_\rho = 0 \qquad 5.13$$

Equation 5.13 represents a different equation for each value of δ which is chosen. Since there are as many values for δ as there are members of the unit cell, the number of equations represented by equation 5.13 will be the number of molecules per unit cell. This system of equations has non-trivial solutions if the determinant of the coefficients of these equations

is zero:

$$\left| \sum_{q} e^{i\underline{k}\cdot(\underline{r}_q - \underline{r}_p)} M_{p\delta, q\rho} + (\xi^F - \epsilon^F)\delta_{\delta\rho} \right| = 0 \qquad 5.14$$

The solutions of equation 5.14 give as many values for ϵ^F as there are molecules per unit cell.

It should be noted that the values of ϵ^F which are obtained from equation 5.14 are not the energies which are obtained from an absorption experiment. In order to obtain the absorption energies, the ground state energy should be subtracted from the values found for ϵ^F. It is shown in Appendix A to this chapter that the energy of the crystal ground state is shifted from its oriented gas value by the addition of a factor which is independent of k. Because of this the k dependence of the dispersion relations for ϵ^F are not altered by subtracting the ground state energy, and properties such as the velocity of the excitons and the differences between the values of ϵ^F will not be affected

B. Crystal Structure of Pyrene

The pyrene crystal is monoclinic with the following unit cell dimensions: a=13.60 Å, b=9.24 Å, c=8.37 Å, β=100.2°.[1] The space group is $C_{2h}^5(P2_1/a)$ with four molecules per unit cell.[1] Figure 5.1 shows a projection of 19 molecules on the ab crystal plane. Each molecule is designated with the number of its unit cell followed by a number from 1 to 4 indicating the molecule's position in the unit cell. The position of molecule 1 with respect to the center of symmetry in terms of projections along

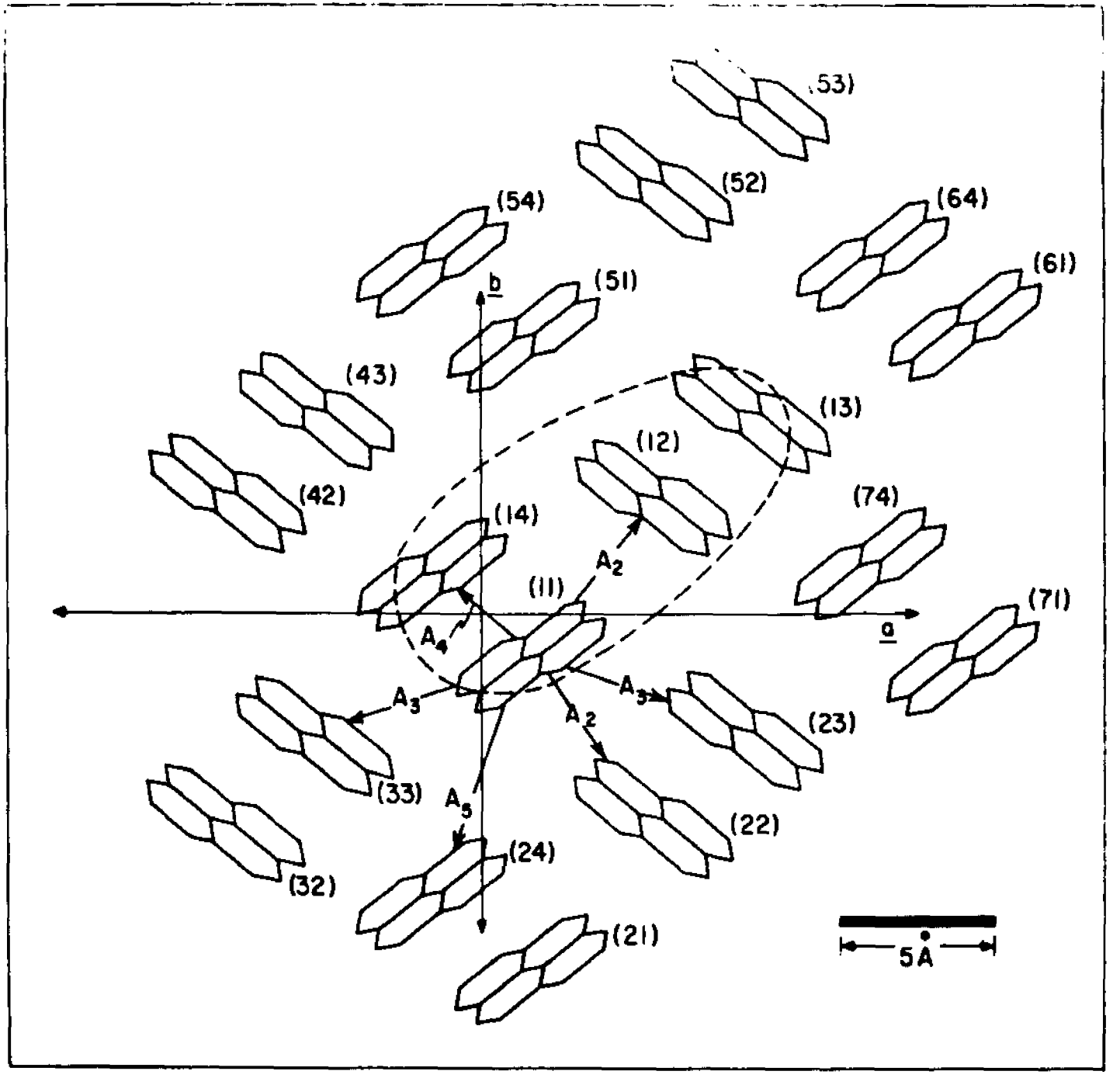

Fig. 5.1. Projection of 19 pyrene molecules on the ab crystal plane

the a and b axes and their perpendicular c' is (1.520 Å, -1.160 Å, 0.463 Å). Molecules 2,3 and 4 are generated from molecule 1 respectively by the following symmetry operations: (1) C_2^b = two fold screw rotation about the b axis, (2) δ^{ac} = glide plane, ac crystal plane, (3) i = inversion through the center of symmetry.

C. The $M_{p\delta,q\rho}$ Interaction Matrix and the Pyrene Structure

The interaction matrix given in equation 5.10 can be written with the aid of equation 5.3 as

$$M_{p\delta,q\rho} = \int a\phi^{F*}_{p\delta} \widetilde{\Pi}_{m\alpha \neq p\delta} \phi^{\circ}_{m\alpha} \sum_{r\beta,s\eta} V_{r\beta,s\eta}\, a\phi^{F}_{q\rho}\, \widetilde{\Pi}\, \phi^{\circ}_{n\beta}\, dV \qquad 5.15$$

The interaction indicated in the above expression is carried out over the coordinates of all the electrons in the crystal. Jortner et al[2] have shown that the $M_{p\delta,q\rho}$ interaction reduces to the sum of two terms.

$$M_{p\delta,q\rho} = \int \phi^{F*}_{p\delta}\, \phi^{\circ *}_{q\rho}\, V_{p\delta,q\rho}\, \phi^{\circ}_{p\delta}\, \phi^{F}_{q\rho}\, dV + \int \left[\left(\sum_P (-)^P P - 1\right)\left(\phi^{F*}_{p\delta}\, \phi^{\circ *}_{q\rho}\right)\right] V_{p\delta,q\rho}\, \phi^{\circ}_{p\delta}\, \phi^{F}_{q\rho}\, dV \qquad 5.16$$

where $\sum_P (-)^P P$ is an operator which permutes the electrons among the molecules; odd permutations are prefixed by a minus sign and even permutations are prefixed by a plus sign. To illustrate the significance of the terms on the right hand side of equation 5.16, suppose that the $p\delta$ molecule contains one elec-

tron numbered 1 and the $q\rho$ molecule contains one electron numbered 2. In this case the first term on the right hand side of equation 5.16 is

$$\text{FIRST TERM ON THE RT. SIDE OF EQN. 5.16} = \int \phi^{F*}_{p\delta}(1)\, \phi^{\circ *}_{q\rho}(2)\, V_{p\delta,q\rho}\, \phi^{\circ}_{p\delta}(1)\, \phi^{F}_{q\rho}(2)\, dV_1 dV_2 \qquad 5.17$$

If the excited state is a triplet, and $V_{p\delta,q\rho}$ does not interact with spin, the right hand side of equation 5.17 will be zero since the spin wave functions are orthogonal (the ground state is a singlet) and can be separated out of the integral. The second term on the right hand side of equation 5.16 for this illustrative example is

$$\text{SECOND TERM ON THE RT. SIDE OF EQN. 5.16} = \int\left[\phi^{F*}_{p\delta}(1)\,\phi^{\circ *}_{q\rho}(2) - \phi^{F*}_{p\delta}(2)\,\phi^{\circ *}_{q\rho}(1)\right] V_{p\delta,q\rho}(1,2)\,\phi^{\circ}_{p\delta}(1)\,\phi^{F}_{q\rho}(2)\, dV_1\, dV_2 \qquad 5.18$$

$$- \int \phi^{F*}_{p\delta}(1)\,\phi^{\circ *}_{q\rho}(2)\, V_{p\delta,q\rho}(1,2)\,\phi^{\circ}_{p\delta}(1)\,\phi^{F}_{q\rho}(2)\, dV_1\, dV_2$$

Equation 5.18 reduces to

$$\text{SECOND TERM ON THE RT. SIDE OF EQN. 5.16} = -\int \phi^{F*}_{p\delta}(2)\,\phi^{\circ *}_{q\rho}(1)\, V_{p\delta,q\rho}(1,2)\,\phi^{\circ}_{p\delta}(1)\,\phi^{F}_{q\rho}(2)\, dV_1 dV_2 \qquad 5.19$$

It is clear from the above integral that electron 2 has been "exchanged" for electron 1 on the left hand side of the integrand. Due to this exchange lack of spin orbit coupling will not reduce this integral to zero. It is concluded therefore

that the $M_{p\delta,q\varphi}$ interaction matrix for the case of one electron per molecule is equal to the exchange interaction arising from the second term on the right hand side of equation 5.16 (if there is no spin orbit coupling and the excited state is a triplet). Jortner et al[2] have shown that this is also true for multi-electron molecules.

The exchange interaction falls off rapidly with the distance between any pair of interacting atoms or molecules. Knox[3] has calculated that the exchange interaction between $\tilde{\pi}$ orbitals in crystalline argon decreases exponentially with the distance between the atoms, falling off by a factor of e every four tenths of an angstrom. More recently Jortner et al[2] have indicated that in crystals of anthracene only the nearest and second nearest neighbors contribute to the exchange interaction. In anthracene the nearest, second nearest and third nearest neighbors are at distances of 5.23, 6.04 and 8.56 Å respectively (the distances given here are between the geometrical centers of the molecules).

On the basis of the previous discussion it will be assumed in dealing with Pyrene that all $M_{p\delta,q\varphi}$ interactions beyond the first four closest different interactions are negligible. These interactions are labeled A_2, A_3, A_4 and A_5 in Figure 5.1, and their corresponding intermolecular distances are 6.03, 7.18, 3.93 and 7.62 Å respectively. All interactions with molecules on either adjacent ab plane are neglected since the closest intermolecular distance for a molecule of this type is 8.37 Å.

D. Energy of an Excited Triplet State in Pyrene

In this section equation 5.14 will be solved for the energy levels of an excited triplet state in pyrene. Equation 5.14 can be written as

$$|D_{\delta\rho}| = 0$$

where

$$D_{\delta\rho} = \sum_{q} e^{i\underline{k}\cdot(\underline{r}_q - \underline{r}_p)} M_{p\delta,q\rho} + (\xi^F - \epsilon^F)\delta_{\delta\rho}$$

It should be noted that the p subscript appearing in the D matrix has not been included in the notation $D_{\delta\rho}$. The reason for this is that each element of the D matrix should be independent of the unit cell for which it is being calculated. The vector $\underline{r}_p$ is the position of the $p\delta$ molecule, and $\underline{r}_q$ is the position of the molecule in unit cell q which is translationally equivalent to the $p\delta$ molecule. To illustrate the calculation of the components of the D matrix in the case of the pyrene structure in Figure 5.1, suppose p is 1. In view of the tight binding approximation only interactions A_2, A_3, A_4 and A_5 will be considered. If $\delta = 1$,

$$D_{11} = \sum_{q} e^{i\underline{k}\cdot(\underline{r}_q - \underline{r}_1)} M_{11,q1} + (\xi^F - \epsilon^F)\delta_{11}$$

Since the interactions which are to be considered do not include any interactions for which $\delta = \rho = 1$, D_{11} becomes

$$D_{11} = \xi^F - \epsilon^F$$

D_{12} is

$$D_{12} = \sum_{q} e^{i\underline{k}\cdot(\underline{r}_q - \underline{r}_1)} M_{11,q2} + (\xi^F - \epsilon^F)\delta_{12}$$

Figure 5.1 indicates that the only interactions of the form

$M_{11,q2}$ among those which are being considered are $M_{11,12}$ and $M_{11,22}$. $\underline{r}_q$ is equal to $\underline{r}_1$ for the $M_{11,12}$ interaction since molecules (11) and (12) are both in the same unit cell. However, $(\underline{r}_q - \underline{r}_1)$ is $-\underline{b}$ for the $M_{11,22}$ interaction since the molecule translationally equivalent to molecule (11) in unit cell 2 is molecule (21).

Therefore D_{12} is

$$D_{12} = M_{11,12} + e^{-i\underline{k}\cdot\underline{b}} M_{11,22}$$

The symmetry of the crystal indicates that

$$M_{11,12} = M_{11,22} = A_2$$

Therefore

$$D_{12} = A_2 \left(1 + e^{-i\underline{k}\cdot\underline{b}}\right)$$

When this procedure is carried out for the other components of the D matrix, equation 5.14 becomes

$$\begin{vmatrix} \xi^F - \epsilon^F & A_2(1+e^{-i\underline{k}\cdot\underline{b}}) & A_3\left[e^{-i\underline{k}\cdot\underline{b}} + e^{-i\underline{k}\cdot(\underline{a}+\underline{b})}\right] & A_4 + A_5 e^{-i\underline{k}\cdot\underline{b}} \\ A_2(1+e^{i\underline{k}\cdot\underline{b}}) & \xi^F - \epsilon^F & A_4 + A_5 e^{-i\underline{k}\cdot\underline{b}} & A_3(1+e^{i\underline{k}\cdot\underline{a}}) \\ A_3\left[e^{i\underline{k}\cdot\underline{b}} + e^{i\underline{k}\cdot(\underline{a}+\underline{b})}\right] & A_4 + A_5 e^{i\underline{k}\cdot\underline{b}} & \xi^F - \epsilon^F & A_2\left[e^{i\underline{k}\cdot(\underline{a}+\underline{b})} + e^{i\underline{k}\cdot\underline{a}}\right] \\ A_4 + A_5 e^{i\underline{k}\cdot\underline{b}} & A_3(1+e^{-i\underline{k}\cdot\underline{a}}) & A_2\left[e^{-i\underline{k}\cdot(\underline{a}+\underline{b})} + e^{-i\underline{k}\cdot\underline{a}}\right] & \xi^F - \epsilon^F \end{vmatrix} = 0 \qquad 5.20$$

B_1 B_2 B_3 B_4

where the columns in the determinant in equation 5.20 have been designated with respect to their corresponding coefficients (B_1, B_2, B_3 or B_4) in the secular equations (equation 5.13). Equation 5.20 is simplified to

$$\begin{vmatrix} \delta & \beta e^{-i\underline{k}\cdot\underline{b}/2} & \gamma e^{-i\underline{k}\cdot(\underline{b}+\underline{a}/2)} & A_4 + A_5 e^{-i\underline{k}\cdot\underline{b}} \\ \beta e^{i\underline{k}\cdot\underline{b}/2} & \delta & A_4 + A_5 e^{-i\underline{k}\cdot\underline{b}} & \gamma e^{i\underline{k}\cdot\underline{a}/2} \\ \gamma e^{i\underline{k}\cdot(\underline{b}+\underline{a}/2)} & A_4 + A_5 e^{i\underline{k}\cdot\underline{b}} & \delta & \beta e^{i\underline{k}\cdot(\underline{a}+\underline{b}/2)} \\ A_4 + A_5 e^{i\underline{k}\cdot\underline{b}} & \gamma e^{-i\underline{k}\cdot\underline{a}/2} & \beta e^{-i\underline{k}\cdot(\underline{a}+\underline{b}/2)} & \delta \\ \uparrow & \uparrow & \uparrow & \uparrow \\ B_1 & B_2 & B_3 & B_4 \end{vmatrix} = 0 \qquad 5.21$$

where

$$\delta = E^F - \epsilon^F$$

$$\beta = 2A_2 \cos\frac{\underline{k}\cdot\underline{b}}{2} \; ; \qquad \gamma = 2A_3 \cos\frac{\underline{k}\cdot\underline{a}}{2}$$

Equation 5.21 could not be solved for ϵ^F for a general direction of $\underline{k}$. However, it was found that solutions to this equation could be obtained for $\underline{k}$ parallel to the $\underline{a}$ or $\underline{b}$ crystal directions. In the case in which $\underline{k}$ is parallel to $\underline{b}$, equation 5.21 is

$$\begin{vmatrix} \delta & \beta e^{-ikb/2} & \gamma e^{-ikb} & A_4 + A_5 e^{-ikb} \\ \beta e^{ikb/2} & \delta & A_4 + A_5 e^{-ikb} & \gamma \\ \gamma e^{ikb} & A_4 + A_5 e^{ikb} & \delta & \beta e^{ikb/2} \\ A_4 + A_5 e^{ikb} & \gamma & \beta e^{-ikb/2} & \delta \end{vmatrix} = 0 \qquad 5.22$$

B_1 B_2 B_3 B_4

After a bit of algebra equation 5.22 becomes

$$\begin{vmatrix} \delta & A_4 e^{ikb/2} + A_5 e^{-ikb/2} & \gamma & \beta \\ A_4 e^{-ikb/2} + A_5 e^{ikb/2} & \delta & \beta & \gamma \\ \gamma & \beta & \delta & A_4 e^{-ikb/2} + A_5 e^{ikb/2} \\ \beta & \gamma & A_4 e^{ikb/2} + A_5 e^{-ikb/2} & \delta \end{vmatrix} = 0 \qquad 5.23$$

$e^{ikb/2} B_1$ B_4 $e^{-ikb/2} B_3$ B_2

Equation 5.23 represents four homogeneous equations. When the equation associated with row 1 of the determinant in equation 5.23 is added to the equation associated with row 4, the result is

$$(\delta+\beta)(e^{ikb/2} B_1 + B_2) + (A_4 e^{ikb/2} + A_5 e^{-ikb/2} + \gamma)(e^{-ikb/2} B_3 + B_4) = 0 \qquad 5.24$$

When the same operation is carried out with rows 3 and 4, one obtains

$$\left(A_4 e^{-ikb/2} + A_5 e^{ikb/2} + \gamma\right)\left(e^{ikb/2} B_1 + B_2\right) + \left(\delta + \beta\right)\left(e^{-ikb/2} B_3 + B_4\right) = 0 \qquad 5.25$$

Equations 5.24 and 5.25 represent two homogeneous equations in two variables, and non-trivial solutions to these equations must satisfy

$$\begin{vmatrix} \delta + \beta & A_4 e^{\frac{ikb}{2}} + A_5 e^{-\frac{ikb}{2}} + \gamma \\ A_4 e^{-\frac{ikb}{2}} + A_5 e^{\frac{ikb}{2}} + \gamma & \delta + \beta \end{vmatrix} = 0 \qquad 5.26$$

$$e^{\frac{ikb}{2}} B_1 + B_2 \qquad e^{-\frac{ikb}{2}} B_3 + B_4$$

Solving equation 5.26 for δ, one obtains

$$\delta = -\beta \pm \sqrt{\gamma^2 + 2\gamma(A_4 + A_5)\cos\frac{kb}{2} + A_4^2 + A_5^2 + 2A_4A_5\cos kb} \qquad 5.27$$

In terms of the original parameters in equation 5.21, the energy ϵ^F from equation 5.27 is

$$\epsilon^F = \xi^F + 2A_2\cos\frac{kb}{2} \mp \sqrt{4A_3^2 + 4A_3(A_4 + A_5)\cos\frac{kb}{2} + A_4^2 + A_5^2 + 2A_4A_5\cos kb} \qquad 5.28$$

where the minus sign before the square root corresponds to the plus sign in equation 5.27, and vice versa.

Equations 5.24 and 5.25 are not the only pair of simul-

taneous equations in two variables which can be extracted from equation 5.23. When the equation associated with row 4 of the determinant in equation 5.23 is subtracted from the equation associated with row 1, the result is

$$(\delta+\beta)\left(e^{\frac{ikb}{2}}B_1-B_2\right)+\left(A_4e^{\frac{ikb}{2}}+A_5e^{-\frac{ikb}{2}}-\gamma\right)\left(B_4-e^{-\frac{ikb}{2}}B_3\right)=0 \qquad 5.29$$

When the same operation is carried out with rows 3 and 4 of equation 5.23, one obtains

$$\left(A_4e^{-\frac{ikb}{2}}+A_5e^{\frac{ikb}{2}}-\gamma\right)\left(B_1-B_2\right)+\left(\delta-\beta\right)\left(B_4-e^{-\frac{ikb}{2}}B_3\right)=0 \qquad 5.30$$

Equations 5.29 and 5.30 represent two homogeneous equations in two variables, and non-trivial solutions to these equations must satisfy

$$\begin{vmatrix} e^{ikb/2}B_1-B_2 \downarrow & B_4-B_3e^{-ikb/2} \downarrow \\ \delta-\beta & A_4e^{\frac{ikb}{2}}+A_5e^{-\frac{ikb}{2}}-\gamma \\ A_4e^{-\frac{ikb}{2}}+A_5e^{\frac{ikb}{2}}-\gamma & \delta-\beta \end{vmatrix}=0 \qquad 5.31$$

Equation 5.31 gives two new solutions,

$$\epsilon^F=\xi^F-2A_2\cos\frac{kb}{2}\pm\sqrt{4A_3^2-4A_3(A_4+A_5)\cos\frac{kb}{2}+A_4^2+A_5^2+2A_4A_5\cos kb} \qquad 5.32$$

Table 5.1 summarizes the solutions for ϵ^F for the case in which $\underline{k}$ is parallel to $\underline{b}$.

For the case in which $\underline{k}$ is parallel to $\underline{a}$ equation 5.21 is

$$\begin{array}{cccc} B_1 & B_2 & B_3 & B_4 \\ \downarrow & \downarrow & \downarrow & \downarrow \end{array}$$

$$\begin{vmatrix} \delta & \beta & \gamma e^{-\frac{ika}{2}} & A_4+A_5 \\ \beta & \delta & A_4+A_5 & \gamma e^{\frac{ika}{2}} \\ \gamma e^{\frac{ika}{2}} & A_4+A_5 & \delta & \beta e^{ika} \\ A_4+A_5 & \gamma e^{-\frac{ika}{2}} & \beta e^{-ika} & \delta \end{vmatrix} = 0 \qquad 5.33$$

After a bit of algebra equation 5.33 becomes

$$\begin{vmatrix} \delta & (A_4+A_5)e^{-\frac{ika}{2}} & \gamma & \beta \\ (A_4+A_5)e^{\frac{ika}{2}} & \delta & \beta & \gamma \\ \gamma & \beta & \delta & (A_4+A_5)e^{-\frac{ika}{2}} \\ \beta & \gamma & (A_4+A_5)e^{\frac{ika}{2}} & \delta \end{vmatrix} = 0 \qquad 5.34$$

$$\begin{array}{cccc} \uparrow & \uparrow & \uparrow & \uparrow \\ B_1 & B_4 e^{\frac{ika}{2}} & B_3 e^{-\frac{ika}{2}} & B_2 \end{array}$$

$\epsilon^F_{b1} = \xi^F + 2A_2 \cos\frac{Kb}{2} + \sqrt{4A_3^2 + 4A_3(A_4+A_5)\cos\frac{Kb}{2} + A_4^2 + A_5^2 + 2A_4A_5\cos Kb}$
$\epsilon^F_{b2} = \xi^F + 2A_2 \cos\frac{Kb}{2} + \sqrt{4A_3^2 + 4A_3(A_4+A_5)\cos\frac{Kb}{2} + A_4^2 + A_5^2 + 2A_4A_5\cos Kb}$
$\epsilon^F_{b3} = \xi^F - 2A_2 \cos\frac{Kb}{2} + \sqrt{4A_3^2 - 4A_3(A_4+A_5)\cos\frac{Kb}{2} + A_4^2 + A_5^2 + 2A_4A_5\cos Kb}$
$\epsilon^F_{b4} = \xi^F - 2A_2 \cos\frac{Kb}{2} + \sqrt{4A_3^2 - 4A_3(A_4+A_5)\cos\frac{Kb}{2} + A_4^2 + A_5^2 + 2A_4A_5\cos Kb}$

Table 5.1. The solutions for ϵ^F for the case in which $\underline{k}$ is parallel to $\underline{b}$.

Equation 5.34 represents four homogeneous equations. When the equation associated with row 1 of the determinant in equation 5.34 is added to the equation associated with row 3, the result is

$$(\delta+\gamma)\left(B_1+B_3e^{-\frac{ika}{2}}\right)+\left[(A_4+A_5)e^{-\frac{ika}{2}}+\beta\right]\left(B_4e^{\frac{ika}{2}}+B_2\right)=0 \qquad 5.35$$

When the same operation is carried out on rows 2 and 4, one obtains

$$\left[(A_4+A_5)e^{\frac{ika}{2}}+\beta\right]\left(B_1+B_3e^{-\frac{ika}{2}}\right)+(\delta+\gamma)\left(B_4e^{\frac{ika}{2}}+B_2\right)=0 \qquad 5.36$$

Equations 5.35 and 5.36 represent two homogeneous equations in two variables, and non-trivial solutions to these equations must satisfy

$$\begin{vmatrix} B_1+B_3e^{-\frac{ika}{2}} & B_4e^{\frac{ika}{2}}+B_2 \\ \delta+\gamma & (A_4+A_5)e^{-\frac{ika}{2}}+\beta \\ (A_4+A_5)e^{\frac{ika}{2}}+\beta & \delta+\gamma \end{vmatrix}=0 \qquad 5.37$$

The solutions to equation 5.37 are given in Table 5.2 as ϵ^F_{a1} and ϵ^F_{a4}.

Equations 5.35 and 5.36 are not the only pair of simultaneous equations in two variables which can be extracted from

equation 5.34. When the equation associated with row 3 of the determinant in equation 5.34 is subtracted from the equation associated with row 1, the result is

$$(\delta-\gamma)(B_1-B_3e^{-\frac{ika}{2}})+[(A_4+A_5)e^{-\frac{ika}{2}}-\beta](B_4e^{\frac{ika}{2}}-B_2)=0 \qquad 5.38$$

When the same operation is carried out on rows 2 and 4 of equation 5.34, one obtains

$$[(A_4+A_5)e^{\frac{ika}{2}}-\beta](B_1-B_3)e^{\frac{ika}{2}}+(\delta-\gamma)(B_4e^{\frac{ika}{2}}-B_2)=0 \qquad 5.39$$

Equations 5.38 and 5.39 represent two homogeneous equations in two variables, and non-trivial solutions to these equations must satisfy

$$\begin{vmatrix} B_1-B_3e^{-\frac{ika}{2}} & B_4e^{\frac{ika}{2}}-B_2 \\ \delta-\gamma & (A_4+A_5)e^{-\frac{ika}{2}}-\beta \\ (A_4+A_5)e^{\frac{ika}{2}}-\beta & \delta-\gamma \end{vmatrix} = 0 \qquad 5.40$$

The solutions to equation 5.40 are given in Table 5.2 as ϵ^F_{a2} and ϵ^F_{a3}.

E. <u>The Eigen Vectors Corresponding to the Energy Levels of an Excited Triplet State in Pyrene</u>

In this section the eigen vectors corresponding to the energy levels in Tables 5.1 and 5.2 will be determined. Since

$\epsilon^F_{a1} = \xi^F + 2A_3 \cos\frac{ka}{2} + \sqrt{4A_2^2 + 4A_2(A_4+A_5)\cos\frac{ka}{2} + A_4^2 + A_5^2 + 2A_4A_5}$
$\epsilon^F_{a2} = \xi^F - 2A_3 \cos\frac{ka}{2} - \sqrt{4A_2^2 - 4A_2(A_4+A_5)\cos\frac{ka}{2} + A_4^2 + A_5^2 + 2A_4A_5}$
$\epsilon^F_{a3} = \xi^F - 2A_3 \cos\frac{ka}{2} + \sqrt{4A_2^2 - 4A_2(A_4+A_5)\cos\frac{ka}{2} + A_4^2 + A_5^2 + 2A_4A_5}$
$\epsilon^F_{a4} = \xi^F + 2A_3 \cos\frac{ka}{2} - \sqrt{4A_2^2 + 4A_2(A_4+A_5)\cos\frac{ka}{2} + A_4^2 + A_5^2 + 2A_4A_5}$

Table 5.2. The solutions for ϵ^F in the case in which $\underline{k}$ is parallel to $\underline{a}$.

the exciton-photon interaction conserves momentum, the exciton wave vector $\underline{k}$ is equal to the wave vector of the interacting photon. In the present experiment the triplet state is excited by light in the visible region, and as a consequence the exciton wave vector is about one thousand times smaller than the extent of the Brillouin zone (π/b or π/a). Because of the relatively small size of the exciton wave vector, the eigen vectors will be calculated in the limit as $\underline{k}$ approaches zero.

The four homogeneous secular equations represented by equation 5.21 can be written as

$$\begin{pmatrix} \xi^F & \beta e^{-i\frac{\underline{k}\cdot\underline{b}}{2}} & \gamma e^{i\underline{k}\cdot(\underline{b}+\frac{\underline{a}}{2})} & A_4+A_5 e^{-i\underline{k}\cdot\underline{b}} \\ \beta e^{i\underline{k}\cdot\underline{b}/2} & \xi^F & A_4+A_5 e^{-i\underline{k}\cdot\underline{b}} & \gamma e^{i\frac{\underline{k}\cdot\underline{a}}{2}} \\ \gamma e^{i\underline{k}\cdot(\underline{b}+\frac{\underline{a}}{2})} & A_4+A_5 e^{i\underline{k}\cdot\underline{b}} & \xi^F & \beta e^{i\underline{k}\cdot(\underline{a}+\underline{b}/2)} \\ A_4+A_5 e^{i\underline{k}\cdot\underline{b}} & \gamma e^{-i\underline{k}\cdot\underline{a}/2} & \beta e^{-i\underline{k}\cdot(\underline{a}+\underline{b}/2)} & \xi^F \end{pmatrix} \begin{pmatrix} B_1 \\ B_2 \\ B_3 \\ B_4 \end{pmatrix} = \epsilon_f \begin{pmatrix} B_1 \\ B_2 \\ B_3 \\ B_4 \end{pmatrix} \qquad 5.41$$

In the limit as k approaches zero, equation 5.41 becomes

$$\begin{pmatrix} \xi^F & \beta & \gamma & A_4+A_5 \\ \beta & \xi^F & A_4+A_5 & \gamma \\ \gamma & A_4+A_5 & \xi^F & \beta \\ A_4+A_5 & \gamma & \beta & \xi^F \end{pmatrix} \begin{pmatrix} B_1 \\ B_2 \\ B_3 \\ B_4 \end{pmatrix} = \epsilon^F(0) \begin{pmatrix} B_1 \\ B_2 \\ B_3 \\ B_4 \end{pmatrix} \qquad 5.42$$

where $\epsilon^F(o)$ is the excited state energy at $\underline{k}=0$.

The eigen vectors associated with the 4x4 matrix in equation 5.42 are obtained in the following manner. Since the sum of the elements in each of the rows is identical, one of the eigen vectors must be

$$|1\rangle = \frac{1}{2}\begin{pmatrix}1\\1\\1\\1\end{pmatrix} \qquad 5.43$$

where the factor $\frac{1}{2}$ is used for normalization. It should be noted that the absolute values of each of the components of eigen vector $|1\rangle$ are equal. This is due to the fact that the excitation is equally likely to be on any one of the four molecules in the unit cell, i.e., $|\beta_n|^2$ = constant. The other three eigen vectors must also have this property. In addition, since the four eigen values ϵ^F are different (see Tables 5.1 and 5.2) and the matrix in equation 5.41 is Hermetian the four eigen vectors must be mutually orthogonal. With the aid of the above restrictions the other three eigen vectors are found to be

$$|2\rangle = \frac{1}{2}\begin{pmatrix}1\\+1\\-1\\-1\end{pmatrix} \qquad 5.44$$

$$|3\rangle = \frac{1}{2}\begin{pmatrix}1\\-1\\-1\\+1\end{pmatrix} \qquad 5.45$$

$$|4\rangle = \frac{1}{2}\begin{pmatrix} 1 \\ -1 \\ +1 \\ -1 \end{pmatrix} \qquad 5.46$$

In order to find out which energies in Tables 5.1 and 5.2 are associated with each of the eigen vectors in equations 5.43 through 5.46, a comparison between the contents of these tables and the eigen values belonging to the eigen vectors (the eigen values calculated from equation 5.42) must be made at $\underline{k}=0$. Table 5.3 is used to make this comparison. Column (a) in Table 5.3 is a listing of each of the eigenvalues associated with each of the $|i\rangle$ eigen vectors. Columns (b) and (c) of Table 5.3 list the contents of Tables 5.2 and 5.1 respectively, evaluated at $\underline{k}=0$. Because of the need to find the absolute value of sums of interactions in columns (b) and (c) of Table 5.3, a comparison cannot be made between the energies in these columns and the eigen values in column (a) without some idea of the relative values of A_2, A_3, A_4 and A_5. Since the exchange interaction falls off exponentially by a factor of e in about 0.4 Å (see section C), the closest interaction should dominate. In view of the fact that molecule 4 is 2 Å closer to molecule 1 (between centers) than any other molecule (see section C), it will be assumed that $|A_4|$ is much larger than $|A_3|$, $|A_2|$, or $|A_5|$. If in addition, A_4 is positive we may write that

$$|2A_2 + (A_4 + A_5)| = 2A_2 + (A_4 + A_5) \qquad 5.47$$

(a)

$\|i\rangle$	$\epsilon^F_{\|i\rangle}(0)$
$\|1\rangle$	$\xi^F + 2A_2 + 2A_3 + (A_4 + A_5)$
$\|2\rangle$	$\xi^F + 2A_2 - 2A_3 - (A_4 + A_5)$
$\|3\rangle$	$\xi^F - 2A_2 - 2A_3 + (A_4 + A_5)$
$\|4\rangle$	$\xi^F - 2A_2 + 2A_3 - (A_4 + A_5)$

(b)

j	$\epsilon^F_{ja}(0)$
1	$\xi^F + 2A_3 + \lvert 2A_2 + (A_4 + A_5)\rvert$
2	$\xi^F - 2A_3 - \lvert 2A_2 - (A_4 + A_5)\rvert$
3	$\xi^F - 2A_3 + \lvert 2A_2 - (A_4 + A_5)\rvert$
4	$\xi^F + 2A_3 - \lvert 2A_2 + (A_4 + A_5)\rvert$

(c)

k	$\epsilon^F_{kb}(0)$
1	$\xi^F + 2A_2 + \lvert 2A_3 + (A_4 + A_5)\rvert$
2	$\xi^F + 2A_2 - \lvert 2A_3 + (A_4 + A_5)\rvert$
3	$\xi^F - 2A_2 + \lvert 2A_3 - (A_4 + A_5)\rvert$
4	$\xi^F - 2A_2 - \lvert 2A_3 - (A_4 + A_5)\rvert$

Table 5.3. (a) Energies of an excited state in Pyrene at $\underline{k}=0$ (solutions to equation 5.42); (b) Table 5.2 evaluated at $\underline{k}=0$; (c) Table 5.1 evaluated at $\underline{k}=0$.

$$|2A_2 - (A_4 + A_5)| = -2A_2 + (A_4 + A_5) \qquad 5.48$$

$$|2A_3 + (A_4 + A_5)| = 2A_3 + (A_4 + A_5) \qquad 5.49$$

$$|2A_3 - (A_4 + A_5)| = -2A_3 + (A_4 + A_5) \qquad 5.50$$

Substituting equations 5.47 through 5.50 into Table 5.3 gives Table 5.4. Table 5.4 indicates that

$$\epsilon^F_{|i\rangle} = \epsilon^F_{a_i}(o) = \epsilon^F_{b_i}(o) \qquad 5.51$$

Therefore, in the case in which A_4 is positive and predominates over the other interactions, energies $\epsilon^F_{a}(o)$ and $\epsilon^F_{b}(o)$ belong to eigen vector $|i\rangle$. However, if A_4 is predominant and negative

$$|2A_2 + (A_4 + A_5)| = -2A_2 - (A_4 + A_5) \qquad 5.52$$

$$|2A_2 - (A_4 + A_5)| = 2A_2 - (A_4 + A_5) \qquad 5.53$$

$$|2A_3 + (A_4 + A_5)| = -2A_3 - (A_4 + A_5) \qquad 5.54$$

(a)

$\|i\rangle$	$\epsilon^F_{\|i\rangle}(o)$
$\|1\rangle$	$\xi^F + 2A_2 + 2A_3 + (A_4+A_5)$
$\|2\rangle$	$\xi^F + 2A_2 - 2A_3 - (A_4+A_5)$
$\|3\rangle$	$\xi^F - 2A_2 - 2A_3 + (A_4+A_5)$
$\|4\rangle$	$\xi^F - 2A_2 + 2A_3 - (A_4+A_5)$

(b)

j	$\epsilon^F_{aj}(o)$
1	$\xi^F + 2A_3 + 2A_2 + (A_4+A_5)$
2	$\xi^F - 2A_3 + 2A_2 - (A_4+A_5)$
3	$\xi^F - 2A_3 - 2A_2 + (A_4+A_5)$
4	$\xi^F + 2A_3 - 2A_2 - (A_4+A_5)$

(c)

k	$\epsilon^F_{bk}(o)$
1	$\xi^F + 2A_2 + 2A_3 + (A_4+A_5)$
2	$\xi^F + 2A_2 - 2A_3 + (A_4+A_5)$
3	$\xi^F - 2A_2 - 2A_3 + (A_4+A_5)$
4	$\xi^F - 2A_2 + 2A_3 - (A_4+A_5)$

Table 5.4. Contents of Table 5.3 for the case in which A_4 is positive and much larger than $|A_2|$, $|A_3|$ or $|A_5|$.

$$|2A_3 - (A_4 + A_5)| = 2A_3 - (A_4 + A_5) \qquad 5.55$$

Substituting equations 5.52 through 5.55 into Table 5.3 gives Table 5.5. Table 5.5 indicates that

$$\epsilon^F_{|1\rangle}(o) = \epsilon^F_{4a}(o) = \epsilon^F_{2b}(o) \qquad 5.56$$

$$\epsilon^F_{|2\rangle}(o) = \epsilon^F_{3a}(o) = \epsilon^F_{1b}(o) \qquad 5.57$$

$$\epsilon^F_{|3\rangle}(o) = \epsilon^F_{2a}(o) = \epsilon^F_{4b}(o) \qquad 5.58$$

$$\epsilon^F_{|4\rangle}(o) = \epsilon^F_{1a}(o) = \epsilon^F_{3b}(o) \qquad 5.59$$

Therefore in the case in which A_4 is predominant and negative ϵ^F_{4a} and ϵ^F_{2b} belong to eigen vector $|1\rangle$, ϵ^F_{3a} and ϵ^F_{1b} belong to eigen vector $|2\rangle$, ϵ^F_{2a} and ϵ^F_{4b} belong to eigen vector $|3\rangle$ and, ϵ^F_{1a} and ϵ^F_{3b} belong to eigen vector $|4\rangle$. The energies associated with each of the eigen vectors $|i\rangle$ are summarized in Table 5.6 for the case in which A_4 is positive and predominant, and for the case in which A_4 is negative and predominant.

$\|i\rangle$	$\epsilon^F_{\|i\rangle}(0)$
$\|1\rangle$	$\xi^F + 2A_2 + 2A_3 + (A_4 + A_5)$
$\|2\rangle$	$\xi^F + 2A_2 - 2A_3 - (A_4 + A_5)$
$\|3\rangle$	$\xi^F - 2A_2 - 2A_3 + (A_4 + A_5)$
$\|4\rangle$	$\xi^F - 2A_2 + 2A_3 - (A_4 + A_5)$

i	$\epsilon^F_{aa,ii}(0)$
1	$\xi^F + 2A_3 - 2A_2 - (A_4 + A_5)$
2	$\xi^F - 2A_3 - 2A_2 + (A_4 + A_5)$
3	$\xi^F - 2A_3 + 2A_2 - (A_4 + A_5)$
4	$\xi^F + 2A_3 + 2A_2 + (A_4 + A_5)$

k	$\epsilon^F_{bb,kk}(0)$
1	$\xi^F + 2A_2 - 2A_3 - (A_4 + A_5)$
2	$\xi^F + 2A_2 + 2A_3 + (A_4 + A_5)$
3	$\xi^F - 2A_2 + 2A_3 - (A_4 + A_5)$
4	$\xi^F - 2A_2 - 2A_3 + (A_4 + A_5)$

Table 5.5. Contents of Table 5.3 for the case in which A_4 is negative and its absolute value is much larger than $|A_2|$, $|A_3|$ or $|A_5|$.

(a)

$A_4 > 0$

$\|i\rangle$	Energies corresponding to each eigen vector
$\|1\rangle$	ϵ^F_{a1} , ϵ^F_{b1}
$\|2\rangle$	ϵ^F_{a2} , ϵ^F_{b2}
$\|3\rangle$	ϵ^F_{a3} , ϵ^F_{b3}
$\|4\rangle$	ϵ^F_{a4} , ϵ^F_{b4}

(b)

$A_4 < 0$

$\|i\rangle$	Energies corresponding to each eigen vector
$\|1\rangle$	ϵ^F_{a4} , ϵ^F_{b2}
$\|2\rangle$	ϵ^F_{a3} , ϵ^F_{b1}
$\|3\rangle$	ϵ^F_{a2} , ϵ^F_{b4}
$\|4\rangle$	ϵ^F_{a1} , ϵ^F_{b3}

Table 5.6. The energies corresponding to each eigen vector $|i\rangle$; (a) for the case in which A_4 is positive and much larger than $|A_2|$, $|A_3|$ or $|A_5|$ and; (b) for the case in which A_4 is negative and its absolute value is much larger than $|A_2|$, $|A_3|$ or $|A_5|$.

F. Optical Selection Rules

In this section we will determine which of the four eigen states in equations 5.43 through 5.46 can be optically excited.

As long as the wavelength of the incident radiation is very large compared to the size of the unit cell, all molecules in a given unit cell will receive the incident radiation in approximately the same phase and the transition probability per unit time is[4]

$$P = c \left| \underline{E}_o \cdot \left(\psi^F, \underline{r}\, \Phi^\circ \right) \right|^2 \delta \left(\hbar\omega - \Delta\epsilon^F \right) \qquad 5.60$$

where c is a constant, $\underline{E}_o$ is the electric field vector of the incident radiation, ψ^F is the wave function corresponding to the excited state, $\underline{r}$ is the sum of the position vectors of all the electrons in the crystal, Φ° is the ground state wave function (equation 5.2), ω is the frequency of the incident radiation, and $\Delta\epsilon^F$ is the difference between the excited state and ground state energies.

In order to obtain the selection rules $(\psi^F, \underline{r}\, \Phi^\circ)$ must be calculated. Since each eigen state $|i\rangle$ is calculated at $\underline{k}=0$, the corresponding excited state wave function ψ_i^F from equation 5.4 is

$$\psi_i^F = k' \sum_{m\alpha} B_\alpha^i \, \Phi_{m\alpha}^F \qquad 5.61$$

The coefficients B_α^i in equation 5.61 are obtained from the components of the eigen vectors in equations 5.43 through 5.46, e.g., $(B_1^1, B_2^1, B_3^1, B_4^1)=(\frac{1}{2},\frac{1}{2},\frac{1}{2},\frac{1}{2})$. Using equation 5.4 the matrix elements $(\psi_i^F, \underline{r}\Phi^\circ)$ for each of the eigen vectors $|i\rangle$ is

$$\left(\psi^F_{\substack{1\\2\\3\\4}}, \underline{r}\,\Phi^\circ\right) = \frac{k'}{2}\sum_m \int\left[\left(\Phi^{F^*}_{m1}\right)_{\pm} + \left(\Phi^{F^*}_{m2}\right)_{\mp} + \left(\Phi^{F^*}_{m3}\right)_{\mp} + \left(\Phi^{F^*}_{m4}\right)_{\pm}\right]\underline{r}\,\Phi^\circ d\tau \qquad 5.62$$

Since each of the unit cells is identical, each integral in equation 5.62 corresponding to a different value of m will be identical, and $(\psi_i^F, \underline{r}\Phi^\circ)$ is

$$\left(\psi^F_{\substack{1\\2\\3\\4}}, \underline{r}\,\Phi^\circ\right) = \frac{Nk'}{2}\int\left(\Phi^{F^*}_{11\,\pm} + \Phi^{F^*}_{12\,\mp} + \Phi^{F^*}_{13\,\mp} + \Phi^{F^*}_{14}\right)\underline{r}\,\Phi^\circ d\tau \qquad 5.63$$

where N is the number of unit cells in the crystal. After substituting for the excited state and ground state crystal functions from equations 5.3 and 5.2 respectively, $(\psi_i^F, \underline{r}\Phi^\circ)$ becomes

$$\left(\psi^F_{\substack{1\\2\\3\\4}}, \underline{r}\,\Phi^\circ\right) = \frac{Nk'}{2}\left[\int \phi^{F^*}_{11}\,\underline{r}_1\,\phi^\circ_{11}\,d\tau \pm \int \phi^{F^*}_{12}\,\underline{r}_2\,\phi^\circ_{12}\,d\tau \mp \int \phi^{F^*}_{13}\,\underline{r}_3\,\phi^\circ_{13}\,d\tau \pm \int \phi^{F^*}_{14}\,\underline{r}_4\,\phi^\circ_{14}\,d\tau\right] \qquad 5.64$$

where $\underline{r}_1$ is the sum of the position vectors of the electrons on the 1^{th} molecule. The first, second, third and fourth integrals in equation 5.64 represent the ground state to excited state transition moments for the molecules numbered 1, 2, 3 and 4 respectively. If we denote the transition moment of the 1^{th} molecule by $\underline{M}_1$, then from equation 5.64

$$\left(\psi^{F}_{\substack{1\\2\\3\\4}}, \underline{r}\,\Phi^{\circ}\right) = \frac{Nk'}{2}\left[\underline{M}_1 \begin{matrix}+\\+\\=\end{matrix} \underline{M}_2 \begin{matrix}=\\+\\+\end{matrix} \underline{M}_3 \begin{matrix}+\\=\\+\end{matrix} \underline{M}_4\right] \qquad 5.65$$

Because the molecules are identical, each will have a transition moment of the same magnitude. Since the allowed molecular excited states for pyrene transform as vectors,[5] $\underline{M}_1$ will have a fixed direction with respect to molecule 1. The transition moments of molecules 2, 3, and 4 are related to $\underline{M}_1$ by the transformation properties of the space group C^5_{2h} (see section B). Using the properties of this space group

$$\underline{M}_2 = C_2^b\,\underline{M}_1 \qquad 5.66$$

$$\underline{M}_3 = \delta_{ac}\,\underline{M}_1 = i\,C_2^b\,\underline{M}_1 = -C_2^b\,\underline{M}_1 \qquad 5.67$$

$$\underline{M}_4 = i\,\underline{M}_1 = -\underline{M}_1 \qquad 5.68$$

After substituting equations 5.66, 5.67 and 5.68 into equation 5.65

$$\left(\psi^{F}_{\substack{1\\2\\3\\4}}, \underline{r}\,\Phi^{\circ}\right) = \frac{Nk'}{2}\left[\underline{M}_1 \begin{matrix}+\\+\\=\end{matrix} C_2^b\,\underline{M}_1 \begin{matrix}=\\+\\+\end{matrix} \left(-C_2^b\,\underline{M}_1\right) \begin{matrix}+\\=\\+\end{matrix} \left(-\underline{M}_1\right)\right] \qquad 5.69$$

Equation 5.69 indicates that only eigen states $|2\rangle$ and $|4\rangle$ have

nonzero values for $(\psi_i^F, \underline{r}\Phi^\circ)$. Therefore using equation 5.60 we see that only eigen states $|2\rangle$ and $|4\rangle$ can be excited. To determine the polarizations needed for excitation of each of these states, the directions of $(\psi_2^F, \underline{r}\Phi^\circ)$ and $(\psi_4^F, \underline{r}\Phi^\circ)$ must be found. $(\psi_2^F, \underline{r}\Phi^\circ)$ and $(\psi_4^F, \underline{r}\Phi^\circ)$ from equation 5.69 are

$$\left(\psi_{\substack{2\\4}}^F, \underline{r}\Phi^\circ\right) = Nk'\left(1 \pm C_2^b\right)\underline{M}_1 \qquad 5.70$$

The matrix which represents a two fold rotation about the $\underline{b}$ axis is

$$C_2^b = \begin{pmatrix} -1 & 0 & 0 \\ 0 & 1 & 0 \\ 0 & 0 & -1 \end{pmatrix} \qquad 5.71$$

where the first row of the matrix transforms the $\underline{a}$ component, the second row transforms the $\underline{b}$ component, and the third row transforms the $\underline{c}$' component (c' is the direction perpendicular to the $\underline{ab}$ plane). Using equation 5.71

$$\left(\psi_{\substack{2\\4}}^F, \underline{r}\Phi^\circ\right) = Nk'\left[\begin{pmatrix} 1 & 0 & 0 \\ 0 & 1 & 0 \\ 0 & 0 & 1 \end{pmatrix} \pm \begin{pmatrix} -1 & 0 & 0 \\ 0 & 1 & 0 \\ 0 & 0 & -1 \end{pmatrix}\right]\begin{pmatrix} M_{1a} \\ M_{1b} \\ M_{1c'} \end{pmatrix} \qquad 5.72$$

Equation 5.72 reduces to

$$\left(\psi_2^F, \underline{r}\Phi^\circ\right) = 2Nk'\begin{pmatrix} 0 \\ M_{1b} \\ 0 \end{pmatrix} \qquad 5.73$$

$$\left(\psi_4^F, \underline{r}\,\underline{\mathcal{E}}^\circ\right) = 2Nk' \begin{pmatrix} M_{1a} \\ 0 \\ M_{1c} \end{pmatrix} \qquad 5.74$$

Equations 5.73 indicate that $(\psi_1^F, \underline{r}\,\underline{\mathcal{E}}^\circ)$ and $(\psi_2^F, \underline{r}\,\underline{\mathcal{E}}^\circ)$ are parallel and perpendicular to the $\underline{b}$ axis respectively. Since the transition probability is proportional to the square of $\underline{E}_o \cdot (\psi^F, \underline{r}\,\underline{\mathcal{E}}^\circ)$, the respective polarizations required to excite eigen states $|2\rangle$ and $|4\rangle$ must be parallel and perpendicular to the $\underline{b}$ axis.

G. Davydov Splitting of the Triplet State in Pyrene

The Davydov splitting of the triplet state is the difference in energy between the allowed triplet transitions at $\underline{k}=0$. Since the eigen states $|2\rangle$ and $|4\rangle$ correspond to the only allowed triplet transitions, the Davydov splitting is

$$\Delta = \left| \epsilon^F_{|2\rangle}(0) - \epsilon^F_{|4\rangle}(0) \right| \qquad 5.75$$

by substituting the values for $\epsilon^F_{|2\rangle}(0)$ and $\epsilon^F_{|4\rangle}(0)$ from Table 5.3 into equation 5.75, one obtains

$$\Delta = 4 \left| (A_2 - A_3) \right| \qquad 5.76$$

H. The Energy Dispersion of Eigen States $|2\rangle$ and $|4\rangle$

Table 5.6 lists the energy dispersion relations which are associated with each of the eigen states. With the aid of

this table and Tables 5.1 and 5.2, a list of dispersion relations for eigen states $|2\rangle$ and $|4\rangle$ can be constructed. Table 5.7 shows such a listing for the case in which A_4 is positive and much larger than all other interactions ($|A_4| \gg |A_2|, |A_3|$ or $|A_5|$). To illustrate the type of approximation used in constructing the elements of this table, let us examine $\epsilon^F_{|2\rangle}$ for the case in which $\underline{k}$ is parallel to $\underline{a}$. In this case Table 5.6 indicates that $\epsilon^F_{|2\rangle}$ is ϵ^F_{a2}. From Table 5.2 ϵ^F_{a2} is

$$\epsilon^F_{a2} = \xi^F - 2A_3 \cos\frac{ka}{2} - \sqrt{4A_2^2 - 4A_2(A_4+A_5)\cos\frac{ka}{2} + A_4^2 + A_5^2 + 2A_4A_5} \qquad 5.77$$

Following the approximation that A_4 is predominant over all other interactions, the second order terms in equation 5.77 are approximately zero and

$$\epsilon^F_{a2} \simeq \xi^F - 2A_3 \cos\frac{ka}{2} - \sqrt{A_4^2 + 2A_4\left(A_5 - 2A_2\cos\frac{ka}{2}\right)} \qquad 5.78$$

In view of the approximation, the second term under the square root sign is small compared with the first and the square root is expanded to give

$$\epsilon^F_{a2} \simeq \xi^F - 2A_3 \cos\frac{ka}{2} - A_4 - A_5 + 2A_2\cos\frac{ka}{2} \qquad 5.79$$

This result is presented in Table 5.7. In the case in which A_4 is negative and predominant the energy dispersion relations for states $|2\rangle$ and $|4\rangle$ are identical to those given in Table 5.7.

$\underline{K}$	$\epsilon^F_{\|2\rangle}$	$\epsilon^F_{\|4\rangle}$
Parallel to $\underline{a}$	$\epsilon^F_{a2} \simeq \xi^F - (A_4 + A_5) - 2(A_3 - A_2)\cos\frac{ka}{2}$	$\epsilon^F_{a4} \simeq \xi^F - (A_4 + A_5) + 2(A_3 - A_2)\cos\frac{ka}{2}$
Parallel to $\underline{b}$	$\epsilon^F_{b2} \simeq \xi^F - (A_4 + A_5\cos kb) - 2(A_3 - A_2)\cos\frac{kb}{2}$	$\epsilon^F_{b4} \simeq \xi^F - (A_4 + A_5\cos kb) + 2(A_3 - A_2)\cos\frac{kb}{2}$

Table 5.7. Energy dispersion of eigen states $|2\rangle$ and $|4\rangle$ for the case in which A_4 is positive and much larger than $|A_2|$, $|A_3|$ or $|A_5|$.

The energy dispersion relations in Table 5.7 are only applicable for excitons moving parallel to the a or b crystal direction. In order to calculate the exciton diffusion constant it is necessary to know the energy dispersion for all directions of exciton motion (see section J). Since equation 5.21 cannot be factored in general, as we have already mentioned, a general dispersion relation must be obtained through appoximation methods. All of the dispersion relations in Table 5.7 indicate that

$$\delta = \mathcal{E}^F - \epsilon^F = A_4 + d \qquad 5.80$$

where d is a factor which is smaller than A_4. In the work which follows we will show that if δ is taken to be in the form given by equation 5.80, equation 5.21 can be solved in approximation for a general dispersion relation which is consistent with the results of Table 5.7. Substituting equation 5.80 for δ, equation 5.21 becomes

$$\begin{vmatrix} A_4+d & a_{12} & a_{13} & A_4+a_{15} \\ a_{12}^* & A_4+d & A_4+a_{15} & a_{24} \\ a_{13}^* & A_4+a_{15}^* & A_4+d & a_{34} \\ A_4+a_{15}^* & a_{24}^* & a_{34}^* & A_4+d \end{vmatrix} = 0 \qquad 5.81$$

where

$$a_{12} = \beta e^{-i\underline{k}\cdot\underline{b}/2}$$

$$a_{13} = \gamma e^{-i\underline{k}\cdot\left(\underline{b}+\frac{\underline{a}}{2}\right)}$$

$$a_{15} = A_5 e^{-i\underline{k}\cdot\underline{b}}$$

$$a_{24} = \gamma e^{i\underline{k}\cdot\frac{\underline{a}}{2}}$$

$$a_{34} = \beta e^{i\underline{k}\cdot\left(\underline{a}+\frac{\underline{b}}{2}\right)}$$

After a bit of algebra equation 5.81 becomes

$$\begin{vmatrix} 2d-(a_{15}+a_{15}^*) & a_{12}-a_{13}-a_{24}^*+a_{34}^* & a_{13}-a_{34}^* & a_{15}-d \\ a_{12}^*-a_{13}^*-a_{24}+a_{34} & 2d-(a_{15}+a_{15}^*) & a_{15}-d & a_{24}-a_{34} \\ a_{13}^*-a_{34} & a_{15}^*-d & A_4+d & a_{34} \\ a_{15}^*-d & a_{24}^*-a_{34}^* & a_{34}^* & A_4+d \end{vmatrix} = 0 \qquad 5.82$$

Since A_4 is assumed to be much larger than any other interaction, the largest terms in the expansion of the above determinant are the ones which are quadratic in A_4. If all other terms are assumed to be negligible, equation 5.82 becomes

$$\left\{\left[2d-(a_{15}+a_{15}^*)\right]^2-\left|a_{12}-a_{13}-a_{24}^*+a_{34}^*\right|^2\right\}A_4^2 = 0 \qquad 5.83$$

Solving equation 5.83 for d, one obtains

$$d = \frac{(a_{45} + a_{45}^*)}{2} \pm \frac{1}{2}\left| a_{12} - a_{13} - a_{24}^* + a_{34}^* \right| \qquad 5.84$$

After substituting for a_{12}, a_{13}, a_{15}, a_{24} and a_{34} from equation 5.81, d becomes

$$d = A_5 \cos \underline{k}\cdot\underline{b} \pm 2(A_2 - A_3) \cos \frac{\underline{k}\cdot\underline{a}}{2} \cos \frac{\underline{k}\cdot\underline{b}}{2} \qquad 5.85$$

By substituting equation 5.85 into equation 5.80, one finds that the energy of the excited state is

$$\epsilon^F = \xi^F - (A_4 + A_5 \cos \underline{k}\cdot\underline{b}) \pm 2(A_3 - A_2) \cos \frac{\underline{k}\cdot\underline{a}}{2} \cos \frac{\underline{k}\cdot\underline{b}}{2} \qquad 5.86$$

For the case in which $\underline{k}$ is parallel to $\underline{a}$, equation 5.86 is

$$\epsilon^F = \xi - (A_4 + A_5) \pm 2(A_3 - A_2) \cos \frac{ka}{2} \qquad 5.87$$

Equation 5.87, as anticipated, is identical to the results in Table 5.7 for $\underline{k}$ parallel to $\underline{a}$. Equation 5.86, as also anticipated, is in agreement with the results of Table 5.7 in the case in which $\underline{k}$ is parallel to $\underline{b}$. These comparisons indicate that the approximate dispersion relations for states $|2\rangle$ and $|4\rangle$ are

$$\epsilon^F_{\substack{|2\rangle \\ |4\rangle}}(\underline{k}) = \xi^F - (A_4 + A_5 \cos \underline{k}\cdot\underline{b}) \mp 2(A_3 - A_2) \cos \frac{\underline{k}\cdot\underline{a}}{2} \cos \frac{\underline{k}\cdot\underline{b}}{2} \qquad 5.88$$

I. Velocity of Triplet Excitons in Pyrene

The velocity of triplet excitons in pyrene can be found from the energy dispersion relation, equation 5.88. In terms of the components of $\underline{k}$ along the $\underline{a}$ and $\underline{b}$ crystal directions, k_a and k_b respectively, equation 5.88 is

$$\epsilon^{F}_{\substack{|2\rangle \\ |4\rangle}}(\underline{k}) = E^{F} - (A_4 + A_5 \cos k_b b) \mp 2(A_3 - A_2)\cos\frac{k_a a}{2}\cos\frac{k_b b}{2} \qquad 5.89$$

The $\underline{a}$ component of the exciton velocity is

$$v_a(\underline{k}) = \frac{1}{\hbar}\frac{\partial \epsilon^{F}}{\partial k_a} = \mp \frac{a}{\hbar}(A_3 - A_2)\sin\frac{k_a a}{2}\cos\frac{k_b b}{2} \qquad 5.90$$

where the distinction between states $|2\rangle$ and $|4\rangle$ has been dropped because the velocities for these states have the same absolute magnitudes. In terms of the Davydov splitting Δ (equation 5.75) the absolute magnitude of the $\underline{a}$ component of the exciton velocity is

$$|v_a(\underline{k})| = \frac{a\Delta}{4\hbar}\sin\frac{k_a a}{2}\cos\frac{k_b b}{2} \qquad 5.91$$

Therefore, by measuring the Davydov splitting one can estimate the absolute magnitude of the $\underline{a}$ component of the velocity. The $\underline{b}$ component of the exciton velocity is

$$\left[v_b(k)\right]_{\substack{|2\rangle \\ |4\rangle}} = \frac{1}{\hbar}\frac{\partial \epsilon^{F}}{\partial k_b} = A_5 b \sin k_b \mp b(A_3 - A_2)\cos\frac{k_a a}{2}\sin\frac{k_b b}{2} \qquad 5.92$$

The presence of A_5 in this equation indicates that a measurement of the Davydov splitting is not sufficient to determine the b component of the exciton velocity.

J. The Diffusion Constant of Triplet Excitons in Pyrene

The a component of the triplet exciton velocity (equation 5.90) can be used to estimate the triplet exciton diffusion constant for motion in the a direction. For lack of further knowledge is will be assumed that exciton scattering can be described by a constant isotropic scattering time. In this approximation the components of the diffusion tensor are[6]

$$D_{ij} = \tau_s \left\langle v_i(\underline{k}), v_j(\underline{k}) \right\rangle \qquad 5.93$$

where τ_s is the constant isotropic scattering time, and $v_i(\underline{k})$ is the i^{th} component of the exciton velocity for all directions of $\underline{k}$. By substituting equation 5.90 into equation 5.93, one obtains

$$D_{aa} = \frac{\tau_s a^2 \Delta^2}{16 \hbar^2} \left\langle \sin^2 \frac{k_a a}{2} \cos^2 \frac{k_b b}{2} \right\rangle \qquad 5.94$$

After carrying out the average indicated in equation 5.94 over the extent of the Brillouin zone (zero to $\frac{\pi}{a}$ for k_a and zero to $\frac{\pi}{b}$ for k_b), D_{aa} becomes

$$D_{aa} = \frac{\tau_s a^2 \Delta^2}{64 \hbar^2} \qquad 5.95$$

APPENDIX

A. The Crystal Ground State Energy

The crystal ground state wave function constructed from equation 5.2 is

$$\psi^{\circ} = k'' \sum_{r\beta} B_{\beta} e^{i\underline{k}\cdot\underline{r}_{r}} \Phi^{\circ} \qquad \text{A.1}$$

where k" is a factor which normalizes ψ°. By operating on this function with the crystal Hamiltonian (equation 5.1), one obtains

$$\sum_{m\alpha} H_{m\alpha} \psi^{\circ} + \sum_{m\alpha,n\beta}{}' V_{m\alpha,n\beta} \psi^{\circ} = \epsilon^{\circ} \psi^{\circ} \qquad \text{A.2}$$

Multiplying both sides of equation A.2 by ψ^{*} and integrating over all the molecules, we have

$$\int \psi^{\circ *} \sum_{m\alpha} H_{m\alpha} \psi^{\circ} dV + \sum_{m\alpha,n\beta}{}' \int \psi^{\circ *} V_{m\alpha,n\beta} \psi^{\circ} dV = \epsilon^{\circ} \int \psi^{\circ *} \psi \, dV \qquad \text{A.3}$$

where ϵ° is the crystal ground state energy.

The first term in equation A.3 is just $\sum_{m\alpha} E^{\circ}_{m\alpha}$, the total ground state energy of the individual molecules. Using equation A.1 the second term in equation A.3 can be written as

$$(k'')^{2} \left[\sum_{t\rho} \sum_{s\eta} B^{*}_{\rho} B_{\eta} e^{i\underline{k}\cdot(\underline{r}_{s} - \underline{r}_{t})} \right] \sum_{m\alpha,n\beta}{}' \Phi^{\circ *} V_{m\alpha,n\beta} \Phi^{\circ} dV \qquad \text{A.4}$$

In order to evaluate the above expression we must evaluate the term in brackets. This is accomplished by looking at the normalization condition for ψ°.

$$\int \psi^{\circ *} \psi^{\circ} dV = 1 = (k'')^2 \sum_{t\rho} \sum_{s\eta} B_{\rho}^{*} B_{\eta} e^{i\underline{k}\cdot(\underline{r}_s - \underline{r}_t)} \int \Phi^{\circ *} \Phi^{\circ} dV \qquad \text{A.5}$$

But Φ° is normalized, so

$$\sum_{t\rho} \sum_{s\eta} B_{\rho}^{*} B_{\eta} e^{i\underline{k}\cdot(\underline{r}_s - \underline{r}_t)} = \frac{1}{(k'')^2} \qquad \text{A.6}$$

With the above relationship one finds that

$$\epsilon^{\circ} = \sum_{m\alpha} E_{m\alpha}^{\circ} + \sum_{m\alpha, n\beta}{}' \int \Phi^{\circ *} V_{m\alpha, n\beta} \Phi^{\circ} dV \qquad \text{A.7}$$

Therefore we find that ϵ° is independent of $\underline{k}$.

References - Chapter 5

1. J.M. Robertson and J.G. White, J. Chem. Soc., 358 (1947).

2. J. Jortner, S.A. Rice, and J.L. Katz, J. Chem. Phys. 42, 309 (1965).

3. R.S. Knox, J. Phys. Chem. Solids 9, 265 (1959).

4. A.S. Davydov, Theory of Molecular Excitons, McGraw-Hill, p.77 (1962).

5. Reference 4, p. 42.

6. P. Avakian, V.Ern, R.E. Merrifield, and A. Suna, Phys. Rev. 165, 974 (1968).

CHAPTER 6

Crystals and Experimental Apparatus for the Davydov Splitting Experiment

A. Availability and Quality of Pyrene Crystals

The pyrene crystals were prepared at, and made available by the Solid State Physics Group of the Brookhaven National Laboratory.

The crystals were prepared by starting with a chemical grade of pyrene (Eastman no.3627) and further purifying it by chromatography, vacuum sublimation, and zone refining.[1] The residual impurity concentration was too small to be detected by gas chromatography (less than 1 ppm). Single crystals were grown by the Bridgman method.

The decay of the delayed fluorescence in a pyrene crystal was recorded with the apparatus shown in Figure 3.8. This decay was found to have a triplet decay constant of 160 sec^{-1}.

B. Preparation of a Sample from the Crystal Boule

A section about 3 mm thick was cleaved from the crystal boule along the ab cleavage plane[2] with a razor. The cleavage plane was located with the aid of cleavage cracks. Both sides of the crystal were then planed with a glass mounted xylene-soaked, "Kleenex" tissue until they were parallel to the ab cleavage plane and had an optical finish. The typical sample was 1 cm^2 in the ab plane and about 1.5 mm thick along the c' direction.

C. Orientation of Sample

During the experiment the crystal was irradiated by linearly polarized light directed normally to the crystal ab plane. The a and b directions of the crystal were oriented with respect to the incident direction of polarization by using the optical properties of the monoclinic unit cell. In the monoclinic unit cell the b axis is a principle axis of the dielectric tensor.[3] As a consequence the other two principle directions lie in the ac plane. By rotating the crystal about its c' axis while observing the transmitted light through a crossed polaroid, two directions of extinction were established. The b axis was distinguished by observing the birefringence along each of these directions. Since the ac plane is a mirror plane in the monoclinic unit cell, the minimum birefringence should be observed for the b direction.

D. Apparatus for Davydov Splitting Experiment

The goals of the Davydov Splitting Experiment were to find: (1) the change in the energy of the (0,0) triplet transition [(0,0) designates a transition from the lowest vibrational level of the ground state to the lowest vibrational level of an excited state] in a pyrene crystal between its values for light polarized perpendicular and parallel to the b direction, and (2) the line width of the absorption line associated with the (0,0) triplet transition for a pyrene crystal.

To accomplish the above aims the absorption spectrum in the region of the (0,0) triplet transition was ob-

tained indirectly by measuring the delayed fluorescence vs. incident wavelength for each of the two polarizations.

The apparatus used in performing the Davydov Splitting Experiment consisted of the following, (1) a high intensity light source, (2) a scanning monochromator, (3) a polarizer, (4) a second order filter, (5) a crystal holder, (6) observation filters, and (7) an electrical system (Figure 6.1).

(1) High Intensity Light Source

A 1000 watt xenon lamp (Hanovia 976C1) was used as the source. In order to prevent damage to other parts of the optical system, the xenon lamp was followed by a 2 cm water heat filter.

(2) Scanning Monochromator

The scanning monochromator consisted of: (a) a monochromator; (b) a syncronous drive mechanism; (c) a motor power supply; and (d) a trigger pickup.

(a) Monochromator

The monochromator was manufactured by Jarrel Ash. It had a quarter meter focal length, and was equipped with a 1180 groove/mm grating having a 6000 Å blaze. With this grating the linear dispersion of the monochromator is advertized to be 33 Å/mm.

(b) Syncronous Drive Mechanism

The syncronous drive mechanism is shown in Figure 6.2. The monochromator was driven by a two-speed reversible syncronous motor, which was connected to the monochromator drive shaft by a bellows coupler. The motor was operated at 1 r.p.m.

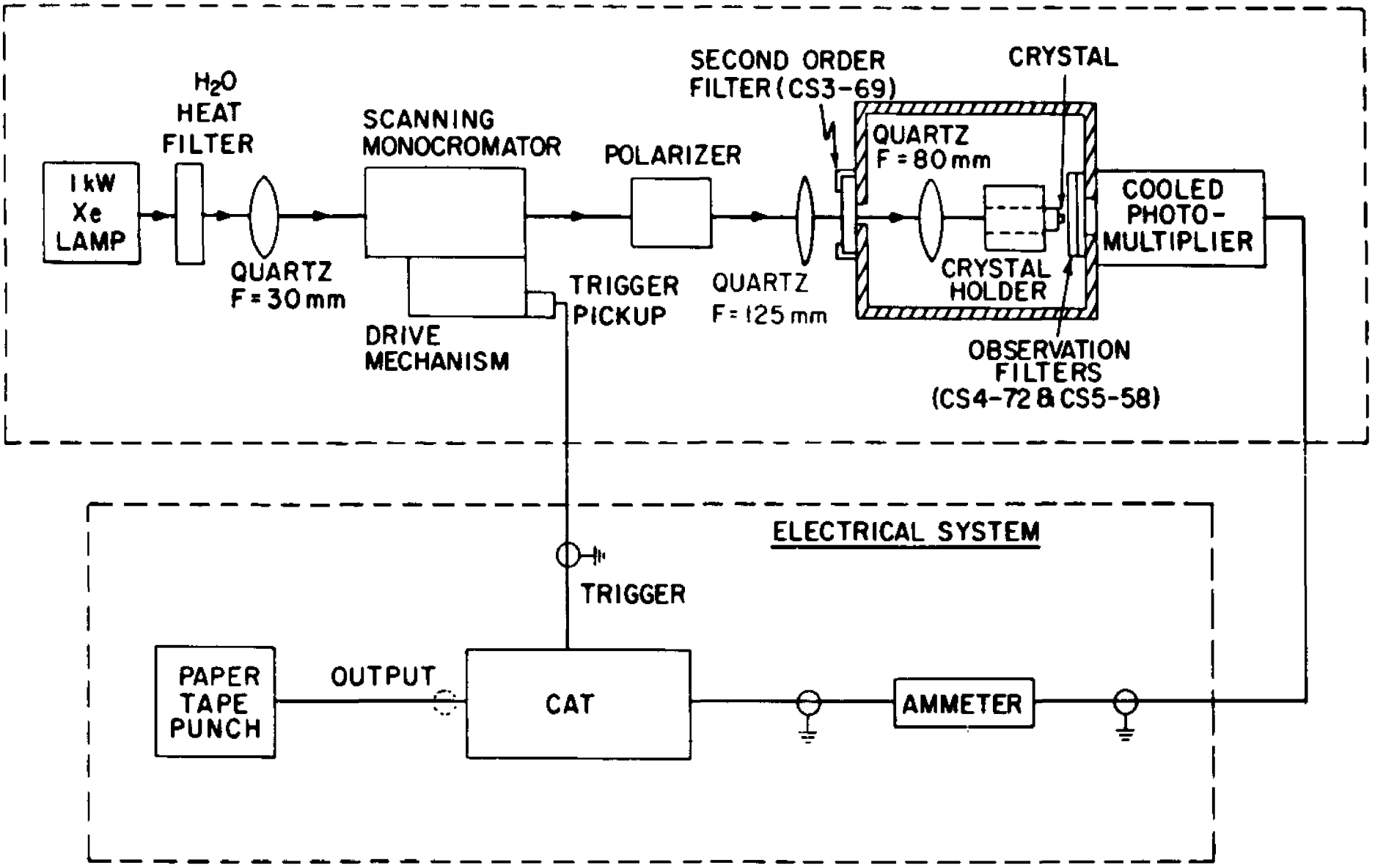

Fig. 6.1. Electrical and optical systems for splitting experiment

1. Cam 1

2. Trigger pickup

3. Cam 2

4. Two speed reversible syncronous motor

5. Monochromator

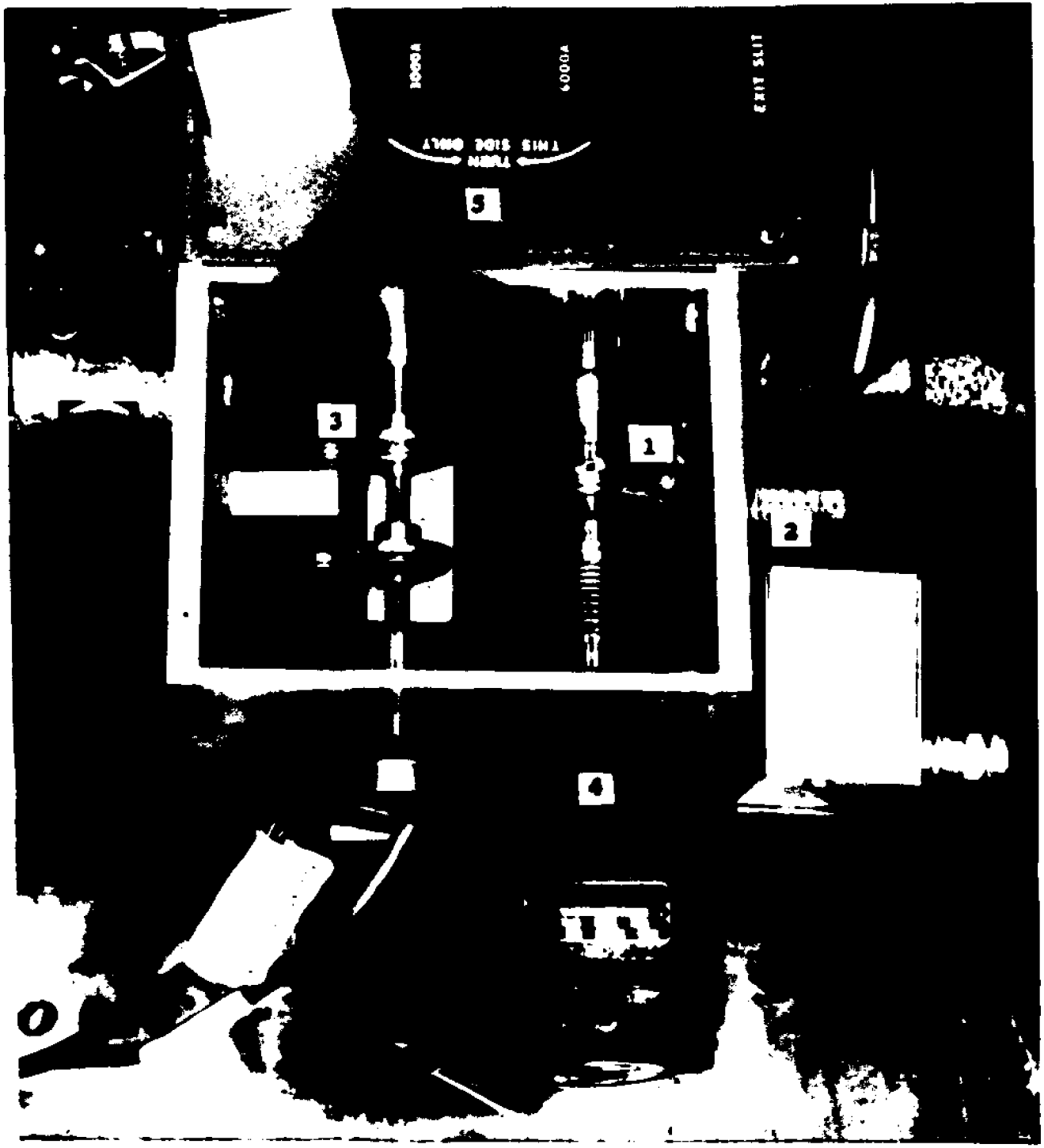

Fig.6.2. Monochromator drive mechanism

in the direction of decreasing wavelength and at 2 r.p.m. in the reverse direction. Data were taken only in the direction of decreasing wavelength. In this direction the wavelength speed was approximately 280 Å per minute. Cam 1, mounted on the drive shaft, was used to trigger (see Trigger Pickup) a computer of average transients (abbrev., CAT) into recording the output from the cooled photomultiplier (see Figure 6.1). A second shaft was coupled through gears to the monchromator drive shaft, and driven at one fifth the motor speed. Cam 2, mounted on this shaft, was used to control the limits to which the monochromator could travel (see Motor Power Supply).

(c) Motor Power Supply

The purpose of the motor power supply was to drive the monochromator cyclically between a desired high and low wavelength. To introduce as little impulse as possible, all switching was done after the motor was shut off and allowed to glide to a stop. The motor power supply illustrated in Figure 6.3 was composed of a microswitch, two time delay relays, a ratchet relay and motor switching relays.

The motor was controlled in the following manner. When the monochromator reached its lower wavelength limit microswitch S_2 was closed by Cam 2 which caused time delay relay 1 to turn the motor power off for three seconds. After the first two seconds time delay relay 2 activated the ratchet relay, which caused the motor switching relays to set the motor up for a fast rewind (2 r.p.m.). One second later power was restored to the motor by relay 1, and the monochromator was driven in the direction of in-

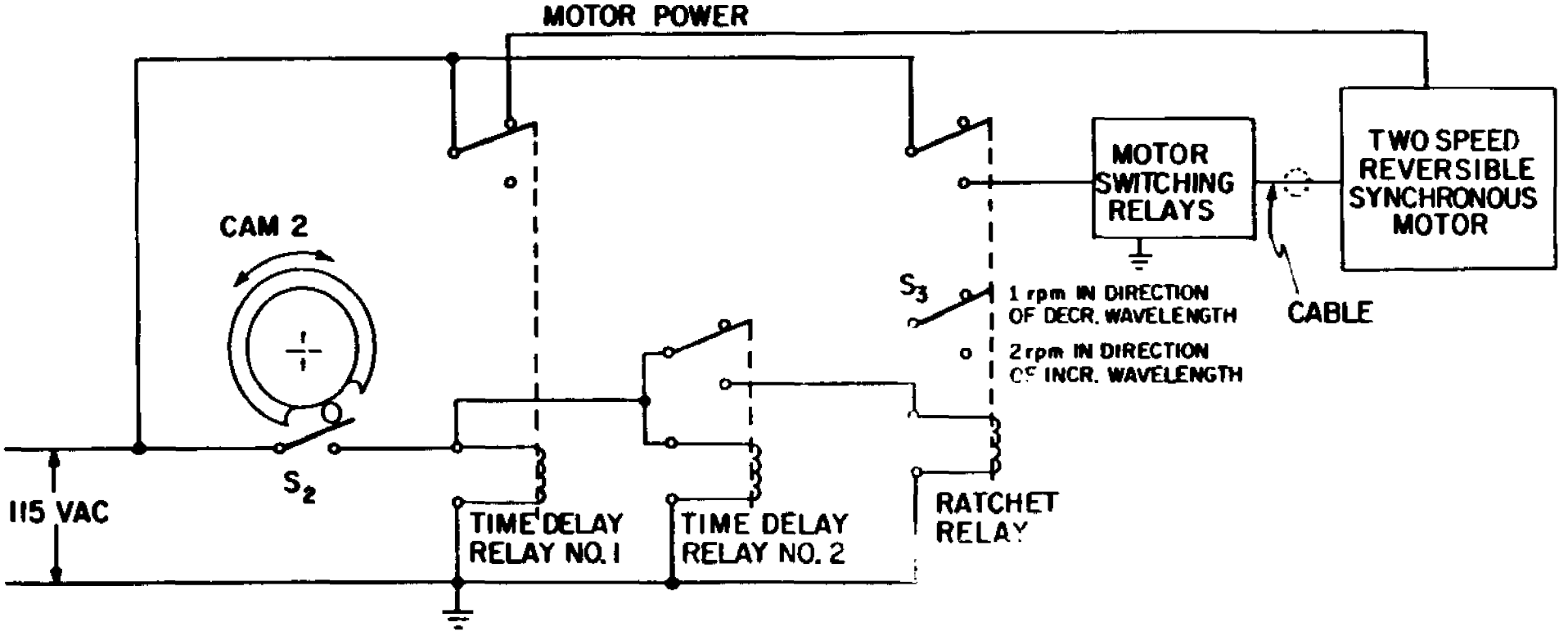

Fig. 6.3. Scanning motor power supply

creasing wavelength. When Cam 2 reached its high wavelength limit, the switching process was repeated, and the motor was reversed into the direction of decreasing wavelength at 1 r.p.m.

(d) Trigger Pickup

The trigger pickup, as mentioned earlier, was used to initiate the recording of data by a CAT (see Electrical System). This trigger pickup, illustrated in Figure 6.4, consisted of a rotating cam, a microswitch, and a pulse circuit.

The trigger pickup operated in the following manner. When S_1 was switched from A to B by Cam 1 the charge on C_1 was transferred to C_2 through resistor R_2. In this way a pulse with a rise time of under one microsecond was generated across R_2. When S_1 was switched back to A, capacitor C_1 recharged in readiness for the next trigger pulse. To inhibit a trigger pulse from occuring during the rewind, the battery E in the pulse circuit was open circuited with the aid of switch S_3 in the motor power supply, and residual charge on C_1 decayed through R_1 and R_4. In order to avoid inertial lags which occur at the beginning of the slow scan, cams 1 and 2 were adjusted so that the trigger pulse occurred about two seconds after the start of the slow scan.

(3) Polarizer

The light leaving the monochromator was polarized by means of a calcite crystal polarizer (Karl Lambrecht Crystal Optics Inc.). It was found that the light from the xenon source-monochromator combination had a preferred horizontal polarization. In order to transmit as much polarized light as possible the axis of the polarizer was set in the horizontal direction.

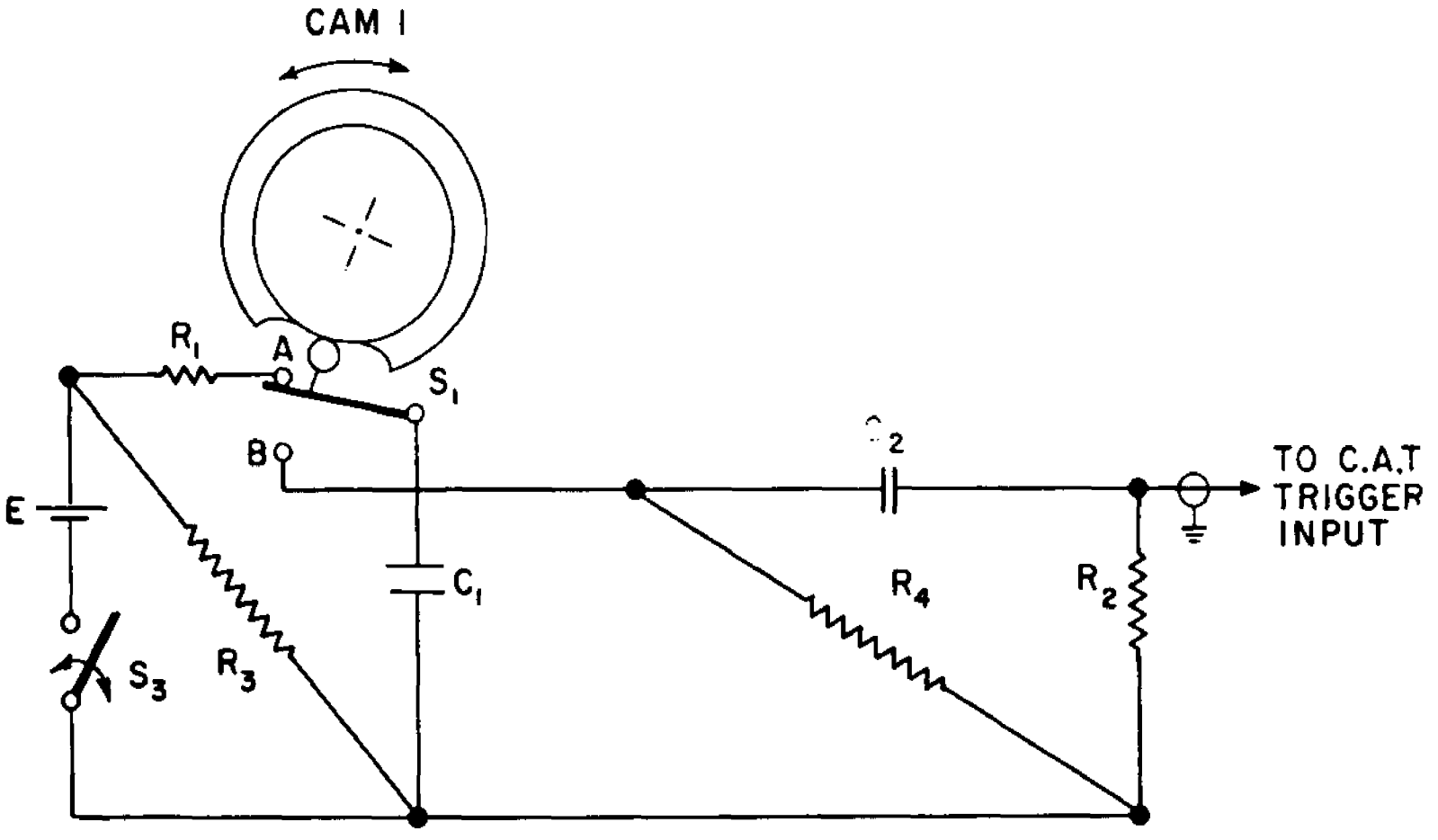

C_1 – 0.1 μf
C_2 – 0.01 μf
R_1 – 1 MΩ
R_2 – 1200Ω
R_3 – 3 MΩ
R_4 – 10,000Ω
E – 12 VOLTS

Fig. 6.4. Trigger pickup circuit

(4) Second Harmonic Filter

According to Avakian,[4] the (0,0) triplet transition in pyrene occurs for unpolarized light of 5935 Å. At this setting the monochromator produces second-order light at 2967 Å. Since the singlet levels in pyrene absorb at wavelengths less than 3800 Å,[5] the second harmonic must be eliminated. This is accomplished by using the Corning CS 3-69 filter which acts as a high wavelength pass filter above 5100 Å.

(5) Crystal Holder

The crystal holder is shown in Figure 6.5. The crystal holder was designed to rotate the crystal about its c' axis. The holder was oriented so that the incident light was normal to the ab plane of the crystal. In order to avoid disrupting the alignment of the optical system, the position of the crystal was controlled remotely. This was accomplished by rotating the crystal holder shaft with a servo motor. The angle between the b axis of the crystal and the plane of polarization of the incident light was monitored by a potential divider which was coupled to the servo motor shaft. The voltmeter used to indicate this angle was calibrated and could be read to within ½ degree.

(6) Observation Filters

The delayed fluorescence emitted by pyrene is composed of wavelengths greater than 4000 Å. In order to keep from detecting the incident light at approximately 5900 Å, a 3400 Å to 5000 Å band pass filter combination (Corning CS4-72 and CS5-58) was used before the photomultiplier.

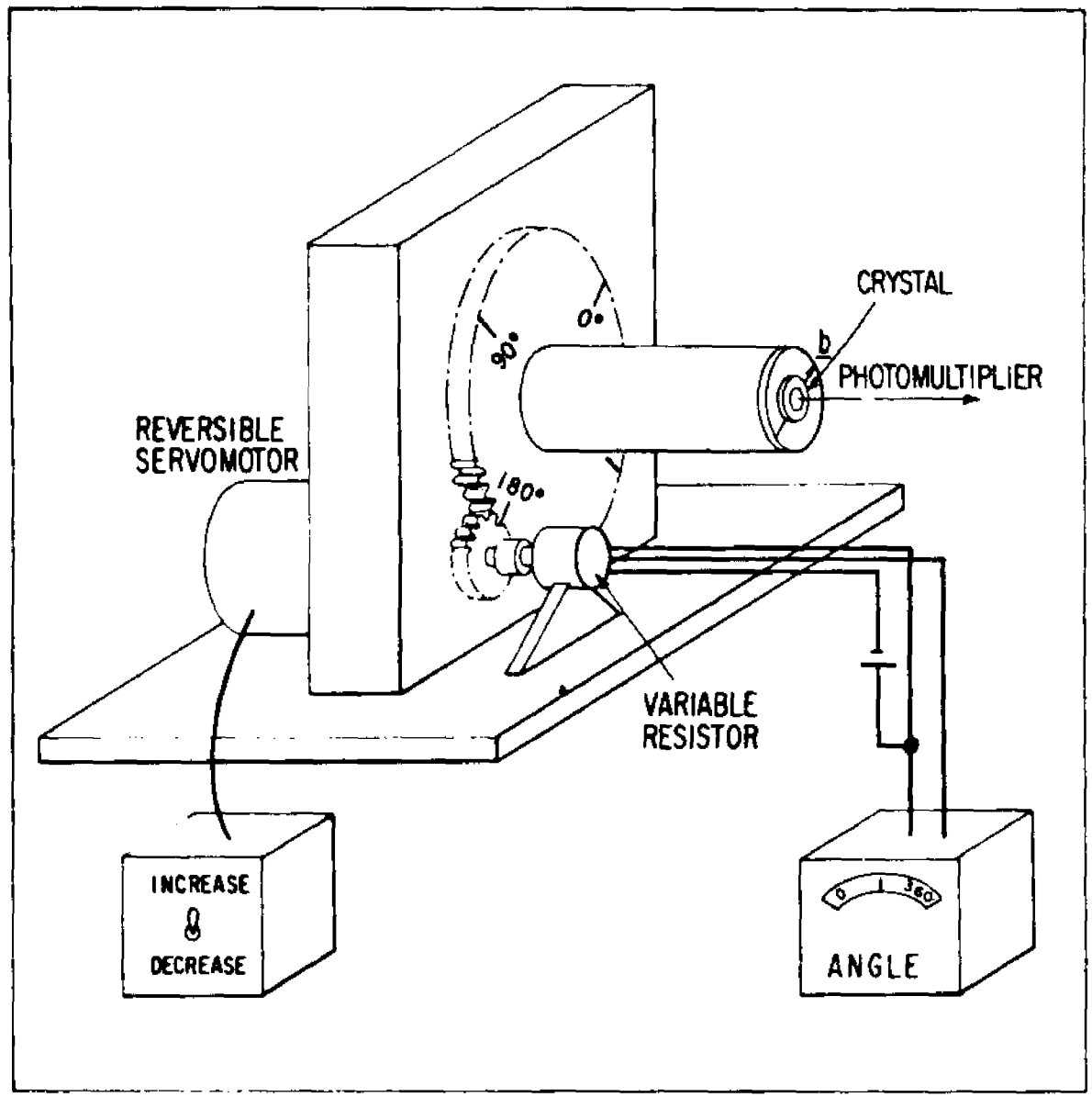

Fig.6.5. Crystal holder

(7) Electrical System

The delayed fluorescence from the pyrene was detected by an EMI 9558 photomultiplier. By cooling the photomultiplier to -20°C with a temperature stabilized tube chamber (Products for Research Inc., Model TE 102-TS), the signal to noise ratio was increased by a factor of one hundred. The current from the photomultiplier was measured by an ammeter (Kiethly Model 150 B) with a time constant of 25 milliseconds. The ammeter provided a one volt full scale output which was connected to the input of a Northern Scientific CAT. The CAT was programmed to sweep through its memory at the rate of 80 milliseconds per channel upon receiving a trigger signal from the monochromator trigger pickup. The resulting data was recorded by a Tally Paper Tape Punch.

The wavelength separation of the channels of the CAT was determined by placing a neon source at the entrance slit (0.1 mm) of the monochromator and recording the spectrum of this source with a photomultiplier at the exit slit (0.1 mm). Since the (0,0 triplet transition in pyrene takes place at 5935 Å[4] (for unpolarized incident light) the neon lines at 5944.8 Å and 5881.9 Å were analyzed in order to obtain the wavelength separation of the channels. The wavelength separation was found to be 0.340 Å per channel.

References - Chapter 6

1. Personal Communication with Dr. W.B. Whitten.

2. M.W. Porter and R.C. Spiller, The Barker Index of Crystals, (W. Heffer and Sons Ltd., Cambridge 1950).

3. S. Bhagvantam, Crystal Symmetry and Physical Properties, (Academic Press, London, p. 182, 1966).

4. P. Avakian and E. Abramson, J. Chem. Phys. 43, 182 (1965).

5. J. Ferguson, J. Chem. Phys. 28, 765 (1958).

CHAPTER 7

Experimental Procedure, Results and Discussion of the Davydov Splitting Experiment

A. Experimental Procedure

P. Avakian and E. Abramson have shown that the absorption peak corresponding to the (0,0) triplet transition in pyrene is centered at 5935 Å for unpolarized excitation.[1] In order to find this absorption peak, the polarizer was removed from the setup in Figure 6.1 (with 1 mm slits on the monochromator) and the wavelength of the incident light was reduced from 6500 Å until delayed fluorescence was observed (the fluorescence varied as the square of the incident excitation). The spectrum of the delayed fluorescence from 6000 Å to 5200 Å was similar to that observed by Avakian and Abramson.[1] By comparing the position of a krypton line at 5870.9 Å with the position of the (0,0) triplet transition peak (the longest wavelength peak in the delayed fluorescence spectrum) and using the channel wavelength separation of 0.340 Å per channel (see chapter 6, section D), the triplet transition peak was found to be located at 5928 Å. At this point cam 2 on the monochromator drive mechanism was adjusted so that the monochromator would cyclically scan over the (0,0) triplet transition peak (see chapter 6, section D) and cam 1 was adjusted so that the trigger pickup generated a pulse 2 seconds after the start of the scan to shorter wavelength. The polarizer was then replaced and the crystal holder was rotated to a position in which the incident light was polarized along either the a or b direction of the crystal. The (0,0) triplet transition peak was recorded in 254 channels of the CAT and signal av-

eraged over 50 scans of the monochromator. A typical signal averaged (0,0) triplet transition peak is shown by 254 solid circles in Figure 7.1.

B. Calculation of the Position of the Maximum of the (0,0) Triplet Transition Peak

In order to find the position of the maximum of the (0,0) triplet transition peak the signal averaged data was fit with an eighth order power series by the method of least squares. A typical fit is illustrated by the solid line in Figure 7.1. The eighth order power series was used because fits with power series of lower order had larger mean square deviations and ninth and tenth order power series gave the same answer for the position of the maximum with little change in mean square deviation. The position of the maximum was found by calculating the ordinate of the power series fit at intervals of a tenth of a channel (in the region of the fit) while storing the abscissa corresponding to the largest ordinate.

C. Results and Discussion

Table 7.1 shows the results of experiments performed on three different samples from the same boule. The polarization was alternated until a total of five runs (each run represents 50 signal averaged scans) at each polarization were made on each sample. Since the wavelength of the excitation decreases with increasing channel number, Table 7.1 indicates that the transition which is excited by a polarized light (state $|4\rangle$) is at lower energy (lower wavelength) than the transition excited by

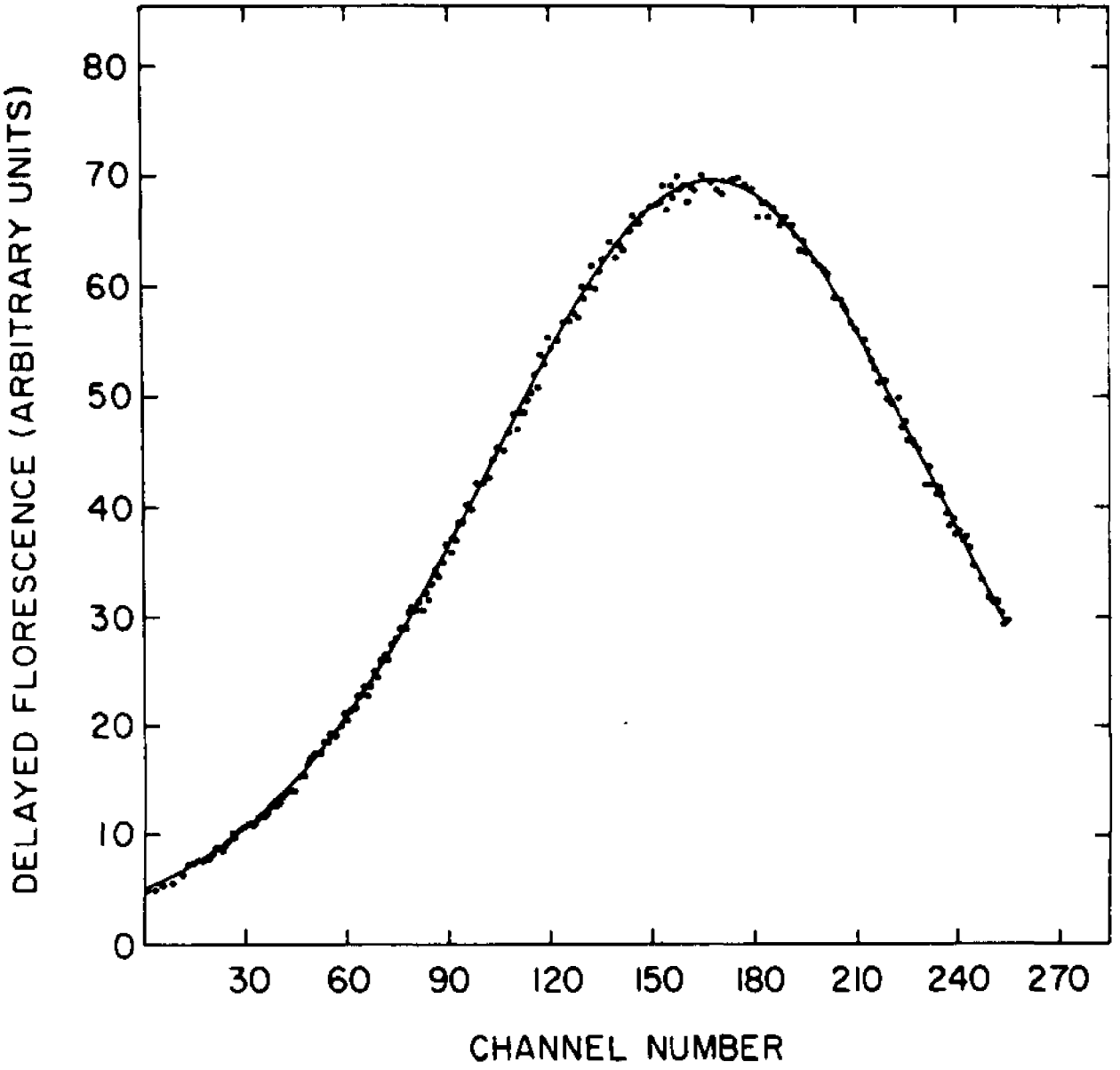

Fig. 7.1. The (0,0) triplet delayed fluorescence peak. The solid circles are experimental data and the solid line is an eighth order polynomial fit.

	CRYSTAL 1		CRYSTAL 2		CRYSTAL 3	
	$\underline{E}_o \parallel \underline{a}$ channels	$\underline{E}_o \parallel \underline{b}$ channels	$\underline{E}_o \parallel \underline{a}$ channels	$\underline{E}_o \parallel \underline{b}$ channels	$\underline{E}_o \parallel \underline{a}$ channels	$\underline{E}_o \parallel \underline{b}$ channels
	164.1	167.3	164.7	166.9	165.5	169.1
	164.1	167.8	165.0	167.3	165.9	168.6
	164.6	167.0	164.9	167.0	166.7	168.1
	164.1	166.7	164.6	167.0	166.8	168.9
	165.1	167.4	165.0	167.2	166.4	168.6
Mean	164.4±.4	167.2±.3	164.8±.2	167.1±.2	166.3±.4	168.7±.3
Mean Davydov splitting	2.8±.7		2.3±.4		2.4±.7	

Table 7.1. Position of the maximum of the (0,0) triplet transition peak for three pyrene crystals

b polarized light (state $|2\rangle$). In addition the delayed fluorescence at the maximum of the b polarized transition peak was found to be 40% greater than the delayed fluorescence at the maximum of the a polarized transition peak. Table 7.1 also indicates that the mean Davydov splittings for samples 1, 2 and 3 are $2.8 \pm .7$, $2.3 \pm .4$ and $2.4 \pm .7$ channels respectively (the variation in the mean deviation of these numbers is due to difference in signal to noise ratio caused by differences in the thicknesses of the three samples). Since the wavelength separation of the channels is 0.340 Å per channel, the Davydov splittings of samples 1, 2 and 3 in Angstroms are $0.95 \pm .24$, $0.78 \pm .14$ and $0.82 \pm .2$ respectively. The average value of the Davydov splitting for the three crystals is $0.85 \pm .21$ Å. In inverse centimeters this splitting is given by

$$\Delta = \frac{(0.85 \pm .21) \times 10^{-8}}{\lambda_{|2\rangle}\, \lambda_{|4\rangle}} \qquad 7.1$$

where $\lambda_{|2\rangle}$ and $\lambda_{|4\rangle}$ are the wavelengths corresponding to the absorption maxima of states $|2\rangle$ and $|4\rangle$ respectively. Since $\lambda_{|4\rangle}$ is only 1 Å larger than $\lambda_{|2\rangle}$, both $\lambda_{|2\rangle}$ and $\lambda_{|4\rangle}$ can be taken to be the unpolarized value of 5928 Å, and Δ is $2.4 \pm .6 cm^{-1}$.

The scattering time can be obtained from the width of the (0,0) triplet absorption line. If this line is approximated by a Lorentzian with a half width at half maximum Γ, the scattering time τ_s from the uncertainty principle will be approximately

$$\tau_s = \frac{\hbar}{2\Gamma} \qquad 7.2$$

Since the delayed fluorescence spectrum is proportional to the square of the absorption spectrum, Γ will correspond to the half width of the delayed fluorescence peak at quarter maximum after correcting for the finite slit width of the monochromator. In order for this correction to be as small as possible, the slit width of the monochromator must be reduced to a practical minimum. In polarized light a reduction of the slit width to $\frac{1}{2}$ mm was found to give inadequate signal to noise ratio. Since the splitting is small compared with the width of the delayed fluorescence peak, the half width at quarter maximum can be determined in unpolarized light. In unpolarized light a reduction of the slit width to $\frac{1}{2}$ mm was found to give adequate signal to noise ratio, and the resultant data had a half width at quarter maximum of 101 channels or 34.5 Å (using 0.340 Å/channel) or 98 cm^{-1} (using 5928 Å as the position of the unpolarized triplet absorption peak). After correcting for the finite slit width of the monochromator, as demonstrated in the Appendix to this chapter, the half width of the absorption spectrum at quarter maximum Γ was found to be 91 cm^{-1}. Using this value for Γ, the scattering time from equation 7.2 is 2.9×10^{-14} sec.

The values of the Davydov splitting and scattering time will now be used to estimate the triplet exciton velocity and diffusion constant. Using equation 5.93, the root mean square value of the a component of the triplet exciton velocity is

$$\sqrt{\langle v_a^2 \rangle} = \sqrt{\frac{D_{aa}}{\tau_s}} \qquad 7.3$$

Substituting in equation 7.3 for the diffusion constant D_{aa} from equation 5.95,

$$\sqrt{\langle v_a^2 \rangle} = \frac{a\,\Delta}{8\,\hbar} \qquad 7.4$$

Using a as 13.60 Å^3 and Δ as $2.4 \pm .6$ cm^{-1} in equation 7.4,

$$\sqrt{\langle v_a^2 \rangle} = (7.7 \pm 1.9) \times 10^3 \text{ cm/sec}$$

Solving equation 7.3 for the diffusion constant D_{aa} and substituting 2.9×10^{-14} sec for τ_s,

$$D_{aa} = (1.7 \pm .8) \times 10^{-6} \text{ cm}^2\text{-sec}^{-1}$$

An estimate of the triplet exciton diffusion length can be made from the diffusion constant and the triplet decay rate. From diffusion theory it is known that the diffusion length L is[4]

$$L = \sqrt{\frac{2D}{\beta}} \qquad 7.5$$

where D is the diffusion constant and β is the particle decay rate. Using 1.7×10^{-6} cm^2/sec for D and 160 sec^{-1} for β (see chapter 1, section A), the diffusion length L is about 1.5 mi-

crons. This diffusion length is much larger than a lattice constant, as one would expect for a triplet exciton (see chapter 1, section A).

In addition to the parameters which have already been obtained by using the Davydov splitting, some information about the molecular wave functions can probably be obtained from this quantity. The Davydov splitting from equation 5.76 is

$$\Delta = 4\left|(A_2 - A_3)\right| \qquad 5.76$$

where A_2 and A_3 are the molecular exchange interactions illustrated in Figure 5.1. By calculating A_2 and A_3 for various wave functions, and using the constraint imposed by equation 5.76, it is conceivable that a proper molecular wave function can be chosen, or at least equation 5.76 may serve as a test for the rejection of certain choices.

Finally, the estimated values of the triplet exciton velocity and scattering time can be used to choose a theoretical model which can best predict these parameters. The motion of an exciton may be described by either a localized or delocalized model. In the localized model, which is commonly called the hopping model,[5] exciton diffusion is described by a random walk process. In the delocalized model, commonly called the band model,[6] the exciton is described by a plane wave which is nearly stationary and the scattering length is taken to be much larger than a lattice constant. Since the scattering length is the product of the triplet exciton velocity and the scattering time,

the scattering length in pyrene is about 0.02 Å (using 7.7×10^{3} cm/sec for the triplet exciton velocity and 2.9×10^{-14} sec for the scattering time). Since this scattering length is much less than a lattice constant, and since the band model requires a length which is long compared to a lattice constant, it is concluded that the localized model affords the best description of the triplet exciton diffusion in pyrene.

APPENDIX

A. Correction in the Half Width at Quarter Maximum of the (0,0) Delayed Fluorescence Peak for the Finite Slit Width of the Monochromator

Due to finite slit width, the light at the exit slit of the monochromator will not be strictly monochromatic. For a monochromator set at a frequency ν', the intensity at the exit slit, for a nearby frequency ν, may be approximated by the triangular distribution[7]

$$I(\nu-\nu') = I(0)\left[\frac{(\nu-\nu')}{s} + 1\right] \quad \text{for } \nu' \le \nu \le (\nu'+s)$$

and

$$I(\nu-\nu') = I(0)\left[-\frac{(\nu-\nu')}{s} + 1\right] \quad \text{for } (\nu'-s) \le \nu \le \nu' \qquad \text{A.1}$$

where s is the slit width in energy units. Since the triplet exciton density is proportional to the incident intensity and absorption coefficient (see equation 2.13) and since the delayed fluorescence is proportional to the square of the triplet exciton density, if the absorption line is assumed to be Lorentzian, the delayed fluorescence is

$$I_f(\nu') = k\left[\int \frac{I(\nu-\nu')}{(\nu-\nu_0)^2 + r^2}\, d\nu\right]^2 \qquad \text{A.2}$$

where k is a constant of proportionality and ν_0 is the frequency at which the absorption is a maximum. Substituting in equation A.2 for the slit intensity distribution $I(\nu-\nu')$ from

equation A.1 and integrating, the delayed fluorescence intensity becomes

$$I_f(\nu') = k I^2(0) \left\{ \frac{1}{2s} \ln \frac{[(\Delta\nu)^2 + \Gamma^2]^2}{[(\Delta\nu - s)^2 + \Gamma^2][(\Delta\nu + s)^2 + \Gamma^2]} + \frac{1}{\Gamma}\left(1 + \frac{\Delta\nu}{s}\right) \tan^{-1} \frac{(\Delta\nu + s)}{\Gamma} \right.$$

$$\left. - \frac{1}{\Gamma}\left(1 - \frac{\Delta\nu}{s}\right) \tan^{-1} \frac{(\Delta\nu - s)}{\Gamma} - \frac{2\Delta\nu}{s\Gamma} \tan^{-1} \frac{\Delta\nu}{\Gamma} \right\}^2 \qquad \text{A.4}$$

where

$$\Delta\nu = \nu' - \nu_0$$

Equation A.4 can be written as

$$I_f(\nu') = I_f(\Delta\nu, \Gamma, s) \qquad \text{A.5}$$

The ratio of the delayed fluorescence at the top of the peak to its value at quarter maximum from equation A.5 is

$$\frac{I_f(0, \Gamma, s)}{I_f(\Delta\nu_{\frac{1}{4}}, \Gamma, s)} = \frac{1}{4} \qquad \text{A.6}$$

where $\Delta\nu_{\frac{1}{4}}$ is the half width of the delayed fluorescence peak at quarter maximum. Since $\Delta\nu_{\frac{1}{4}}$ and s are experimental numbers, Γ can be found by changing its value until the ratio on the left hand side of equation A.6 is 4; the corresponding value of Γ is then the true half width at half maximum of the absorption spectrum. For the present experiment $\Delta\nu_{1/4}$ was found to be 98 cm^{-1}. Since the linear dispersion of the monochromator is 33 Å/mm, a 1 mm slit represents an s of 16.5 Å or 47 cm^{-1} (using

5928 Å as the average wavelength of the (0,0) triplet transition peak). Using the above numbers for $\Delta\nu_{1/4}$ and s in equation A.6, the value of Γ is 91 cm^{-1}, as reported in section C.

References - Chapter 7

1. P. Avakian and E. Abramson, J. Chem. Phys. 43, 182 (1965).
2. P. Avakian and R.E. Merrifield, Mol. Cryst. 5, 37 (1968).
3. J.M. Robertson and J.G. White, J. Chem. Soc., 358 (1947).
4. R.D. Present, Kinetic Theory of Gases, (McGraw-Hill Book Co., Inc., New York, N.Y., 1958), p.66.
5. M. Trlifaj, Czech. J. Phys. 6, 533 (1956).
6. J. Jortner, S.A. Rice, J.L. Katz and S.I. Choi, J. Chem. Phys. 42, 309 (1965).
7. D.M. Dennison, Phys. Rev. 31, 503 (1928).